Performance Analysis of Space Frequency Block Coded OFDM Free-Space Optical Communication Systems with Polarization Diversity over Atmospheric Turbulent Channel

A thesis submitted to the Department of Electrical and Electronic Engineering of

Bangladesh University of Engineering and Technology in partial fulfillment of the requirement for the degree of

DOCTOR OF PHILOSOPHY IN ELECTRICAL AND ELECTRONIC

ENGINEERING

by

Md. Shariful Islam

B. Sc. in Electrical and Electronic Engineering, BUET
M. Sc. in Electrical and Electronic Engineering, BUET

Department of Electrical and Electronic Engineering

BANGLADESH UNIVERSITY OF ENGINEERING AND TECHNOLOGY

November 2022

The thesis entitled **"Performance Analysis of Space Frequency Block coded OFDM Free-Space Optical Communication Systems with Polarization Diversity over Atmospheric Turbulent Channel"** submitted by Md. Shariful Islam (Roll no: 0416064001 P, Session: April 2016) has been accepted as satisfactory in partial fulfillment of the requirements for the degree of **Doctor of Philosophy in Electrical and Electronic Engineering** on **26 November 2022**.

BOARD OF EXAMINERS

1.

Dr. Satya Prasad Majumder
Professor, Department of Electrical and Electronic Engineering
BUET, Dhaka-1205, Bangladesh

Chairman

2.

Dr. Md. Aynal Haque
Professor and Head, Department of Electrical and Electronic Engineering
BUET, Dhaka-1205, Bangladesh

(Ex-Officio)

3.

Dr. Mohammed Imamul Hassan Bhuiyan
Professor, Department of Electrical and Electronic Engineering
BUET, Dhaka-1205, Bangladesh

Member

4.

Dr. Mohammad Faisal
Professor, Department of Electrical and Electronic Engineering
BUET, Dhaka-1205, Bangladesh

Member

5.

Dr. Lutfa Akter
Professor, Department of Electrical and Electronic Engineering
BUET, Dhaka-1205, Bangladesh

Member

6.

Dr. Md. Saiful Islam
Professor, Institute of Information and Communication Technology,
BUET, Dhaka-1205, Bangladesh

Member

7.

Dr. Ramjee Prasad
Professor, Future Technologies for Business Ecosystem Innovation
Aarhus University, Herning, Denmark

Member
(External)

8.

Dr. Subrata Kumar Aditya
Professor, Department of Electrical and Electronic Engineering
Dhaka University, Dhaka-1000, Bangladesh

Member
(External)

CANDIDATE'S DECLARATION

It is hereby declared that, this thesis or any part of it has not been submitted elsewhere for the award of any degree or diploma.

Signature of the candidate

Md. Shariful Islam

Dedication

To my Family

Acknowledgement

Firstly, I would like to express my heartiest gratitude to almighty Allah for upholding me with perseverance, wisdom and strength throughout this journey and allowing everything to happen miraculously. His blessings have brought me success and smooth accomplishment to this research program at BUET.

Secondly, I would like to express my heartfelt gratitude to my supervisor Prof. Dr. Satya Prasad Majumder for giving me the opportunity to work under him in the field of Free-Space Optical Communication System. I would like to thank him for his constant guidance, supervision, encouragement and kind cooperation, particularly in justifying proper research direction of the thesis and ensuring that the research aims and objectives are fulfilled over the past six years.

I would then like to thank my Ph. D committee members, Prof. Md. Kamrul Hasan, Prof. Mohammed Imamul Hassan Bhuiyan, Prof. Mohammad Faisal, Prof. Lutfa Akter and Prof. Md. Saiful Islam for their generous help and numerous advices during every stage of the program. I have learnt from them not only the knowledge but also the invaluable methodologies to solve problems. Special thanks to Dr. Ramjee Prasad, Distinguished Professor, Department of Business Development and Technology, Aarhus University, Denmark and Dr. Subrata Kumar Aditya, Professor Department of EEE, DU for their professional inspiration, motivation and dynamic guidance for my higher studies.

Finally, my whole-hearted thanks should go to my parents for their principles and unconditional love for me. I sincerely pray to Allah for their good health and peaceful life. I am deeply thankful to my beloved wife, Achia Noor Akter who has constantly supported me to finish this journey. I would also like to express my endless love to my son (Aayan Islam) and daughter (Sara Binte Islam), who always cherished me in every moment of my life with the sacrifices of their needs.

Abstract

Free-space optical (FSO) communication system is an emerging technology for future broadband optical data communication network due to its lucrative properties like required no license, cost effective, simple hardware architecture, high data rate, full duplex communication, easy to deployment, etc.. During the last two decades, the user demand for data rate increased tremendously. To meet up the current data rate demand, FSO technology can play as a key parallel technology to enhance the capacity of the existing data communication network. However, there are some adverse weather effects like molecular absorption, scattering, beam divergence, background radiation, rain, snow, fog etc. severely limits the performance of FSO communication links. Beside these, pointing error due to earth quake, building sway and building vibration due to heavy mechanical load may occurs link failure which drastically degrades the performance of FSO communication links. Huge numbers of research works have already been published regarding how to mitigate the limitations of FSO communication system. Various methods of mitigation techniques like aperture averaging, diversity, adaptive optics, coding, modulation, relay transmission, background noise rejection, jitter isolation and rejection, hybrid RF/FSO link etc. are already employed by many of the researchers. In this dissertation, several analytical models are developed for a non-Hermitian OFDM FSO system followed by differential quadrature phase shift keying (DQPSK) modulation with polarization diversity over atmospheric turbulent channel.

Firstly, an analytical model is developed to evaluate the signal to noise ratio (SNR) and bit error rate (BER) of a non-Hermitian OFDM FSO system followed by DQPSK modulation in presence of atmospheric turbulence. To perform non-Hermitian OFDM, two different laser sources are required for transmitting real and imaginary part separately. Secondly, analysis is also carried out for the same system model with polarization diversity to overcome the requirement of two laser sources and evaluated the cross polarization induced crosstalk, signal to crosstalk plus noise ratio (SCNR)

and BER performance of the system in presence of all atmospheric turbulent conditions. The effect of pointing error on system BER performance is also carried out. Further analysis is also carried out to mitigate the fading due to atmospheric turbulence by applying aperture averaging technique. Thirdly, a novel analytical model is developed to evaluate the output SCNR and average BER for Space Frequency Block Coded non-Hermitian coherent-optical OFDM DQPSK FSO system with polarization diversity under turbulent atmospheric conditions. For a given BER, the SFBC coding gain is also numerically determined. Fourthly, the analysis is extended to compare the coding gain of SFBC with STBC for the same system parameters. Results are compared in terms of SCNR, BER, power penalty and receiver sensitivity. Finally, the numerically evaluated performance results for different system and channel parameters are validated by numerical simulations. Optimum system design parameters are also determined. The results of this dissertation may be used for the future development of FSO communication systems.

Contents

List of Tables

List of Figures

List of Symbols

A_o	Fraction of the collected power
A	Aperture Averaging Factor
B	Receiver bandwidth
C_n	Refractive index structure parameter
D	Receiver aperture diameter
E	Electron charge
f_c	Carrier frequency
G	Mean gain of APD
$g(t)$	Pulse shape
$h(t)$	Channel impulse response
h_{mn}	Normalized fading channel coefficient
I_0	Modified Bessel function of zero order
I	Received optical signal irradiance
I_b	Background radiation intensity
i_{sig}	Signal current
$i_d(t)$	Output current of the photodetector
k_x	Wave number
K	Boltzmann constant
θ_m	Mean angular misalignment angle
L	Link distance in meter
ε_X	Complex fading coefficient
ε_F	Complex crosstalk coefficient
M_T	Number of transmitters
M_R	Number of receivers
N	Number of OFDM Subcarrier
$n(t)$	Represent the photodetector shot noise, preamplifier thermal noise and zero mean Gaussian noise with variance σ_n^2
P_T	Average transmitted optical power

P_r	Average received optical power
P_{LO}	Power of the local oscillator
P_b	Background radiation power
φ_n	Complex orthonormal waveform
$f(I)$	Probability density function of channel irradiance, I
R_b	Bit rate/data rate
R_d	Detector responsivity
R_L	Load resistance of the receiver
R_C	Code rate
R	Detector aperture radius
$s(t)$	Output optically coded signal
T	Receiver Temperature in Kelvin
T_s	Symbol duration
T_b	Bit period
Λ	Wave length
Ω	Resistance in ohms
σ_I^2	Rytov variance
σ_S^2	Jitter variance
SI	Scintillation Index
Z	Distance of wave propagation from the transmitter
A	Effective numbers of large-scale eddies
B	Effective numbers of small-scale eddies
γ	Ratio between the equivalent beam width and the pointing error standard deviation.
Λ	Wave length
E	Normalized timing error
ω_c	Angular optical carrier frequency
ω_{eff}	Effective beam waist
ω_{zeq}	Equivalent beam width
ρ_0	Coherence length

List of Abbreviations and Acronyms

APD	Avalanche Photo Diode
ASE	Amplified Spontaneous Emission
AWGN	Additive White Gaussian Noise
BER	Bit Error Rate
BPSK	Binary Phase Shift Keying
CP	Cyclic Prefix
CO-OFDM	Coherent Optical Orthogonal Frequency Division Modulation
DDMZI	Dual Drive Mach Zehnder Interferometer
DQPSK	Differential Quadrature Phase Shift Keying
DSP	Digital Signal Processor
ECC	Error Control Coding
EGC	Equal Gain Combining
FEC	Forward Error Correction
FSK	Frequency Shift Keying
FSO	Free-Space Optical
FWM	Four-Wave Mixing
IFFT	Inverse Fast Fourier Transformation
IM/DD	Intensity Modulation Direct Detection
I/Q	In-phase/Quadrature
LAN	Local Area Network
LASER	Light Amplification by Stimulated Emission of Radiation
LD	Laser Diode
LED	Light Emitting Diode
LOS	Line of Sight
LO	Local Oscillator
LPF	Low Pass Filter
LQPCM	Linear Quantized Pulse Code Modulation
MIMO	Multiple Input Multiple Output
MISO	Multiple Input Single Output
MRC	Maximal Ratio Combining

MZI	Mach Zehnder Interferometer
NLOS	Non-Line of Sight
OCDMA	Optical Code Division Multiple Access
OFC	Optical Fiber Communication
OFDM	Orthogonal Frequency Division Multiplexing
OOK	On-off Keying
OPPM	Optical Pulse Position Modulation
PAPR	Peak to Average Power Ratio
PBC	Polarized Beam Combiner
PBS	Polarized Beam Spilliter
PDF	Probability Density Function
PE	Pointing Error
PPM	Pulse Position Modulation
P/S	Parallel to Serial
RF	Radio Frequency
RIC	Real Imaginary Combiner
RIS	Real Imaginary Separator
SCNR	Signal to Crosstalk plus Noise Ratio
SE	Selection Combining
SFBC	Space Frequency Block Coding
SISO	Single Input Single Output
SI	Scintillation Index
SIMO	Single Input Multiple Output
SNCR	Signal to Noise plus Crosstalk Ratio
SNR	Signal to Noise Ratio
S/P	Serial to Parallel
STBC	Space Time Block Coding
WDM	Wavelength Division Multiplexing

Chapter 1

INTRODUCTION

Chapter-1

INTRODUCTION

1.1   Introduction

Free-space optical communication (FSO) or better still, laser communication is an optical point to point communication technology that uses light propagating in free space (means air, outer space, vacuum etc.) to wirelessly transmit data or information for telecommunication or computer networking. FSO communication has emerged as an alternative to RF and Microwave (MW) communications due to its inherent merits of license free bandwidth and lower hardware cost. FSO communication technology is useful for metropolitan area network where the physical connections such as optical fiber cable are impractical due to high cost or other considerations. FSO transmits invisible, eye-safe light beams from one telescope to other telescope using low power infrared lasers in the terahertz spectrum. The transmitted laser light focused on highly sensitive photodetector receivers and from the photodetectors currents, the transmitted information are carried out. FSO systems can function over a distance of several kilometers as long as there is a clear line of sight (LOS) between the source and the destination. The data transmission rate, range, and reliability of free-space optical communication (FSO) systems are affected by a number of atmospheric phenomena such as rain, haze, cloud, fog, snow, and pointing errors due to building sway, earthquake, etc. result is loss of alignment between transmitter and receiver. Thick fog with over 300 dB/km of attenuation limits the link length to around 100 m. Even under clear air conditions with no atmospheric scattering, the FSO communication link still suffers from fading due to scintillation. Scintillation fade margins are 2 to 5 dB for FSO links of 500 meters or less, which is well below margins for the atmospheric attenuation. For the link range beyond 1 km, scintillation may cause severe impact on the performance of FSO links, thus resulting in the link deterioration, i.e., higher outage probability and ultimately complete link failure.

1.2 Literature Review

Free Space Optical (FSO) communication is a very promising technology for the broadband optical and tactical military communications networks due to its large bandwidth, unlicensed spectrum, high transmission security, high bit rates, require less power, full duplex communication and simple and quick deploy ability and lower setup cost [1-6]. The performance of the free space optical communication systems can be severely limited by its only real data transmission, misalignments between the transmitter and receiver and atmospheric turbulences which cause intensity fluctuations of the received signal and degrade the bit error rate performance significantly [7-12].

In FSO communication, it is very essential to maintain constant line of sight connection between transmitter and receiver for perfect reception of transmitting information. A slight misalignment can lead to failure of FSO link. Due to some unavoidable phenomenon like earthquake, building sway, dynamic load thermal expansion etc. the alignment between transmitter and receiver is distorted results in pointing error. Some authors reported [13-18] the effect of pointing error on terrestrial FSO link performance. The refractive index fluctuation due to the change of temperature, which results in atmospheric turbulence, also limits the performance of terrestrial FSO link. Atmospheric turbulence is classified into weak, moderate and strong turbulence. Analysis of atmospheric turbulence has been carried out by a number of researchers and several theoretical models have been developed to characterize its behavior. The simplest and most widely reported model is the log-normal turbulence, which is mathematically convenient and tractable [8, 19-24]. The log-normal model is based on the Rytov approximation, which requires the unperturbed phase gradient to be large, compared to the magnitude of the scattering field wave [20, 21, 25, 26]. However, the log-normal model only covers the weak turbulence regime with a single scattering event. For turbulence in the saturation regime with multiple scatterings, the lognormal model becomes invalid [23, 27-29]. The strength of turbulence can be described by the log intensity variance and the range of value for lognormal model is less than 1.2 [23, 24, 26].

For describing the turbulence strength, another important parameter called scintillation index (*S.I.*), which is the log intensity variance normalized by the square of the mean

irradiance. In [29], the author reported that the scintillation index does not only saturate, but also decreases after it reaches the maximum value while the strength of turbulence continues rising. In [1], Andrews et al first proposed Gamma-Gamma model valid for all turbulence regimes based on the assumption that the laser beam propagating through the turbulent medium consists of refraction and scattering effects. For saturation regime, many researchers considered the negative exponential model to describe the signal fluctuations [1, 27, 29, 30].

In order to extend the FSO system's reliability, different fading mitigation techniques such as spatial diversity [31], adaptive optics [32], aperture averaging [33], saturated optical amplifiers [34], modulation techniques and coding [20, 27] are used. The diversity techniques comprising space, time, frequency and polarization have been adapted to improve impairments in performance due to the atmospheric turbulence. To ensure the maximum power efficiency, the types of modulation schemes in FSO systems are very crucial. Amplitude shift keying (ASK), phase shift keying (PSK), quadrature phase shift keying (QPSK), differential quadrature phase shift keying (DQPSK) and polarization shift keying (PolSK) are the most common modulation formats adopted for FSO communication systems. On-off keying (OOK) format is the simplest and most widely used scheme but it is highly sensitive to the atmospheric turbulence [20, 27, 35].

Orthogonal frequency division multiplexing (OFDM) is one of the most popular techniques for broadband wireless communications and is known for its increased robustness against frequency selective fading, narrow-band interference, and high channel efficiency [36-41]. In [36], the author reported that the OFDM signal after Inverse Fast Fourier Transform (IFFT) is complex and bipolar, while in IM/DD optical link, a real and positive RF signal is required to drive the laser diode [36]. In [37], the idea of transmitting the real and imaginary parts of a complex-valued OFDM signal separately via two chips of a RGB-LED is mentioned. For optical communication, OFDM can be considered as special case of multiple subcarrier modulation, where multiple independent bit streams are modulated onto subcarriers at different frequencies, multiplexed in the RF domain and transmitted over free space using intensity modulation direct detection (IM/DD) scheme [42-44]. To perform optical DQPSK, signal transmission format is realized by an optical modulator consisting

of nested Mach- Zehnder interferometer (MZI), which consists of two MZIs for optical in-phase and quadrature phase components [45-47]. DD-MZI is robust against a laser chirp and provides high spectral efficiency [46]. In [48], the authors used balanced photodetector circuit for optical DQPSK demodulation, where the small change in phase of the optical carrier is detected perfectly.

Various research works on FSO considered the polarization state of the light beam to be stable and the effect of cross polarization due to atmospheric turbulence is not taken into account [49, 50-52]. The experimental results showed that the state of polarizations (SOPs) for an optical beam propagating over a long turbulence channel were maintained, which proved that the SOPs were the most stable properties compared with the amplitude and phase and also reported that polarization shift keying modulation scheme is considered to reduce the laser phase noise [53, 54]. In [55], the authors reported the effect of polarization on the performance of an FSO link in terms of degradation in signal to noise ratio considering Gaussian distribution of phase fluctuation in presence of atmospheric turbulence. In case of optical fiber transmission, the effect of cross polarization induced crosstalk on the BER performance of a PDM-QPSK coherent homodyne transmission system is also reported [56].

Different coding techniques have already been utilized with FSO communication system under the presence of atmospheric turbulence to mitigate the fading due to imperfect channel estimation. Space-time block coding can effectively be used with OFDM in non-flat fading channels [57-59]. In order to utilize the diversities in frequency and space, different forms of space-frequency coded OFDM, such as space-frequency block coded OFDM (SFBC-OFDM) have also been proposed and evaluated [60-65]. It is also reported that SFBC not yet been proposed for free space optical communication system to reduce the fading effect due to the presence of atmospheric turbulence.

1.3   Research Motivation

During the last two decades, free space optical (FSO) communications system have been getting research interest due to its unlicensed frequency spectrum, very high data rate and ease of connectivity. The use of FSO communication is increasing day by day to mitigate

the public increasing demand of high data rate which is the motivating force behind research in this field. For a number of applications, the FSO technology presents many advantages over RF spectrum. Such an advantage is the immunity of FSO to the electromagnetic interference, thus making it the preferred option in certain applications where there is a requirement for a very low level of interference or no interference at all [66-70]. Another advantage offered by FSO over RF is the increased security owing to the laser's narrow beam, which makes detection, interception and jamming very difficult. Nowadays, FSO is widely used for both short distance and long-distance communication such as near-ground radio-frequency wireless short-distance connections and in satellite communications which is long distance communication. To enhance the capacity and performance of FSO communication system, different coding technology like space time block coding (STBC) [34, 35, 37], forward error control (FEC) coding such as low-density parity check (LDPC) coding [71-74], turbo coding [75-77], convolutional coding [78, 79], Reed Solomon coding [80, 81] etc. has already been reported by several researchers. In this thesis, we proposed space frequency block coding technology to improve the existing performance of FSO communication system.

1.4 Objectives of the Research

The main objective of this thesis is to analyze the performance of a Non-Hermitian OFDM FSO system followed by DQPSK modulation considering space frequency block code and polarization diversity over atmospheric turbulent channel. Some objectives of this thesis are -

i. To develop the analytical model to evaluate the performance of OFDM optical DQPSK FSO system with polarization diversity to evaluate the SNR and BER performance considering the effect of turbulence.

ii. To develop an OFDM FSO System with Space Frequency Block coding (SFBC) and to analyze the system performance in presence of atmospheric turbulence. To extend the analytical development to evaluate the performance of OFDM SFBC system with polarization diversity over turbulent channel.

iii. To extend the analytical development to compare the performance between SFBC OFDM system with polarization diversity and STBC OFDM system with polarization diversity.

1.5   Background History of FSO Communication

Around 800 BC, ancients Greeks and Romans used fire beacons for signaling and by 150 BC the American Indians were using smoke signals for the same purpose of signaling. During the years 1790─1794, an optical telegraph based on a chain of semaphores was used by French naval navigators. But what can be termed the first optical communication in an unguided channel was the 'photo-phone' experiment by Alexander Graham Bell in 1880 [82-84]. In his experiment, Bell modulated the Sun radiation with voice signal and transmitted it over a distance of about 200 meters. The receiver was made of a parabolic mirror with a selenium cell at its focal point. However, the experiment did not go very well because of the crudity of the devices used and the intermittent nature of the sun radiation.

During 1935-1940, a several number of experiments have been carried out using modulated electric light sources for transmitting information by the Australian, German and Japanese armies. The technology used in those experiments was obtained from the recording of optical sound tracks on the motion picture film. In the early 1930s Mr. Sony, who established the Sony Corporation in Japan, carried out research that involved prototyping a modulated light communication system. These systems provided the military with the high directivity and a high security before the microwave hardware became available [84, 85]. During the Second World War, an infrared optical telegraph was developed to ensure a secure data transmission link. However, difficulties in inserting the technology in operational systems were greater than envisioned by the early pioneers due to: 1) accurate pointing and tracking systems were not available; and 2) the optical components were unreliable and needed improving [86].

The fortune of FSO changed in the 1960s with the discovery of optical sources, most importantly, the laser. A flurry of FSO demonstrations was recorded in the early 1960s into 1970s. Some of these included the: spectacular transmission of television signal over a 30-mile (48 km) distance using a GaAs light emitting diode by researchers working in the MIT Lincolns Laboratory in 1962 [86]; a record 118 miles (190 km) transmission of voice modulated He-Ne laser between Panamint Ridge and San Gabriel Mountain, USA in May 1963 [86]; and the first TV-over-laser demonstration in March 1963 by a group of researchers working in the North American Aviation [86]. The first laser link to handle

commercial traffic was built in Japan by the Nippon Electric Company (NEC) around 1970. The link was a full duplex 0.6328μm He-Ne laser FSO between Yokohama and Tamagawa, a distance of 14 km [86]. In the same year the demonstration of the first semiconductor laser that required no cooling, but could be operated at the room temperature, was reported by Hayashi *et al*. [87]. From here onwards, FSO communications we have seen a rapid development in FSO communication in both commercial and military operations.

FSO has also been heavily researched for deep space applications by NASA and ESA with programs such as the then Mars Laser Communication Demonstration (MLCD) and the Semiconductor-laser Inter-satellite Link Experiment (SILEX) respectively [88]. In spite of early knowledge of the necessary techniques to build an operational laser communication system, the usefulness and practicality of a laser communication system was until recently questionable for many reasons [86]. First, existing communications systems were adequate to handle the demands of the time. Second, considerable research and development were required to improve the reliability of components to assure reliable system operation. Third, a system in the atmosphere would always be subject to interruption in the presence of heavy fog. Fourth, use of the system in space where atmospheric effects could be neglected required accurate pointing and tracking optical systems which were not then available. In view of these problems, it is not surprising that until now, FSO had to endure a slow penetration into the access network.

With the rapid development and maturity of optoelectronic devices, FSO has now witnessed a re-birth. Several successful field trials have been recorded in the last few years in various parts of the world which have further encouraged investments in the field [89]. This has now culminated into the increased commercialization and the deployment of FSO in today's communication infrastructures. At the present time, as a method of exploiting more bandwidth and utilizing the broad array of new services, FSO technology is seen as a cost-effective method to solve the high-bandwidth bridge (the "last mile") [36, 90, 91]. FSO applications, in both military and civilian fields in particular the access network, have been reported in the last few years in various parts of the world [92-97]. For example, the FSO technology was successfully used to continually transmit the image between the Waterhouse Centre and the studio during the Sydney Olympic Games in 2000 [98]. As a

commercially complementary technology to the radio frequency (RF) (in the range of about 3 kHz to 30 GHz) and the millimeter-wave (30 GHz to 300 GHz) wireless systems, FSO has now emerged as a commercially viable complementary technology to radio frequency (RF) and millimeter wave wireless systems for reliable and rapid deployment of data, voice and video within the access networks [99-101]. RF and millimeter wave based wireless networks can offer data rates from tens of Mbps (point-to-multipoint) up to several hundred Mbps (point-to-point). However, there is a limitation to their market penetration due to spectrum congestion, licensing issues and interference from unlicensed bands [102-104]. The future emerging license-free bands are promising, but still have certain bandwidth and range limitations compared to the FSO [105]. The short-range FSO links are used as an alternative to the RF links for the last or first mile to provide broadband access network to homes and offices as well as a high bandwidth bridge between the local and wide area networks. In 2008, the first 10 Gbps FSO system was introduced to the market, making it the highest-speed commercially available wireless technology [106]. Efforts is continuing to further increase the capacity via integrated FSO/fiber communication system and wavelength division multiplexed (WDM) FSO system which is currently at experimental stages [107-109].

The earlier skepticism about FSO's efficacy, its shrinking acceptability by service providers and slow market penetration are now rapidly fading away judging by the number of service providers, organizations, government and private establishments that now incorporate FSO into their network infrastructure [110]. Terrestrial FSO has now proven to be a viable complementary technology in addressing the contemporary communication challenges, most especially the bandwidth/high data rate requirements of end users at an affordable cost [111]. The fact that FSO is transparent to traffic type and data protocol makes its integration into the existing access network far more rapid. Nonetheless, the atmospheric channel effects such as thick fog, smoke and turbulence as well as the attainment of 99.999% availability still pose the greatest challenges to long range terrestrial FSO [87, 110, 112].

1.6   FSO Communication System's Features, Limitations and Applications

Some features of FSO communication systems are as follows-

i. **Very high bandwidth:** The frequency range of an optical carrier spans from 10^{12} Hz to 2000 THz data bandwidth. Since the amount of data transmitted is directly related to the bandwidth of the carrier, FSO communication allows 10^5 times greater information capacity compared to the RF technology [19, 36, 49].

ii. **Unlicensed spectrum:** The spectrum of RF frequencies is very congested and almost saturated. So, it is now very difficult and expensive to allocate additional RF frequencies because of the variations in the regulatory authorities in different countries, such as the Office of Communications (OfCom) in the UK and the Federal Communications Commission (FCC) in the USA. On the other hand, FSO technology offers license-free spectrum and shorter deployment time [113-115].

iii. **Cost-effective:** For similar data rate, the development cost of FSO links is much lower than that of an RF system. No additional cost of trenching and right of way is required for FSO to deliver a comparable bandwidth to optical fiber [101, 110, 112].

iv. **Narrow beam size:** A typical laser beam has a diffraction limited divergence in between 0.01 to 0.1 mrad [83], which concentrates the optical power within an extremely narrow area that provides the FSO system adequate spatial isolation from potential interference. Therefore, independent FSO communication systems exist with virtually unlimited degrees of frequency reuse and data interception by unintended users becomes extremely difficult. However, a precise alignment for FSO links is required at the expense of tight beam size [87, 116-118].

v. **Very quick deployment:** FSO technology requires very short time to setup and easily portable. It also only takes a short time to redeploy the FSO link easily to another location [19, 112, 114, 119].

For better performance of an FSO communication link, there might be minimized some challenges like-

i. **Atmospheric turbulence:** Atmospheric turbulence is a random phenomenon which is occurred due to the random variations of temperature and pressure of the atmosphere along the propagation path of the transmitted light beam. The performance of an FSO link is limited by atmospheric turbulences which deteriorated the amplitude and phase of the transmitted light signal.

ii. **Absorption and scattering:** The atmospheric absorption and scattering is a wavelength dependent phenomenon. When the laser light propagates through the atmosphere, it interacts with various molecules (like water molecule, carbon-dioxide, ozone etc.) [120, 121] and aerosol particles presents in the atmosphere which results in absorption and scattering loss and it is described by Beer's law [122].

iii. **Beam divergence:** Due to diffraction, a beam divergence is caused near the receiver aperture. So, some fraction of light beam is not collected by the receiver, which is called beam divergence loss or geometric loss [25].

iv. **Background noise and sky radiance:** The main sources of background noise are: i) diffused extended noise from the atmosphere, ii) the sun and other stellar objects and iii) scattered light collected by the receiver [13, 123].

v. **Pointing error:** In FSO communication, it is very essential to maintain a constant line of sight connection between transmitter and receiver. A slight misalignment can lead to failure of FSO link. So, the beam used is highly directional and consider a very narrow beam divergence. Pointing error may occur for various reason like- building sway, earthquake, dynamic load of the mechanical system etc. [14-18, 124]. Pointing error may also be caused for beam wander variance due to atmospheric turbulence [125].

Several numbers of typical applications of the FSO technology are discuss below-

i. **Last mile access:** The FSO technology can be used to communicate between the end users and the fiber optics backbone and overcome the last mile bottleneck problem [126].

ii.   **Multi-campus communication network:** FSO technology can provides as a back-up links for multi-campus communication at Gigabit or Fast- Ethernet speeds [113-115].

iii.   **In hospital:** FSO technology can be used in hospital for communicate with doctors for emergency [127].

iv.   **Cellular communication back-haul:** To carry traffic between base station and switching centers in 3G/4G networks and also transport the IS-95 code division multiple access (CDMA) signals from micro- and macro- cell sites to the base stations [110].

v.   **Back up to optical fiber link:** FSO technology can be considered as a back-up in circumstances where the communication link is down or unavailable [110, 113, 116].

vi.   **Disaster recovery/temporary links:** FSO system can be used for disaster recovery [114, 116, 119].

vii.   **Difficult terrains:** Where the right of way is unavailable or too expensive such as across rivers, in the inner city and across rail tracks etc. [101, 128].

viii.   **HDTV:** FSO technology is used to broadcast live high-definition signals in remote locations to the central office [19, 36, 87].

1.7 Outline of the Dissertation

This dissertation consists of total six chapters.

Chapter 1 is concentrated on the purpose and present state of FSO communication system and importance of FSO communication system.

A detail analytical expression of output current, signal to noise ratio and bit error rate of a non-Hermitian coherent-optical OFDM FSO communication system followed by DQPSK modulation is provided in Chapter 2. The effect of pointing error on BER performance of the system is also shown in this chapter.

In Chapter 3, the analysis is extended by considering polarization diversity and the effect of cross polarization induced crosstalk on FSO system's BER performance is determined and shown.

A detail illustration of SFBC for FSO communication system is provided in Chapter 4.

The bit error rate performance of SFBC is compared with STBC and the comparative results are provided in Chapter 5.

Finally, concluding remarks and some proposals for future works are given in Chapter 6.

Chapter 2

NON-HERMITIAN OFDM FSO SYSTEMS

Chapter-2

NON-HERMITIAN OFDM FSO SYSTEMS

2.1 Introduction

For free space optical (FSO) communication system, only real valued signal can be transmitted. In OFDM based optical communication system, Hermitian symmetry is generally imposed before performing the inverse fast Fourier transforms (IFFT) so as to generate LED/LASER compatible real valued signal. However, the constraint of Hermitian symmetry doubles the sizes of the IFFT and FFT, resulting in the increase of the transceiver complexity. To avoid this complexity, non-Hermitian OFDM is proposed and analyzed in this chapter.

2.2 Differential QPSK (DQPSK) Modulation

In DQPSK modulation, the information bits are encoded as the phase change from one symbol period to the next rather than an absolute phase. At the receiver end, the phase change is detected rather than absolute phase which avoids the need for synchronized local carrier. The resultant transmitted signal can be represented as-

$$x(t) = A\cos\{2\pi f_c t + \theta(k)\}; \qquad kT \leq t \leq (k+1)T \tag{2.1}$$

$$where, k = 1:4 \quad and$$

$$\theta(k) - \theta(k-1) = \begin{cases} \pi & if \quad (I(k), Q(k)) = (0,0) \\ 3\pi/2 & if \quad (I(k), Q(k)) = (1,0) \\ 0 & if \quad (I(k), Q(k)) = (1,1) \\ \pi/2 & if \quad (I(k), Q(k)) = (0,1) \end{cases}$$

A DQPSK transmitter includes a DQPSK modulator, two modulator drivers and a precoder. The mapping from new input bits to the carrier phase change can be achieved by a precoder which maps the input bits to a new set of bits as follows-
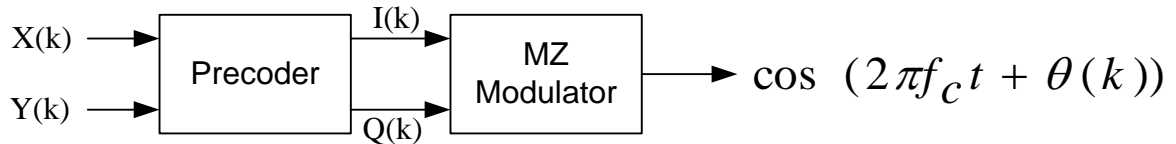
Fig. 2.1: DQPSK Transmitter

The precoder current outputs (I(k), Q(k)) are a function of the current inputs (X(k), Y(k)) and previous outputs (I(k-1), Q(k-1)) of the precoder. The truth table of the precoder is given in Table-2.1 and the precoder mapping from input symbol (X(k), Y(k)) to symbol (I(k), Q(k)) is shown in Table-2.2.

Table-2.1: Truth table for the precoder

X(k)	Y(k)	I(k)	Q(k)
0	0	$\overline{I(k-1)}$	$\overline{Q(k-1)}$
0	1	$\overline{Q(k-1)}$	I(k-1)
1	0	Q(k-1)	$\overline{I(k-1)}$
1	1	I(k-1)	Q(k-1)

Table-2.2: Mapping of the differential encoder and the modulator

Current Input		Previous Precoder Output		Previous Modulator Phase	Current Precoder Output		Current Modulator Phase	Modulator Phase Change
X(k)	Y(k)	I(k-1)	Q(k-1)	θ(k-1)	I(k)	Q(k)	θ(k)	Δθ
0	0	0	0	45	1	1	225	180
0	0	0	1	315	1	0	135	180
0	0	1	0	135	0	1	315	180
0	0	1	1	225	0	0	45	180
0	1	0	0	45	1	0	135	90
0	1	0	1	315	0	0	45	90
0	1	1	0	135	1	1	225	90
0	1	1	1	225	0	1	315	90
1	0	0	0	45	0	1	315	270
1	0	0	1	315	1	1	225	270
1	0	1	0	135	0	0	45	270
1	0	1	1	225	1	0	135	270
1	1	0	0	45	0	0	45	0
1	1	0	1	315	0	1	315	0
1	1	1	0	135	1	0	135	0
1	1	1	1	225	1	1	225	0

An optical demodulator with balance photodetectors circuit can demodulate the DQPSK signal without the need for local carrier shown in Fig. 2.2.
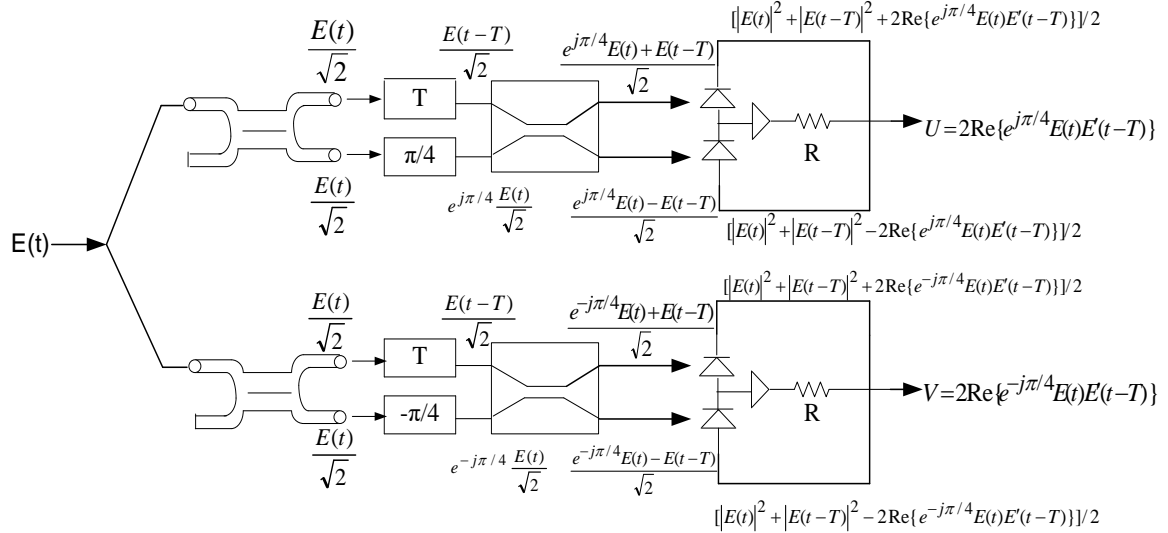
Fig. 2.2: DQPSK optical demodulator with balance photodetectors.

E is the received electric field which is phase modulated. The two outputs from the optical coupler are the sum and difference of the input signals. The resultant differential photodetectors outputs U and V are a function of the phase difference of the input signal E.

$$
\begin{aligned}
U &= \mathrm{Re}\{e^{j\pi/4}E(t)E'(t-T)\} = \mathrm{Re}\{e^{j\pi/4}e^{j\theta(k)}e^{-j\theta(k-1)}\} \\
&= \mathrm{Re}\{e^{j\pi/4}e^{j(\theta(k)-\theta(k-1))}\} = \cos(\pi/4 + \Delta\theta) \\
V &= \mathrm{Re}\{e^{-j\pi/4}E(t)E'(t-T)\} = \mathrm{Re}\{e^{-j\pi/4}e^{j\theta(k)}e^{-j\theta(k-1)}\} \\
&= \mathrm{Re}\{e^{-j\pi/4}e^{j(\theta(k)-\theta(k-1))}\} = \cos(-\pi/4 + \Delta\theta) = \sin(\pi/4 + \Delta\theta)
\end{aligned}
\tag{2.2}
$$

By using the values of *U* and *V*, we can map the transmitted input bit stream as shown in Table-2.3.

Table-2.3: Receiver mapping of phase change to bits

$\Delta\theta$	U	V	Logic(U)=X	Logic(V)=Y
0	$1/\sqrt{2}$	$1/\sqrt{2}$	1	1
$\pi/2$	$-1/\sqrt{2}$	$1/\sqrt{2}$	0	1
π	$-1/\sqrt{2}$	$-1/\sqrt{2}$	0	0
$3\pi/2$	$1/\sqrt{2}$	$-1/\sqrt{2}$	1	0

2.3 Orthogonal Frequency Division Modulation (OFDM)

In OFDM the subcarrier frequencies are chosen so that the signals are mathematically orthogonal over one OFDM symbol period. Modulation is achieved digitally using an inverse fast Fourier transform (IFFT) and as a result, the required orthogonal signals can be generated precisely and in a very computationally efficient way. In FDM/WDM there are frequency guard bands between the subcarriers. At the receiver the individual subcarriers are recovered using analog filtering techniques. Fig. 2.3 shows spectra for FDM/WDM and OFDM.
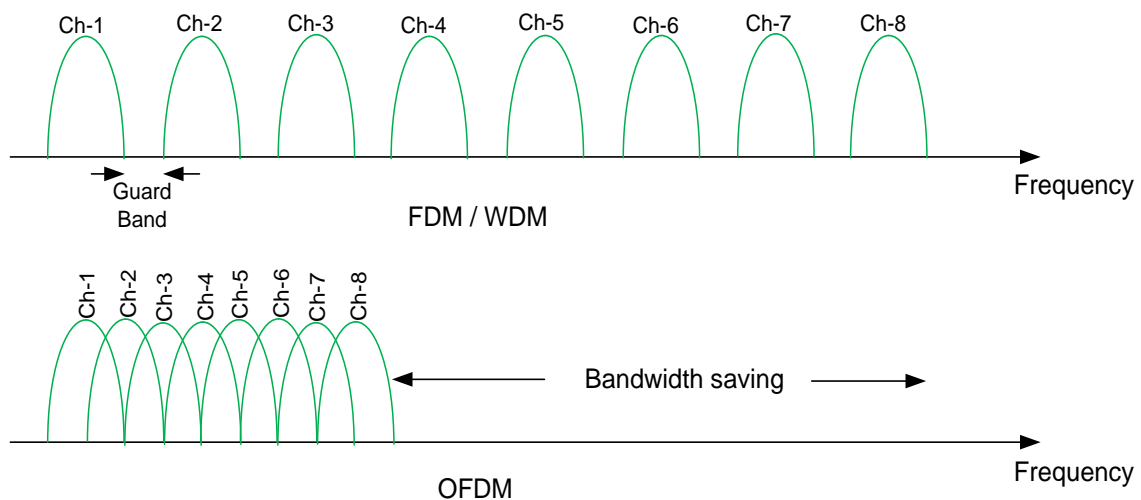
Fig. 2.3: Spectral efficiency of OFDM compare to conventional FDM

In OFDM the spectra of individual subcarriers overlap, but because of the orthogonality property, as long as the channel is linear, the subcarriers can be demodulated without interference and without the need for analog filtering to separate the received subcarriers. Demodulation is performed by a fast Fourier transform (FFT). In Fig. 2.4, the block diagram representation of OFDM modulator and demodulator are shown.
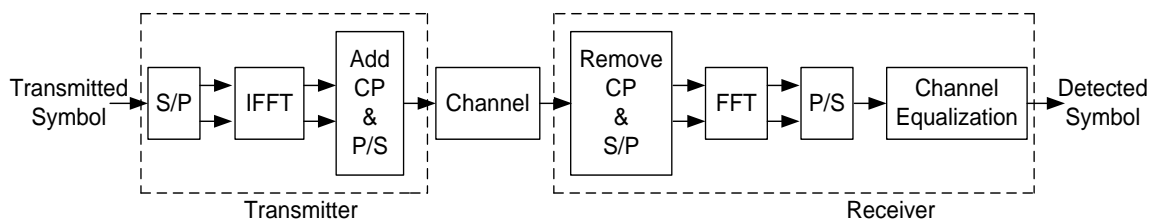
Fig. 2.4: Basic block diagram of OFDM

As the IFFT block is the main component in the transmitter and the FFT in the receiver, and these are the functions which distinguish OFDM from single carrier systems. Let X(m) be the complex number representing the constellation point on the *m*th subcarrier of a given symbol. Then the baseband time domain samples for that symbol are given by x(k)-

$$x(k) = \frac{1}{N}\sum_{m=0}^{N-1} X(m)\, e^{\frac{j2\pi km}{N}} \qquad ; \qquad 0 \le k \le N-1 \tag{2.3}$$

where, and N is the size of the IFFT. The forward FFT corresponding to (2.3) is-

$$X(m) = \frac{1}{N}\sum_{k=0}^{N-1} x(k)\, e^{\frac{-j2\pi km}{N}} \qquad ; \qquad 0 \le m \le N-1 \tag{2.4}$$

In most OFDM systems, a cyclic prefix (CP) is added to the start of each time domain OFDM symbol before transmission. In other words, a number of samples from the end of the symbol are appended to the start of the symbol. Although the CP introduces some redundancy, and reduces the overall data rate, the use of the CP eliminates both inter symbol interference (ISI) and inter carrier interference (ICI) from the received signal and is the key to simple equalization in OFDM. Fig.2.5 shows the time domain sequence of OFDM symbols.
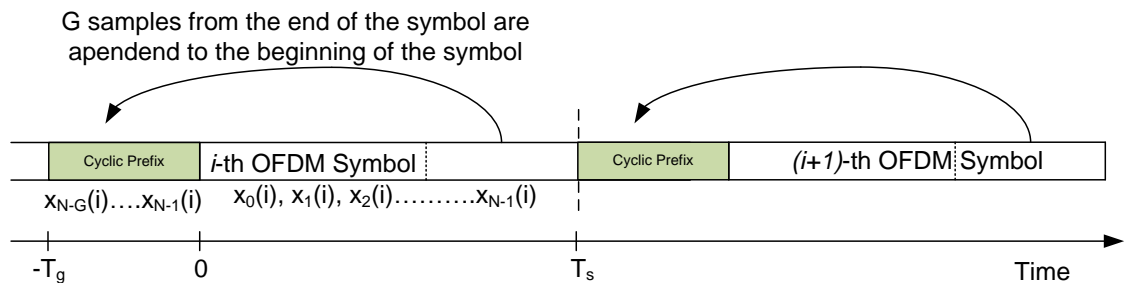
Fig. 2.5: Time domain sequence of OFDM symbols showing the cyclic prefix [129].

2.4 Non-Hermitian OFDM

A block diagram representation of a non-Hermitian OFDM FSO system is shown in Fig. 2.6. In the transmitter part the serial data are converted to parallel first which are then fed into IFFT block. After performing IFFT, a cyclic prefix (CP) is added and the resultant

signal is converted into parallel to serial. As no Hermitian symmetry is imposed before IFFT operation, so the resultant signal is complex valued. Now, to get real valued signals, a real-imaginary separator (RIS) is used to separate *Re* part and *Im* part of the complex-valued signal. The digital real and imaginary data are digital-to-analog converted and then transmit through the atmospheric channel using two separate laser sources. At the receiver end, the analog data is first converted to digital and then using a real-imaginary combiner (RIC) to generate complex-valued signal. The serial data is converted to parallel and then remove the CP. After FFT operation the parallel data is serial converted and finally get the desired output signal.
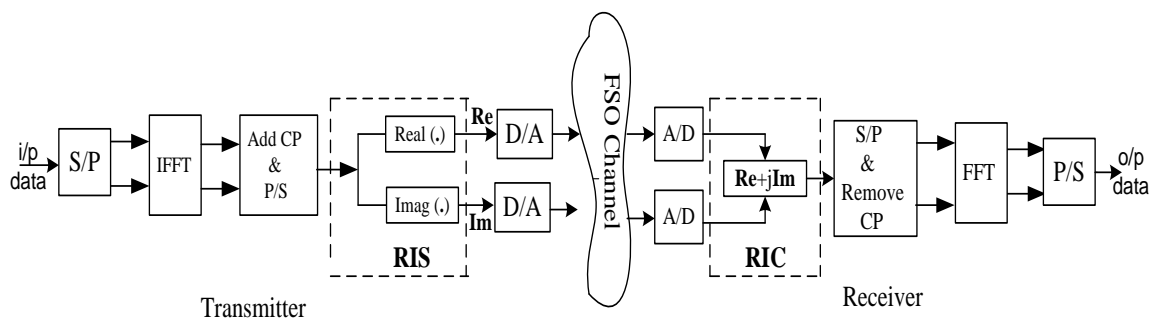
Fig 2.6: Block diagram representation of Non-Hermitian OFDM transmitter and receiver [130].

2.5 FSO Transmission Channels

FSO links contain the transmission, absorption and scattering of light by the atmosphere. Under normal conditions, the atmosphere has variety of different molecules and small suspended particles (aerosols) which interacts with light. This interaction produces a wide variety of optical phenomena such as selective attenuation of radiation, absorption at specific optical wavelengths due to the molecules, scattering due to the sky-blue color, the red sunset, radiative emission of an optical beam etc., and scintillation due to the variation of the air's refractive index under the effect of temperature and pressure.

The performance of any opt-electronic system depends not only on its intrinsic design features resulting from its design and the technology used, but also on its behavior in its operational environment. However, the construction of such a system, made up of a transmitter and a receiver in free atmosphere, necessitates proper knowledge of specific optical properties of the atmosphere. Scattering and absorption of the radiation from the

medium affect spectral transmission of the propagation medium. Therefore, it is useful to know how opt-electronic systems behave in differing climatic and weather conditions and particularly under prevailing environmental conditions.

2.5.1 Atmospheric turbulence

Atmospheric turbulence results in random fluctuation of the atmospheric refractive index along the path of the optical beam traversing the atmosphere. This refractive index fluctuation is the direct end product of random variations in atmospheric temperature [131]. These random temperature changes are a function of the atmospheric pressure, altitude and wind speed. The relationship between the temperature of the atmosphere and its refractive index is given by [132]-

$$\eta = 1 + 77.6(1 + 7.52 \times 10^{-3} \lambda^{-2}) \frac{P}{T_e} \times 10^{-6} \tag{2.5}$$

where, P is the atmospheric pressure in mbar, T_e is the temperature in Kelvin and λ is the wavelength in µm.

And the rate of change in the refractive index with respect to the atmospheric temperature is calculated as-

$$-\frac{d\eta}{dT_e} = 77.6(1 + 7.52 \times 10^{-3} \lambda^{-2}) \frac{P}{T_e^2} \times 10^{-6} \tag{2.6}$$

In homogeneities caused by turbulence can be viewed as discrete cells, or eddies of different temperature, acting like refractive prisms of different sizes and indices of refraction. The interaction between the laser beam and the turbulent medium results in random phase and amplitude variations (scintillation) of the information-bearing optical beam which ultimately results in performance degradation of FSO links.

The smallest and the largest of the turbulence eddies are termed the inner scale l_0, and the outer scale L_0, of turbulence respectively. Typically, l_0 is on the order of a few millimeters

while L_0 is on the order of several meters [1, 8]. These weak lens-like eddies shown graphically in Fig. 2.7 result in a randomized interference effect between different regions of the propagating beam causing the wave front to be distorted in the process. Under the influence of the inertial forces, the larger size eddies break up into smaller eddies until the inner scale size l_0 is reached. The family of eddies bounded above by the outer scale L_0 and below by the inner scale l_0 forms the inertial sub-range. The outer scale denotes the scale below which the turbulent properties are independent of the parent flow. Scale size smaller than the inner scale l_0 belongs to the viscous dissipation range. In this range, the turbulent eddies disappear, and the remaining energy is dissipated in the form of heat. This phenomenon is known as Kolmogorov theory [30, 133] shown in Fig. 2.7.
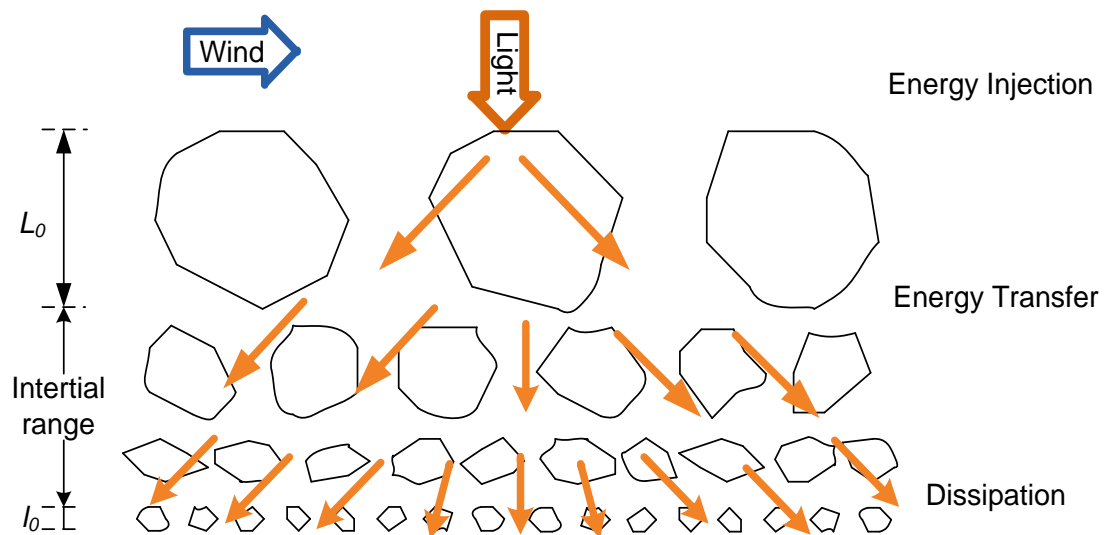
Fig. 2.7: Kolmogorov cascade theory of turbulence eddies

Depending on the size of the turbulent eddies and transmitter beam size, there are three types of atmospheric turbulence effects are observed:

i. **Turbulence-induced beam wander:** Beam wander is a phenomenon which is experienced when the size of turbulence eddies is larger than the beam size. It will result in random deflection of the beam from its propagating path and leads to link failure. Beam wander is a major concern in case of uplink as the beam size is often smaller than the turbulence eddy side and it will result in the beam displacement by several hundred meters. When a collimated beam with W_0

beam size, passing through the atmospheric turbulent channel, the beam wander variance at zero zenith angle is written by [134, 135]-

$$\sigma_{BW}{}^2 = 0.54 L^2 \left(\frac{\lambda}{2W_0}\right)^2 \left(\frac{2W_0}{r_0}\right)^{\frac{5}{3}}$$

(2.7)

where, r_0 is used for atmospheric coherence diameter and its written by-

$$r_0 = \left(0.432 k^2 \int_0^L C_n{}^2(h)dh\right)^{-\frac{3}{5}}$$

(2.8)

ii. **Turbulence-induced beam spreading:** If the eddy size is smaller than the beam size, then a small portion of the beam will be diffracted and scattered independently. This will lead to reduction in the received power density and will also distort the received wave front. However, the effect of turbulence-induced beam spreading will be negligible if the transmitter beam diameter is kept smaller than the coherence length of the atmosphere [136] or if the receiver aperture diameter is kept greater than the size of first Fresnel zone [137].

iii. **Turbulence-induced beam scintillation:** When the eddy size is of the order of beam size, then the eddy will act like lens that will focus and de-focus the incoming beam. This will lead to redistribution of signal energy resulting in temporal and spatial irradiance fluctuations of the received signal [138]. This intensity fluctuation of the received signal is known as scintillation and is the major cause of degradation in the performance of the FSO system.

2.5.2   Atmospheric turbulence models

An atmospheric turbulence channel is called a 'slow fading channel' as it is static during the symbol period. The Rytov variance, σ_l^2 for a plane wave is used as a measure of turbulence strength. It is a variance of log-intensity function, its expression is as [69, 87, 139]-

$$\sigma_l^2 = 1.23 \times C_n^2 \times k^{7/6} \times L^{11/6}$$

(2.9)

where, $C_n{}^2$ represents refractive index structure parameter, k ($=2\pi/\lambda$) represents the wave-number and L is the link distance. To calculate the turbulence, Hufnagel–Velley model is considered usually to find the profile model of $C_n{}^2$ as a function of height, h [69, 140].

$$C_n^2(h) = 0.00594 \left(\frac{w}{27}\right)^2 (10^{-5} h)^{10} \exp\left(-\frac{h}{1000}\right) + 2.7 \times 10^{-16} \exp\left(-\frac{h}{1500}\right)$$
$$+ C_n^2(0) \exp\left(-\frac{h}{1000}\right)$$

(2.10)

$$w = \left[\frac{1}{15 \times 10^3} \int_{5 \times 10^3}^{20 \times 10^3} \left\{w_s h + w_g + 30\exp\left(-\left(\frac{h - 9400}{4800}\right)^2\right)\right\} dh\right]^{\frac{1}{2}}$$

(2.11)

where, w is the rms wind speed, $C_n{}^2(0)$ is the ground level value of $C_n{}^2$, w_s and w_g represents the beam slew rate and ground level wind speed respectively. The typical average value of $C_n{}^2$ is 10^{-15} m$^{-2/3}$ and a range from 10^{-17} m$^{-2/3}$ to 10^{-12} m$^{-2/3}$ corresponds to turbulence regimes from weak to strong, respectively [69].

Depending on the turbulence strength, generally three types of atmospheric turbulence models are used which are as follows-

      a) Log Normal Distribution

      b) Gamma-Gamma Model and

      c) Negative Exponential Model

2.5.2.1 Log- Normal distribution

The atmospheric turbulence impairs the performance of an FSO link by causing the received optical signal to vary randomly thus giving rise to signal fading. The fading strength depends on the link length, the wavelength of the optical radiation and the refractive index structure parameter C_n^2 of the channel. The log-normal distribution is generally used to model the fading associated with the weak atmospheric turbulence regime. This model is mathematically tractable and it is characterized by the Ryotov variance σ_l^2. The turbulence induced fading is termed weak when $\sigma_l^2 < 1$ and this defines the limit of validity of the log-normal model. Beyond the weak turbulence regime, other

models such as the gamma-gamma and the negative exponential will have to be considered. The Ryotov variance σ_l^2 can be calculated by equation (2.9).

The amplitude of the random path gain, $H = e^X$, where X is normal with mean μ_X and variance σ_l^2. Thus, the logarithm of the field amplitude scale factor is normally distributed. The optical intensity $I = H^2$ is also log normally distributed in this case [141]. The probability density function for H is written by-

$$f_H(a) = \frac{1}{\sqrt{2\pi\sigma_l^2}\,a}\exp\left(-\frac{(\log_e a - \mu_x)^2}{2\sigma_l^2}\right), \quad a > 1 \tag{2.12}$$

So that the mean path intensity is unity, such that $E[H^2] = 1$. For the *log-normal* distribution, the scintillation index, defined as-

$$S.I. = \frac{E[H^4]}{E^2[H^2]} - 1 \tag{2.13}$$

This index can be related to the parameter σ_l^2 by S.I. $= e^{4\sigma_l^2} - 1$. Typical values appearing in the literature for S.I. are in the range 0.4–1.0.

2.5.2.2   Gamma-Gamma model

To account the effect of strong atmospheric turbulence, we considered the Gamma-Gamma distribution model for the probability density function of channel irradiance *I,* which is modeled as [7, 8, 87]-

$$P(I) = \frac{2(\alpha\beta)^{(\alpha+\beta)/2}}{\Gamma(\alpha)\Gamma(\beta)} I^{\frac{(\alpha+\beta)}{2}-1} K_{(\alpha-\beta)}(2\sqrt{\alpha\beta I}), I > 0 \tag{2.14}$$

where, *I* is for optical signal intensity, the second kind of the modified Bessel function is represented by $K_{\alpha-\beta}$ where $\alpha-\beta$ is its order and symbol Γ is the gamma function. The small-scale and large-scale eddies are represented by α and β respectively. The expression of α and β are expressed as [87, 139]-

$$\alpha = \left[\exp\left\{ \frac{o.49\sigma_l^2}{(1+1.11\sigma_l^{\frac{12}{5}})^{\frac{7}{6}}} \right\} - 1 \right]^{-1} \quad and \quad \beta = \left[\exp\left\{ \frac{o.51\sigma_l^2}{(1+0.69\sigma_l^{\frac{12}{5}})^{\frac{5}{6}}} \right\} - 1 \right]^{-1} \tag{2.15}$$

where, σ_l^2 represents the Rytov variance. Its expression is as-

$$\sigma_l^2 = 0.5 \times C_n^2 \times k^{7/6} \times L^{11/6} \tag{2.16}$$

The parameters $\alpha > 0$ and $\beta > 0$ are linked to the so–called scintillation index as-

$$S.I = \frac{1}{\alpha} + \frac{1}{\beta} + \frac{1}{\alpha\beta} \tag{2.17}$$

2.5.2.3   Negative exponential model

Negative exponential channel is generally considered under strong irradiance fluctuations. Beyond the saturation regime, the turbulence approaches the limits, also known as the fully developed speckle regime where the link range extends several kilometers and the number of independent scatterings becomes large [88, 142]. The amplitude fluctuation of the field traversing the turbulent medium in this situation is experimentally verified to obey the Rayleigh distribution implying negative exponential statistics for the irradiance which is expressed as [7, 28, 143]-

$$P(I) = \frac{1}{I_0} \exp(-\frac{I}{I_0}) \tag{2.18}$$

Where, I_0 ($I_0 > 0$) is said as the mean irradiance or noise turbulence variance which is often normalized to unity. During the saturation regime, the value of the scintillation index, $S.I.$ $\rightarrow 1$.

2.6   BER Performance of a Non-Hermitian OFDM FSO System Followed by DQPSK Modulation

In this section, an analytical model is described to evaluate the bit error rate (BER) performance of a non-Hermitian OFDM FSO system followed by differential quadrature phase shift keying (DQPSK) modulation. Analysis is presented for an OFDM-DQPSK FSO

link considering an optical receiver based on dual detection optical QPSK demodulator with direct detection. Analytical model is developed to find the expressions for output current and SNR in presence of weak atmospheric turbulence. The conditional bit error rate for a given turbulence induced fading is also derived. Average SNR and BER are obtained considering the turbulence induced fading to be log-normal distribution.

2.6.1 System model

The complete block diagram representation of the proposed non-Hermitian OFDM FSO system is shown in Fig. 2.8. Transmitting part and receiving part are shown in Fig. 1(a) and Fig. 1(b) respectively. Here the serial data input is first put into parallel and then each parallel branch data is QPSK modulated before IFFT operation. After IFFT operation, by adding cyclic prefix (CP) and parallel to serial operation the complex bipolar data is put into a Real Imaginary separator. The separated real and imaginary data is quantized using multi-level quantizer. After that, for optical DQPSK, the quantized digital bit streams change the phase of the continuous wave optical carrier light from laser diode to the DDMZI. Two Mach-Zehnder modulators are required for an optical QPSK modulator which further has a $\pi/2$ phase difference between them [47]. Each of the MZ drivers is biased at its null and driving voltage levels are set so that the carrier phase on each arm shifts by either $+\pi/2$ or $-\pi/2$. In proposed system, we consider low atmospheric turbulence, so we use Log-normal Model for the probability density function of the low atmospheric turbulence. Then the received light is passing through a coupler and then using balanced detection technique to detect carrier phase change due to the change of input bit streams to the DDMZI. The receiver circuit is based on the principle of differential detection. A balanced detection circuit has been designed, where the beam is split into a sense beam and a reference beam and a separate photodiode is used to measure each [48]. The two photocurrents are subtracted and converted to a voltage by a transimpedance amplifier. The sense beam passes through the sample to be measured, whereas the reference beam is unaffected. With no change in sample transmission, the two photocurrents are nulled, a changing transmission produce a differential output voltage.
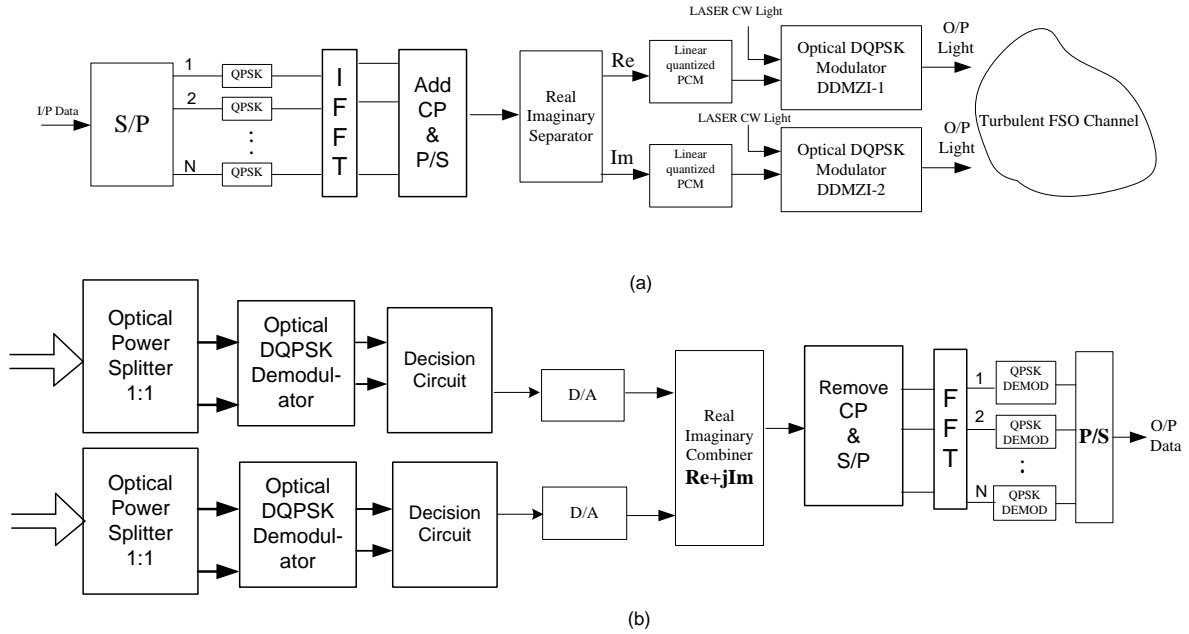
Fig. 2.8: System model of an OFDM-based FSO link: (a) Transmitting part using DDMZI and (b) Receiving part using balanced photodetection circuit.

By using decision circuit, this voltage is used to estimate the transmitted phase, which is then converted to the transmitted symbol. After the decision circuit, the detected carrier phase change converted into digital binary sequences and then de-quantizes the sequences and put them into a real imaginary combiner. After removing CP and serial to parallel operation data streams are put into FFT block and after QPSK demodulation and parallel to serial operation we finally get the output bit streams.

2.6.2 BER analysis

2.6.2.1 Analysis of the transmitted signal

Signal at the output of QPSK modulator can be represented as-

$$s_i(t) = \sqrt{\frac{2E_s}{T_s}}\, a_i \cos\{2\pi f_{rc}t + (2i-1)\pi/4\} \quad ;$$
$$where,\ i = 1:4, \quad for \quad 0 \angle t \angle T_s \tag{2.19}$$

where, the symbol period, $T_s=2T_b$, T_b represents the bit duration and symbol energy, $E_s=2E_b$, E_b represents the bit energy. The complex envelop of OFDM signal is given by-

$$s_i(t) = \sqrt{\frac{2E_s}{T_s}} \sum_{k=0}^{\infty} \sum_{n=0}^{N-1} s_{k,n,i}(t)\, \varphi_n(t-kT) \quad ;$$

$$where, \ i=1:4 \ and \ T=NT_s$$

(2.20)

where, $S_{k,n,I}$ carries the ith information to be sent over the kth symbol interval; $t \in [kT, (k+1)T]$ and nth sub band (n=0,1,2,3…………N-1). N is the no. of OFDM subcarrier. The set of complex orthonormal waveform, $\{\varphi_n(t)\}_{n=0}^{N-1}$ is represented as –

$$\varphi_n(t) = \begin{cases} e^{j2\pi(n-\frac{N-1}{2})t/T} & ; t \in (0,T) \\ 0 \ ; \ otherwise \end{cases}$$

(2.21)

The nth subcarrier frequency is $f_c + \dfrac{2n-(N-1)}{2T}$. Now for simplicity, set k=0 for first symbol interval, $t \in (0,T)$ in equation (2.21) then-

$$v(t) = \sqrt{\frac{2E_s}{T_s}} \sum_{n=0}^{N-1} s_{0,n,i}\, e^{j\frac{2\pi nt}{NT_s}} e^{\frac{-j\pi(N-1)t}{NT_s}} \quad ; \quad 0 \le t \le NT_s$$

$$= \sqrt{\frac{2E_s}{T_s}} \sum_{n=0}^{N-1} a_{0,n,i}\, \cos\,[2\pi f_{rc}+(2i-1)\pi/4]\, e^{\frac{j2\pi nt}{NT_s}} e^{\frac{-j\pi(N-1)t}{NT_s}}$$

$$= \sqrt{\frac{2E_s}{T_s}} \sum_{n=0}^{N-1} a_{0,n,i}\, \frac{1}{2}\,[e^{j\{2\pi f_{rc}+(2i-1)\pi/4\}}+e^{-j\{2\pi f_{rc}+(2i-1)\pi/4\}}]\, e^{\frac{j2\pi nt}{NT_s}} e^{\frac{-j\pi(N-1)t}{NT_s}}$$

(2.22)

Note that the term, $e^{\frac{-j\pi(N-1)t}{NT_s}}[e^{j\{2\pi f_{rc}+(2i-1)\pi/4\}}+e^{-j\{2\pi f_{rc}+(2i-1)\pi/4\}}]$ is not a function of n and can be combined with the carrier term, $e^{j2\pi f_c t}$. Now the complex envelop is written by-

$$v(t) = \sqrt{\frac{E_s}{2T_s}} \sum_{n=0}^{N-1} a_{0,n,i}\, e^{j\frac{2\pi nt}{NT_s}} \quad ; \quad 0 \le t \le NT_s$$

(2.23)

and the corresponding carrier is-

$$e^{j2\pi f_c t}[e^{j\left\{2\pi f_{rc}+(2i-1)\frac{\pi}{4}-\frac{\pi(N-1)t}{NT_s}\right\}} + e^{-j\left\{2\pi f_{rc}+(2i-1)\frac{\pi}{4}+\frac{\pi(N-1)t}{NT_s}\right\}}]$$

The real and imaginary part of the signal, *v(t)* is then separated using real imaginary separator. The output of linear quantized PCM is represented as-

$$v_R(t) = \mathrm{Re}\left\{\sqrt{\frac{E_s}{2T_s}}\sum_{n=0}^{N-1}a_{0,n,i}\ e^{j\frac{2\pi nt}{NT_s}}\right\}; \qquad 0 \le t \le NT_s$$

$$= \sqrt{\frac{P_b}{2}}\sum_{n=o}^{N-1}a_{0,n,i}\ \cos(\frac{2\pi nt}{NT_s}) \tag{2.24}$$

$$where,\ E_s = lE_b\,, T_s = lT_b\,, P_b = \frac{E_b}{T_b}\,, l = \log_2 M$$

In equation (2.24), *M* represents the quantization level and *l* is the number of bits required for different level of quantization. P_b represents the required bit power. Now the output light of DDMZI is given by-

$$E_{out} = E_{in}\left[\cos(\pi\frac{v_R(t)}{V_\pi}) + \cos(\pi\frac{\tilde{v}_R(t)}{V_\pi})\ e^{\frac{j\pi}{2}}\right]$$

$$= E_{in}\left[\cos(\pi\frac{v_R(t)}{V_\pi}) + j\cos(\pi\frac{\tilde{v}_R(t)}{V_\pi})\right] \tag{2.25}$$

where, E_{in} is the input optical signal.

$$E_{in} = A_0 e^{j\omega_0 t}$$

$$E_{out} = A_0 e^{j\omega_0 t}\left[\cos(\pi\frac{v_R(t)}{V_\pi}) + j\cos(\pi\frac{\tilde{v}_R(t)}{V_\pi})\right]$$

$$= A_0 e^{j\omega_0 t}\cos\theta + jA_0 e^{j\omega_0 t}\cos\tilde{\theta}$$

$$= A_0\sqrt{\cos^2\theta + \cos^2\tilde{\theta}}\; e^{j(\omega_0 t + \tan^{-1}\frac{\cos\tilde{\theta}}{\cos\theta})}$$

$$= A_0\sqrt{1 - \sin^2\theta + 1 - \sin^2\tilde{\theta}}\; e^{j(\omega_0 t + \alpha)}$$

$$\cong A_0\sqrt{2 - \theta^2 - \tilde{\theta}^2}\, e^{j(\omega_0 t + \alpha)} \quad ; \quad \sin\theta \approx \theta, \sin\tilde{\theta} \approx \tilde{\theta},\; \alpha_0 = \tan^{-1}\frac{\cos\tilde{\theta}}{\cos\theta}$$

$$\cong A_0\sqrt{2 - \frac{\pi^2 v_R^2(t)}{V_\pi^2} - \frac{\pi^2 \tilde{v}_R^2(t)}{V_\pi^2}}\; e^{j(\omega_0 t + \alpha_0)}$$

$$\cong A_0\sqrt{2 - \frac{\pi^2}{N^2 V_\pi^2}\left(\frac{P_b}{2} + \frac{P_b}{2}\right)}\; e^{j(\omega_0 t + \alpha_0)}$$

$$\cong A_0\sqrt{2 - \frac{\pi^2 P_b}{N^2 V_\pi^2}}\; e^{j(\omega_0 t + \alpha_0)}$$

$$(2.26)$$

2.6.2.2 Analysis of the received signal

After the transmission of turbulence channels the received optical signal can expressed as-

$$E_{out} \cong \sqrt{I}\, A_0\sqrt{2 - \frac{\pi^2 P_b}{N^2 V_\pi^2}}\; e^{j(\omega_0 t + \alpha_0)} \tag{2.27}$$

where, I is the turbulent channel coefficient. Here we consider Log- normal turbulence model for low atmospheric turbulence effect. The probability density function (pdf) of I can be modeled as -

$$f_I(I) = \frac{1}{\sqrt{2\pi\sigma^2}\, I}\, e^{\frac{-(\ln(I) - \mu)^2}{2\sigma^2}} \qquad ; I > 0 \tag{2.28}$$

Now the output current of the balanced photodetector is written by-

$$i(t) = i_1(t) - i_2(t)$$

$$= R_d \, \text{Re} \left[\left\{ E_{out}(t-T) + E_{out}(t)e^{\frac{j\pi}{4}} \right\}^2 - \left\{ E_{out}(t-T) - E_{out}(t)e^{\frac{j\pi}{4}} \right\}^2 \right]$$

$$= R_d \, 2\text{Re} \left[E_{out}(t) E_{out}(t-T)e^{\frac{j\pi}{4}} \right] \qquad ; T = T_s$$

$$= 2R_d \left(\sqrt{I} A_0 \sqrt{2 - \frac{\pi^2 P_b}{N^2 V_\pi^2}} \right)^2 \cos(\frac{\pi}{4} + \omega_0 t + \alpha_0)$$

$$= 2R_d A_0^{\ 2} I \left(2 - \frac{\pi^2 P_b}{N^2 V_\pi^2} \right) \cos(\frac{\pi}{4} + \omega_0 t + \alpha_0)$$

(2.29)

2.6.2.3 SNR and BER analysis

The conditional signal to noise ratio (SNR) condition on turbulence is represent as-

$$SNR(I) = \frac{Signal \ power}{Noise \ power} = \frac{|i(t)|^2}{\sigma_n^{\ 2}} = \frac{|i(t)|^2}{\sigma_{th}^{\ 2} + \sigma_{sh}^{\ 2}}$$

$$= \frac{\left| 2R_d A_0^{\ 2} I \left(2 - \frac{\pi^2 P_b}{N^2 V_\pi^2} \right) \cos(\frac{\pi}{4} + \omega_0 t + \alpha_0) \right|^2}{\frac{4kTB}{R_L} + 2eBR_d P_b I} \qquad ; B = \frac{1}{N \times l \times T_b}$$

$$\cong \frac{\left\{ 2R_d A_0^{\ 2} I \left(2 - \frac{\pi^2 P_b}{N^2 V_\pi^2} \right) \right\}^2}{\frac{4kTB}{R_L} + 2eBR_d P_b I}$$

(2.30)

Average SNR can be obtained as-

$$SNR_{average} = \int_0^\infty SNR(I). f_I(I) \, dI$$

(2.31)

Now the conditional BER is given by-

$$BER(I) = \frac{1}{2} erfc \left(\frac{\sqrt{SNR(I)}}{2} \right)$$

(2.32)

So, the average BER can be written by-

$$BER_{average} = \int_0^\infty BER(I). f_I(I) \, dI$$

(2.33)

For closed form expression, let consider-

$$\zeta = 2R_d A_0^{\ 2} \left(2 - \frac{\pi^2 P_b}{N^2 V_\pi^{\ 2}} \right) \text{ and } \sigma_T^2 = \frac{4kTB}{R_L} + 2eBR_d P_b I$$

$$\frac{\sqrt{SNR(I)}}{2} = 0.5 \left(\frac{\zeta I}{\sigma_T} \right)$$

Now, conditional BER is written as-

$$BER(I) = \frac{1}{2} \left[1 - \frac{2}{\sqrt{\pi}} \sum_{k=0}^{\infty} \frac{(-1)^k \left(0.5 \frac{\zeta}{\sigma_T} \right)^{2k+1} I^{2k+1}}{k|(2k+1)} \right] \tag{2.34}$$

For k=0, $\quad BER(I) \approx \frac{1}{2} - \frac{1}{\sqrt{\pi}} \left(0.5 \frac{\zeta}{\sigma_T} \right) I \tag{2.35}$

$$f_I(I) = \frac{1}{\sqrt{2\pi\sigma^2} I} e^{\frac{-(\ln(I)-\mu)^2}{2\sigma^2}} = \frac{1}{\sqrt{2\pi}\sigma I} \left[\exp \left\{ \left(\ln(I) + \frac{\sigma^2}{2} \right)^2 \right\} \right]^{\left(-\frac{1}{2\sigma} \right)}$$

$$= \frac{1}{\sqrt{2\pi}\sigma} I^{-\left(\frac{1}{\sigma}+1 \right)} \exp \left(-\frac{\sigma}{2} \right) \tag{2.36}$$

Finally, the average BER can be written as-

$$BER_{average} = \int_0^{\infty} BER(I).f_I(I)\, dI$$

$$= \int \left[\frac{1}{2} - \frac{1}{\sqrt{\pi}} \left(0.5 \frac{\zeta}{\sigma_T} \right) I \right] \left[\frac{1}{\sqrt{2\pi}\sigma} I^{-\left(\frac{1}{\sigma}+1 \right)} \exp \left(-\frac{\sigma}{2} \right) \right] dI$$

$$\approx \frac{1}{2\sqrt{2\pi}\sigma} \exp \left(-\frac{\sigma}{2} \right) \int I^{-\left(\frac{1}{\sigma}+1 \right)} dI - \frac{1}{\sqrt{2\pi}\sigma} \left(0.5 \frac{\zeta}{\sigma_T} \right) \exp \left(-\frac{\sigma}{2} \right) \int I^{-\left(\frac{1}{\sigma} \right)} dI$$

$$\approx -\frac{1}{2\sqrt{2\pi}} \exp \left(-\frac{\sigma}{2} \right) I^{-\left(\frac{1}{\sigma} \right)} + \frac{1}{\sqrt{2\pi}\sigma} \left(0.5 \frac{\zeta}{\sigma_T} \right) \exp \left(-\frac{\sigma}{2} \right) \left(\frac{1}{\sigma} - 1 \right)^{-1} I^{-\left(\frac{1}{\sigma}-1 \right)}$$

$$\tag{2.37}$$

2.6.3 Results and discussions

The parameters are used for analysis are listed in table 2.4. The BER performance of an OFDM based DQPSK modulated FSO link is analyzed. The analytical results are comparing with the simulation results, which are shown in Fig. 2.9. Result shows that the analytical results are close to the numerical simulation results. The change in average signal to noise ratio due to the change of OFDM subcarrier with receiver power is shown in Fig. 2.10.

Table 2.4: System Parameters used for simulation results

Parameters	Values
Coupling co-efficient,α	1
Characteristic of the MZ, V_0	500mV to 8V
Temperature, T	300K
Thermal Resistance, R_L	50Ω
FFT size	64 to 512
Laser wavelength, λ	1550nm& 850nm
PIN photodetector Responsivity, Rd	0.85
Quantization level	64
Link distance, L	Up to 3675m
Received power, Pr	-40 to 0 dBm
QPSK phase	45^0
Structure parameter, C_n^2	$10^{-14}m^{-2/3}$
Mean variance, μ	1
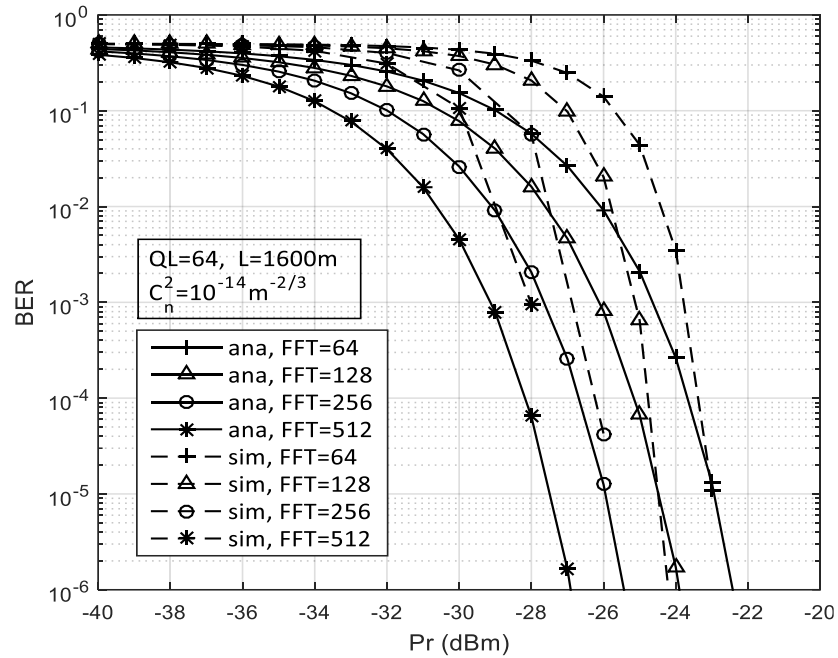
Fig. 2.9: Compare analytical and simulation results of BER performance curve

In Fig. 2.11, it is clearly shown that atmospheric turbulence degrades the BER performance. Analytical results show that, the power requirements increased to 4dB due to atmospheric turbulence at a BER of 10^{-12} for link distance of 2000m.
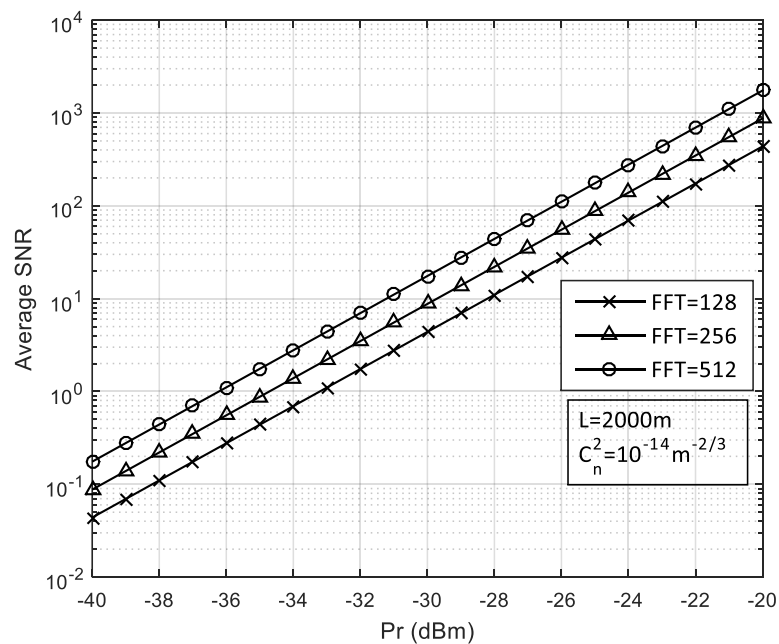
Fig.2.10: Average SNR for different OFDM carrier.
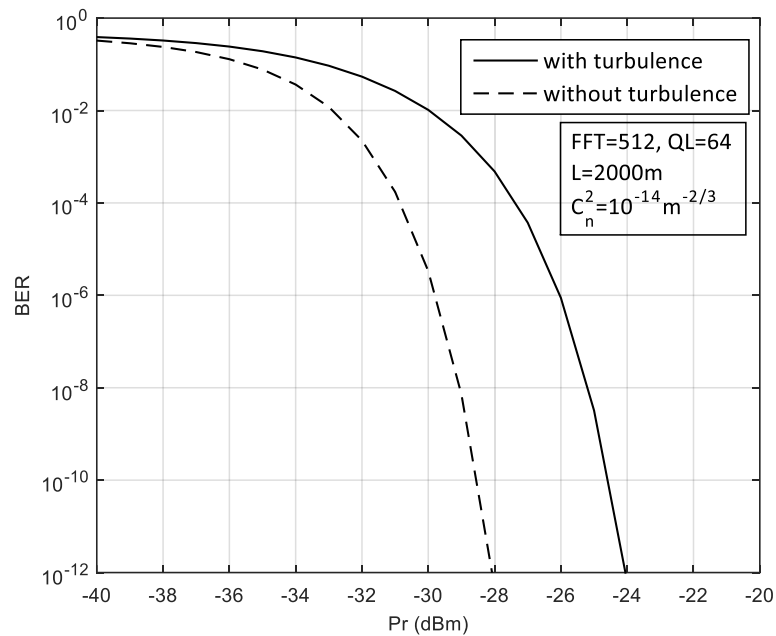
Fig. 2.11: BER performance curve for with and without atmospheric turbulence.

The BER performance is severely affected by the background radiation, which is shown in Fig. 2.12. Results show that, due to background radiation, around 1.4 dB more power required for 2000m link distance at a BER of 10^{-12}.
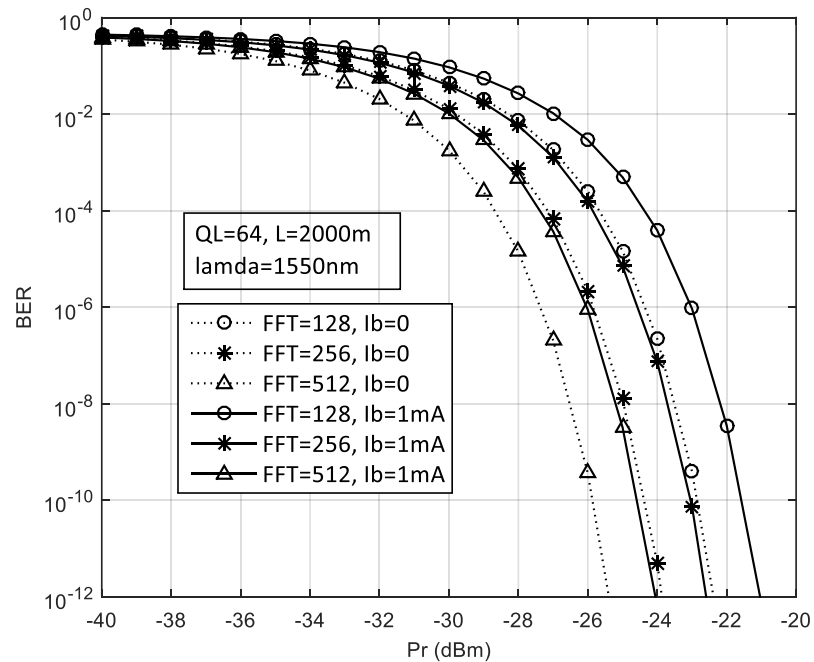
Fig. 2.12: Effect of background radiation on BER performance.
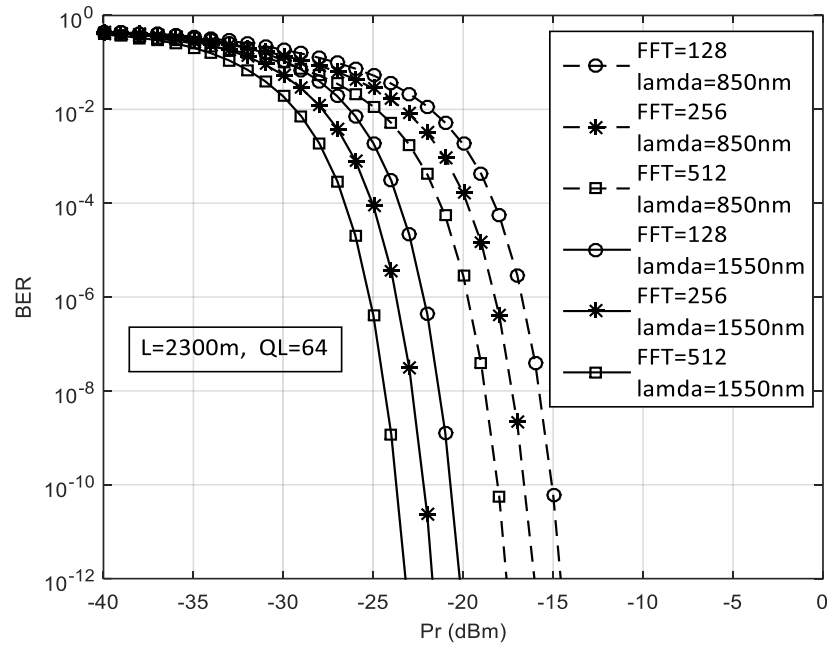
Fig. 2.13: BER curve for different FFT length at two different wavelengths.

In Fig. 2.13, it is clearly shown that a significant amount of improvement in BER performance is found if the wavelength is shifted from 850nm to 1550nm.
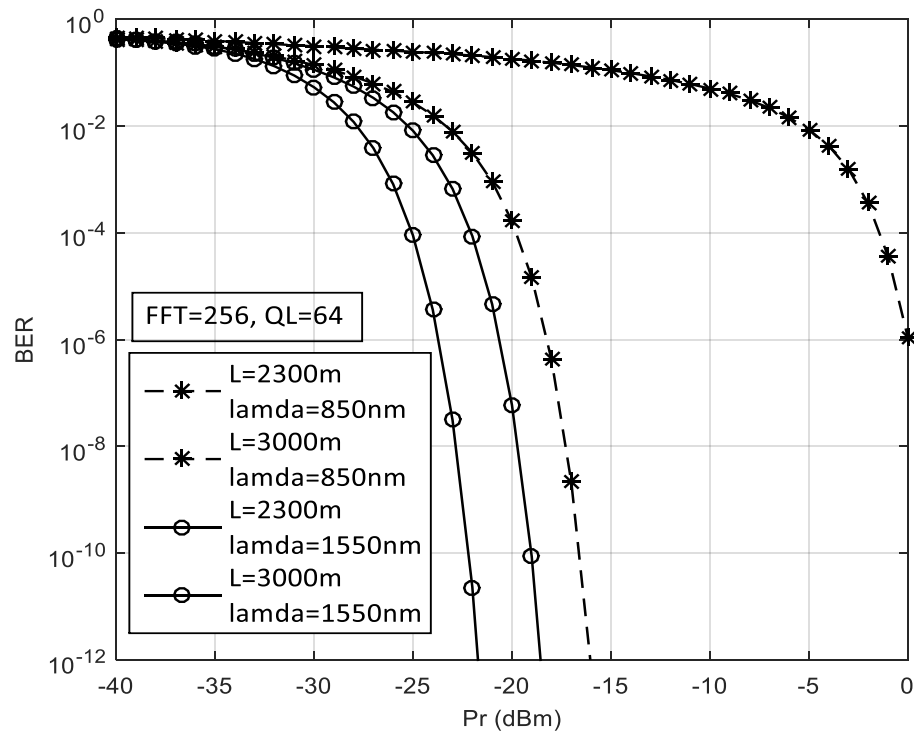
Fig.2.14: BER curve for two different link distances at two different wavelengths.

And the BER performance falls drastically with respect to the wavelength and link distance are include in Fig. 2.14. At a BER of 10^{-6}, our proposed system suffers 3dB and 18dB power penalty for wavelength1550nm and 850nm respectively due to increase link distance from 2300m to 3000m. Again, increasing link distance also increases the power requirements.

In proposed systems, data transmission up to 3675m link distance possible shown in Fig. 2.15 considering the BER of 10^{-6}. Fig. 2.16 shows the SNR sensitivity due to increase link distance along with the change of OFDM sub carrier.
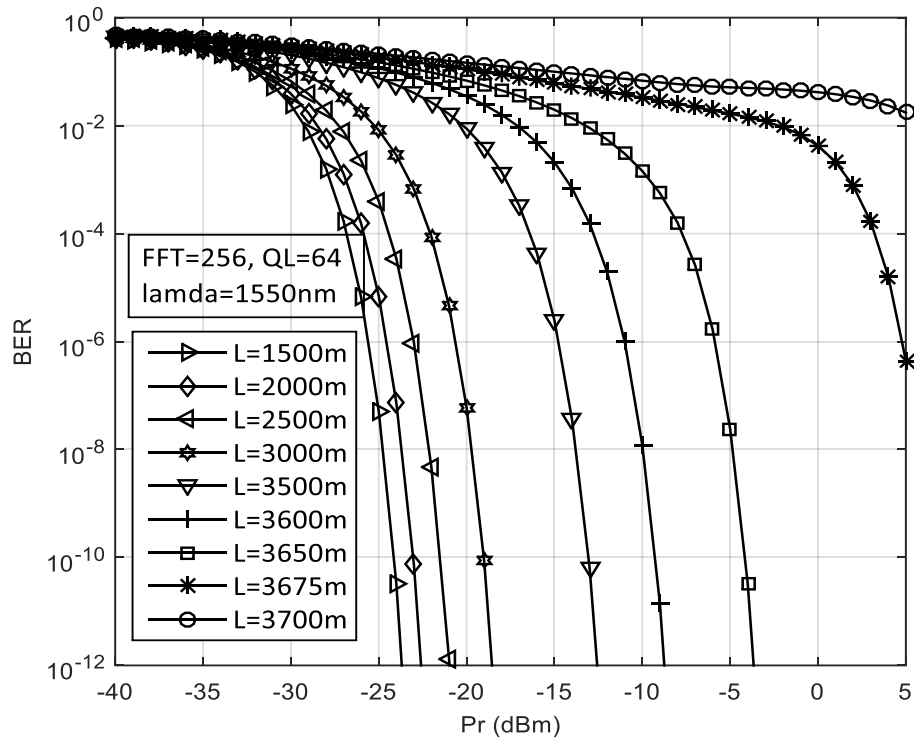
Fig. 2.15: Effect of increasing link distance on BER performance curve.

Receiver sensitivity improvements curve is shown in Fig. 2.17. The amount of improvements is found from the BER versus received power curve and provided in Table 2.5. The power penalties due to increase link distance for different OFDM subcarrier is shown in Fig. 2.18.
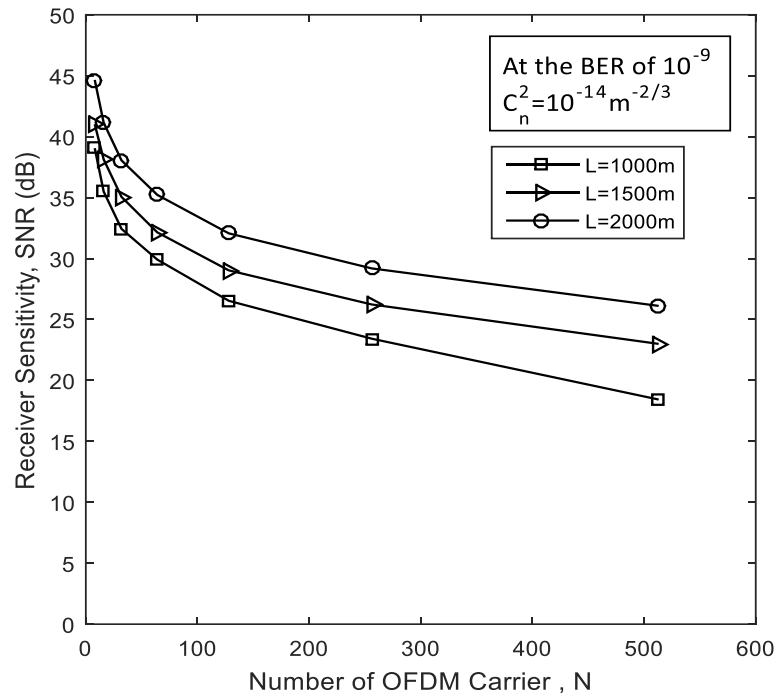
Fig. 2.16: SNR Sensitivity curve due to increasing OFDM sub carrier.
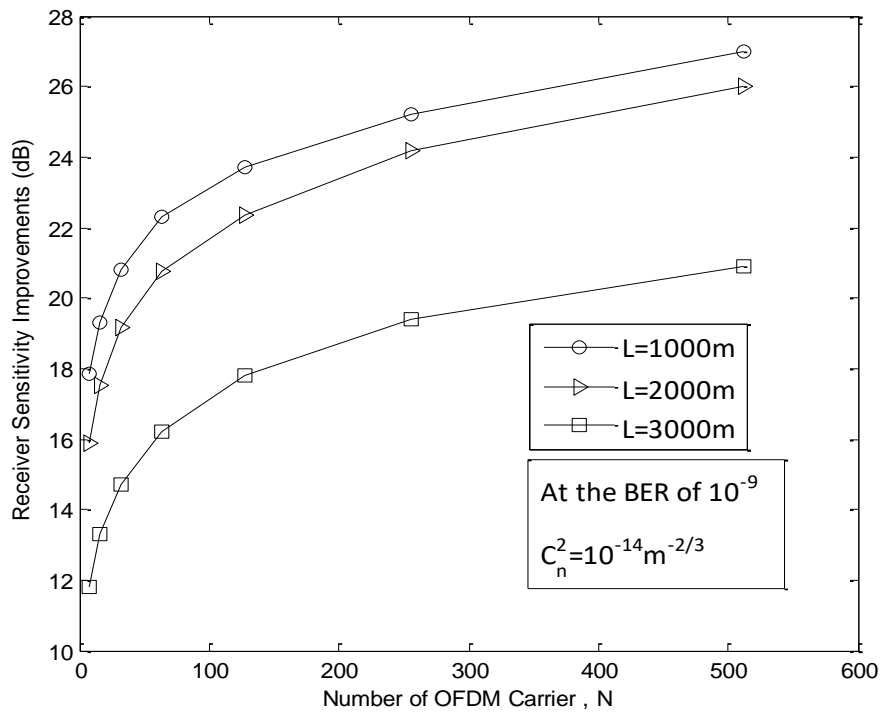
Fig. 2.17: Receiver Sensitivity Improvements curve due to increasing OFDM sub carrier.
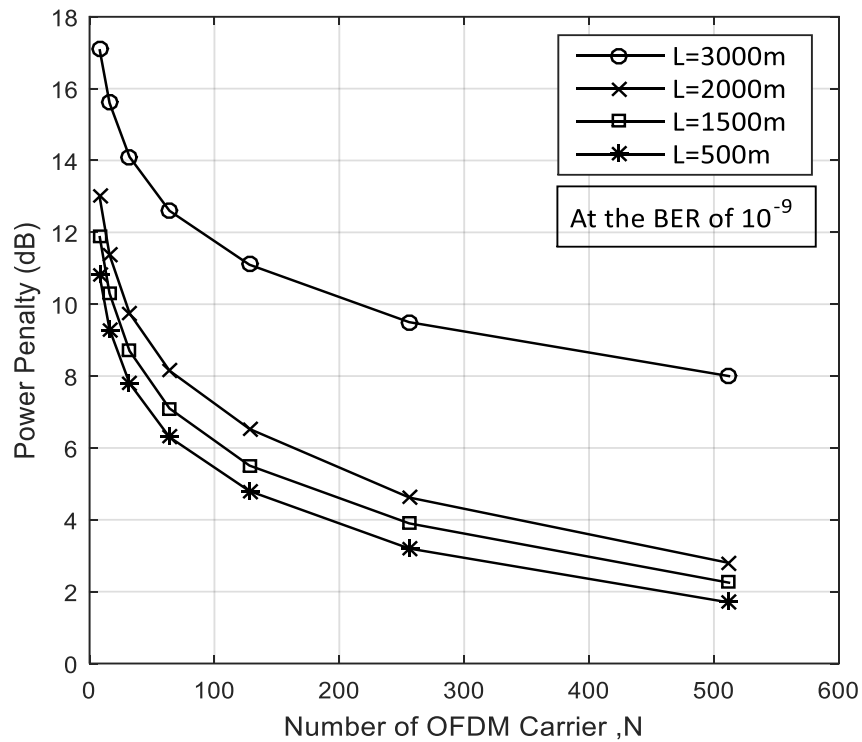
Fig. 2.18: Power penalty curve for increasing number of OFDM carrier.

Table 2.5: Receiver sensitivity improvements for different number of OFDM subcarriers

Number of OFDM Subcarrier / Link Length	8 (dB)	16 (dB)	32 (dB)	64 (dB)	128 (dB)	256 (dB)	512 (dB)
1000 m	17.84	19.3	20.8	22.3	23.7	25.2	27
2000 m	15.9	17.53	19.1	20.75	22.37	24.2	26
3000 m	11.8	13.3	14.7	16.2	17.8	19.4	20.9

Proposed analytical results also compare with the work published in IEEE Photonics journal [36] and the experimental work [39] which is shown in Fig. 2.19 and Fig. 2.20 respectively.
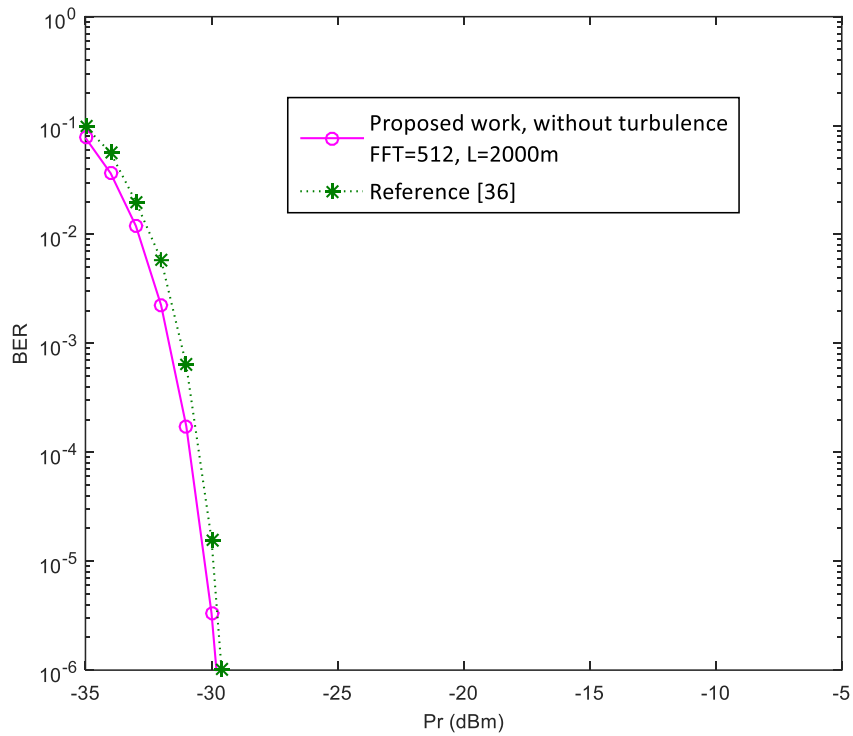
Fig. 2.19: Compare proposed results of BER performance curve with reference [36] considering no atmospheric turbulence.
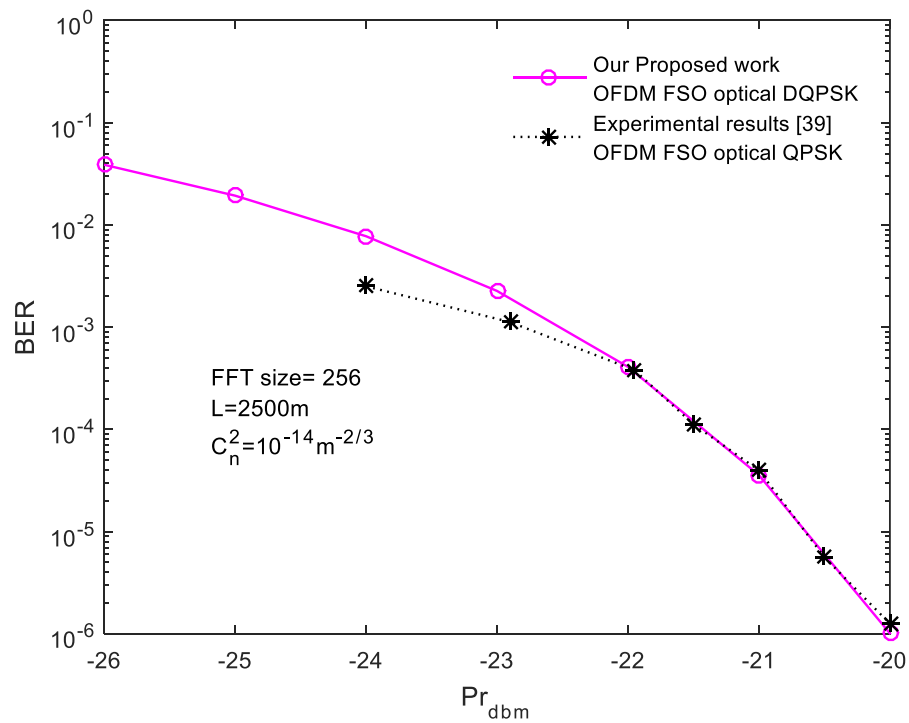
Fig. 2.20: Compare proposed results of BER performance curve with the experimental work of reference [39].

2.7 Effect of Pointing Error on Non-Hermitian OFDM FSO System's BER Performance

2.7.1 Pointing error

The performance of an FSO link is severely limited by not only the atmospheric turbulence but also the pointing error. The pointing error is occurred when the current position of antenna is deviated from the desired position and due to this the line of sight between transmitter and receiver is lost and degrades the system bit error rate performance. Pointing error may arise due to building sway, mechanical misalignment and mechanical vibrations existence in the systems, earthquake, errors in tracking systems etc. There are two components of pointing error which are jitter and boresight error. Boresight seemed as fixed error whereas jitter is a random error and it is superimposed over the boresight error.

2.7.2 Probability density function of pointing error

A Gaussian beam with beam waist *w* propagating through the atmospheric turbulence can be approximated as [144]-

$$w = w_0 \left[1 + \varepsilon \left(\frac{\lambda z}{\pi w_0^2} \right)^2 \right]^{\frac{1}{2}} \tag{2.38}$$

where, w_0 is the beam waist at $z = 0$ and

$$\varepsilon = \left(1 + \frac{2w_0^2}{\rho_0^2(z)} \right) \qquad \rho_0(z) = (0.55 C_n^2 k^2 z)^{-\frac{3}{5}}$$

$\rho_0(z)$ is the coherence length. The fraction of the collected power at a receiver of radius *a* in the transverse plane of the incident wave can be approximated as Gaussian form and expressed as [14]-

$$h(r; z) \approx A e^{\left(-\frac{2r^2}{w_{eq}^2} \right)} \tag{2.39}$$

where, A is the fraction of the collected power at radial distance, $r = 0$ and w_{eq} represents the equivalent beam width of the received light at the receiver. By using the following equations, equivalent beam width of the received light at the receiver is calculated [14].

$$\upsilon = \frac{\sqrt{\pi}\,a}{\sqrt{2}\,w}, \qquad w_{eq}^2 = w^2\,\frac{\sqrt{\pi}\,erf(\upsilon)}{2\upsilon\exp(-\upsilon^2)}, \qquad A = |erf(\upsilon)|^2$$

where, w represents the beam waist, which is evaluated at e^{-L} at a distance L from the transmitter. The radial displacement r at the receiver is modeled by a Rayleigh distribution-

$$f(r) = \frac{r}{\sigma_s^2}e^{\left(-\frac{r^2}{2\sigma_s^2}\right)}, \qquad r > 0 \tag{2.40}$$

where, σ_s^2 is the jitter variance at the receiver. By using equations (2.39) and (2.40) we get the probability distribution function of h as-

$$f_p(h) = \frac{\gamma^2}{A^{\gamma^2}}h^{\gamma^2-1} \qquad ; \quad 0 \leq h \leq A \tag{2.41}$$

where, $\gamma = \dfrac{w_{eq}}{2\sigma_s}$, represents the ratio between the equivalent beam radius and pointing error standard deviation.

2.7.3 BER performance analysis

2.7.3.1 Analysis of SNR and BER

The conditional signal to noise ratio (SNR) is represent as-

$$
\begin{aligned}
SNR(h,I) &= \frac{Signal\ power}{Noise\ power} = \frac{|i(t)|^2}{\sigma_n^2} = \frac{|i(t)|^2}{\sigma_{th}^2 + \sigma_{sh}^2} \\[2mm]
&= \frac{\left|2R_dA_0^2Ih\left(2 - \dfrac{\pi^2 E_b}{N^2 T_b V_\pi^2}\right)\cos(\dfrac{\pi}{4} + \omega_0 t + \alpha_0)\right|^2}{\dfrac{4kTB}{R_L} + 2eBR_dP_bI} \qquad ; B = \frac{1}{N \times l \times T_b} \\[2mm]
&\cong \frac{\left\{2R_dA_0^2Ih\left(2 - \dfrac{\pi^2 E_b}{N^2 T_b V_\pi^2}\right)\right\}^2}{\dfrac{4kTB}{R_L} + 2eBR_dP_bI}
\end{aligned}
\tag{2.42}
$$

The conditional BER is now given by-

$$BER_{cond.}(h, I) = \frac{1}{2} erfc\left(\frac{\sqrt{SNR(h, I)}}{2}\right)$$

(2.43)

Therefore, the average BER is calculated as follows-

$$BER_{average} = \int_{0}^{A}\int_{0}^{\infty} BER_{cond.}(h, I). f(I). f_p(h) dI\ dh$$

(2.44)

2.7.3.2 Results and discussion

The value of the parameters used in analytical simulation process are listed in Table-2.6. The BER performance of the proposed system is analyzed. Considering, both weak and strong atmospheric turbulence, the system BER performance versus received optical power with respect to different normalized pointing error are shown in Fig. 2.21 and Fig. 2.22 respectively.

Table-2.6: List of the parameters value used for analytical simulation.

Parameters	Values
Characteristic of the MZ, V_0	500mV to 8V
Temperature, T	300K
Thermal Resistance, R_L	50Ω
FFT size, N	256
Laser wavelength, λ	1550nm & 850nm
Responsivity, R_d	0.85
Detector aperture radius, a	20cm
Received power, Pr	-30 to -20 dBm
QPSK phase	45^0
Structure parameter, C_n^2	$10^{-14}m^{-2/3}$ - $10^{-16}m^{-2/3}$
Normalized beamwidth, w/a	1-10
Normalized pointing error standard deviation, σ_s/a	1.1-2
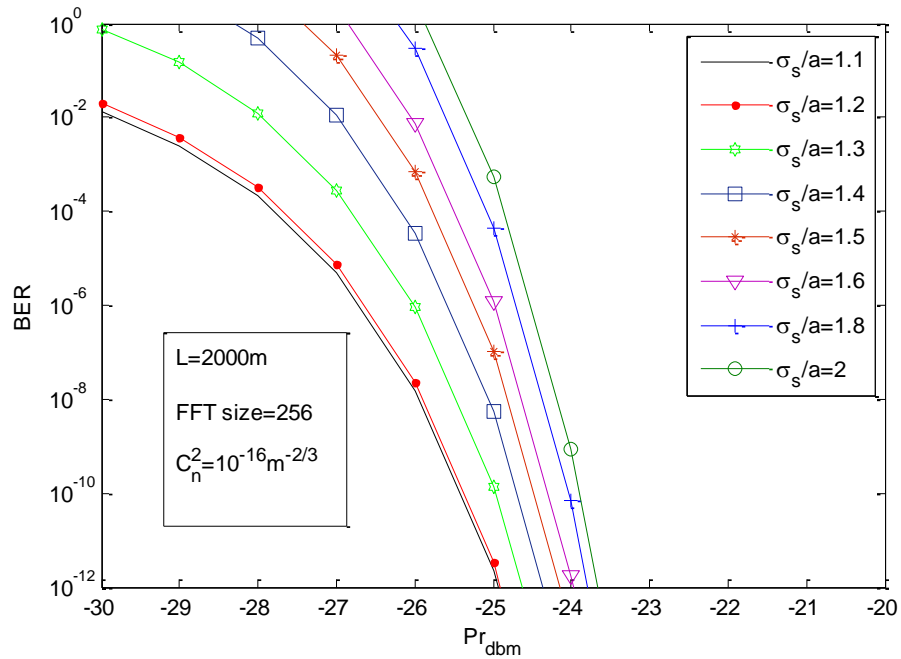
Fig.2.21: BER performance versus received optical power for weak atmospheric turbulence ($C_n^2 = 10^{-16}m^{-2/3}$) with different normalized pointing error.
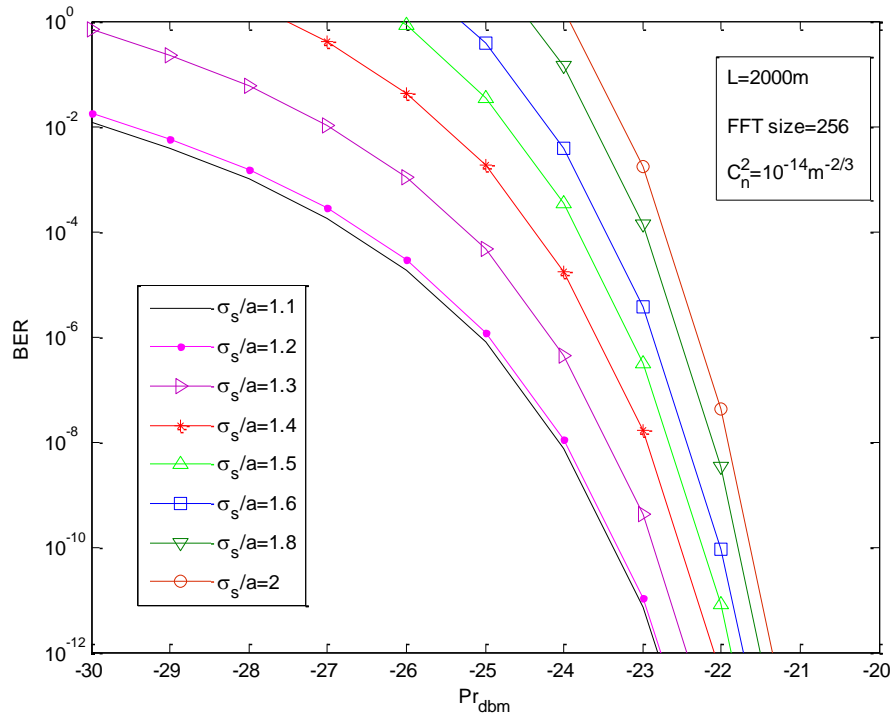
Fig. 2.22: BER performance versus received optical power for strong atmospheric turbulence ($C_n^2 = 10^{-14}m^{-2/3}$) with different normalized pointing error.
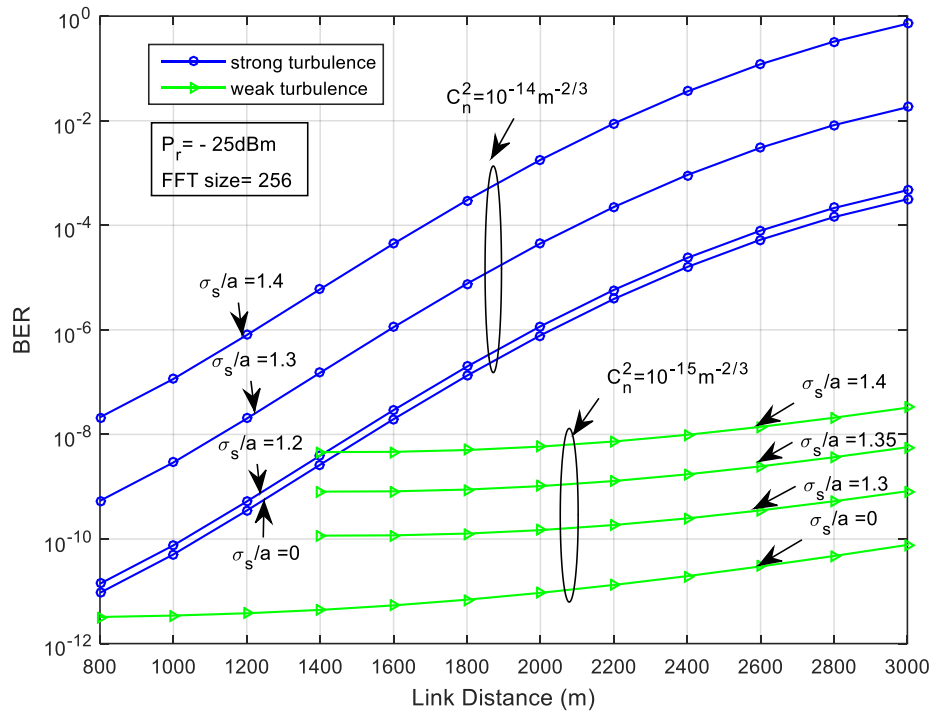
Fig. 2.23: BER versus Link length for both strong and weak atmospheric turbulence considering normalized pointing error as a parameter.

Results show that the system suffers almost 1.95dB and 1.25dB power penalty due to normalized pointing error standard deviation 2 and 1.5 respectively against strong turbulence and 1.7dB and 1.05dB power penalty due to normalized pointing error standard deviation 2 and 1.5 respectively against weak turbulence at a BER of 10^{-9}. In Fig. 2.23, the impact of pointing error on the system BER performance with respect to link distance is shown. The maximum allowable link length considering normalized pointing error as a variable is shown in Fig. 2.24. Results show that system suffers almost 5330m, 3080m and 2100m link distance penalty due to strong atmospheric turbulence for normalized pointing error 1.3, 1.4 and 1.5 respectively at a BER of 10^{-6}.
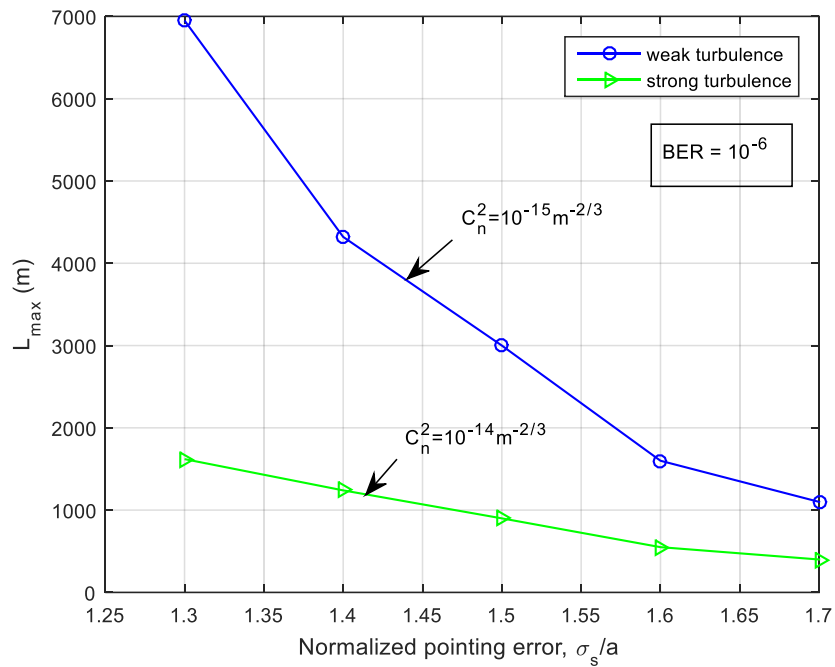
Fig. 2.24: Maximum allowable link length versus normalized pointing error to compare the performance between weak and strong turbulence at a BER of 10⁻⁶.

2.8 Summary

An analytical model for non-Hermitian OFDM FSO system using optical DQPSK modulation is presented in this chapter. Analytical expressions are developed for output SNR and conditional BER considering weak atmospheric turbulence and also for strong turbulence with pointing error. BER performance results are evaluated analytically and verified with semi numerical simulation for different system parameters. It is found that the system BER performance deteriorates significantly due to the pointing error between transmitter and receiver at a given BER.

Chapter 3

Multiplex and Diversity of Polarization for FSO Systems

Chapter-3

MULTIPLEX AND DIVERSITY OF POLARIZATION FOR FSO SYSTEMS

3.1 Introduction

Polarization of light is very useful technique to improve the BER performance of an FSO system. The state of polarization is considered as the most stable parameter for Free-space optical communication system in presence of atmospheric turbulence. Atmospheric turbulence provides distortion in signal intensity and cross polarization induces crosstalk in the received signal which severely limits the performance of a FSO communication system and also degrades the bit error rate performance significantly. Two analytical approaches are presented in this chapter, one is for an FSO system considering polarization multiplexing and another is for an FSO system with polarization diversity. In both cases, the system performance is evaluated taking into account the cross-polarization induced crosstalk and fading effect of atmospheric turbulence.

3.2 Polarization of Light

Polarization, in Physics, is defined as a phenomenon caused due to the wave nature of electro-magnetic radiation. When an electric field interacts with magnetic field result is electro-magnetic wave. Light generally considered as a transverse electro-magnetic wave because the light particle vibrates perpendicularly with the direction of motion of the light waves. The electric field moves in one direction and magnetic in another though always perpendicularly and the direction of motion which is perpendicular to both. These electric and magnetic vibrations can occur in numerous planes. A light wave that is vibrating in more than one plane is known as unpolarized light. The light emitted by the sun, by a lamp or a tube light are all unpolarized light sources. The polarization of light is shown in Fig. 3.1 where a linear polarizer is used.
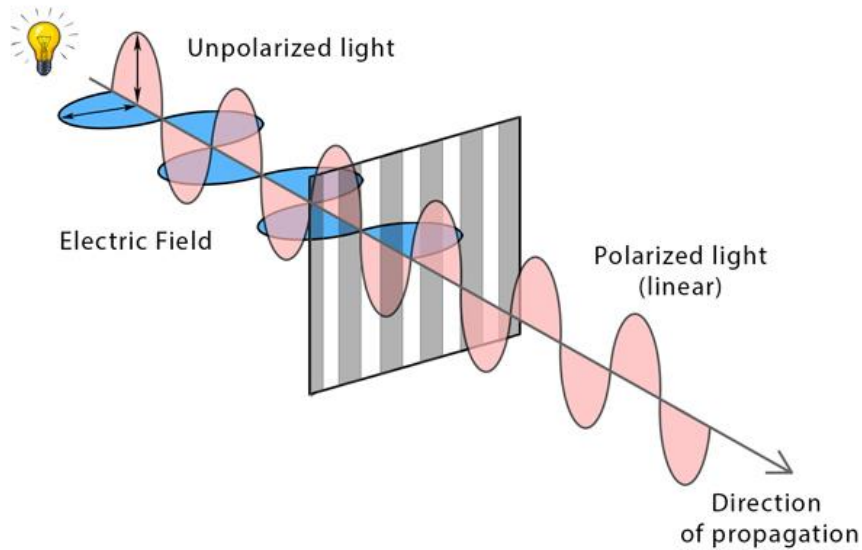
Fig. 3.1 Polarization of light

3.2.1   Polarized Wave

The projected electric field amplitude along horizontal and vertical axis can represented by the following parametric equations [50, 145]-

$$\vec{E}_x = A_x e^{j(\omega t - k\hat{z})}.\vec{x}$$

$$\vec{E}_y = A_y e^{j(\omega t - k\hat{z} + \varphi)}.\vec{y} \tag{3.1}$$

Where, A_x and A_y represents the projected electric field amplitude onto $\vec{x}$ and $\vec{y}$ axis respectively. The phase difference between $\vec{E}_x$ and $\vec{E}_y$ is denoted by φ which actually represents the shape of the electric field. The polarization of an electric field can be described by a single equation as [144, 145]-

$$\frac{\vec{E}_x^2}{A_x^2} + \frac{\vec{E}_y^2}{A_y^2} - \frac{2\vec{E}_x\vec{E}_y}{A_x A_y}cos\varphi = sin^2\varphi \tag{3.2}$$

The shape traced out in a fixed plane by the electric field vector is a description of the polarization state. Another conventional representation of polarization states is Stokes parameters which are [50]-

$$S_0 = \frac{A_x^2 + A_y^2}{2}$$

$$S_1 = \frac{A_x^2 - A_y^2}{2}$$

$$S_2 = 2A_x A_y \cos\varphi$$

$$S_3 = 2A_x A_y \sin\varphi \tag{3.3}$$

The physical interpretation of Stokes parameters are as follows [50]-

$S_0 \longrightarrow$ Optical intensity.

$S_1 \longrightarrow$ Optical intensity difference between horizontal and vertical polarized components. For a linearly polarized wave, a positive or negative S_1 corresponds to the polarization in $\vec{x}$ and $\vec{y}$ axis respectively.

$S_2 \longrightarrow$ A positive S_2 indicates $+45^0$ linear polarizations, while a negative S_2 indicates -45^0 linear polarizations.

$S_3 \longrightarrow$ A positive S_3 indicates right hand circular polarization while a negative S_3 indicates left hand circular polarization.

3.2.2 Polarized Beam Splitter (PBS)

A polarized beam splitter split the incoming continuous wave light signal into two polarized horizontal and vertical light wave perpendicular to each other which is shown in Fig. 3.2.
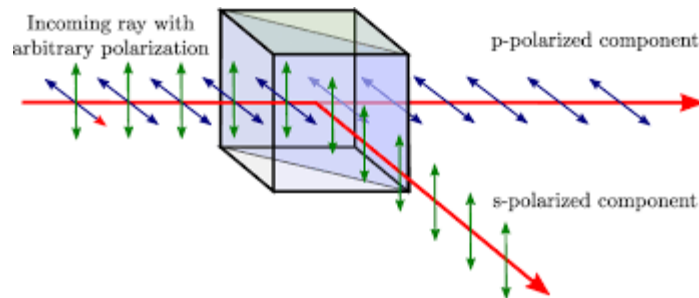
Fig.3.2: Polarized beam splitter

3.2.3 Polarized Beam Combiner (PBC)

A polarized beam combiner combines two linearly polarized light waves into a single light wave by superimposing it. In Fig. 3.3, a polarized beam combiner is shown.
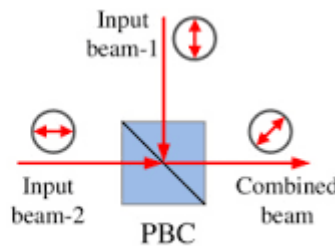
Fig. 3.3: Polarized beam combiner

3.3 BER Performance of a Polarization Multiplexed OFDM FSO System

3.3.1 System model

A detail block diagram of a polarization division multiplexing coherent DQPSK FSO system is shown in Fig. 3.4. For optical DQPSK modulator, dual drive Mach- Zehnder interferometer (DD-MZI) is required which contains two MZIs, one for in-phase and another for quadrature phase components. The polarization beam splitter splits the input continuous wave laser electric field at the transmitter which is orthogonally polarized and passed through two optical QPSK modulators. For X and Y polarizations, the phase difference between them is 90^0. Each modulator modulates the laser output with in-phase (I) and quadrature phase (Q) data indexed by $X_{I,k}$ and $X_{Q,k}$ respectively. The polarized light

is combined by using a PBC and transmitted through turbulent channel. The received signal is split by PBS and fed to the upper 90^0 hybrid for X-polarized light and lower 90^0 hybrid for Y-polarized light. The 45^0 linearly polarized output light from a local oscillator with respect to the received polarization is also feed by the two 90^0 hybrids. By applying homodyne balance detection techniques, the data decision is carried out from the receiver circuit.
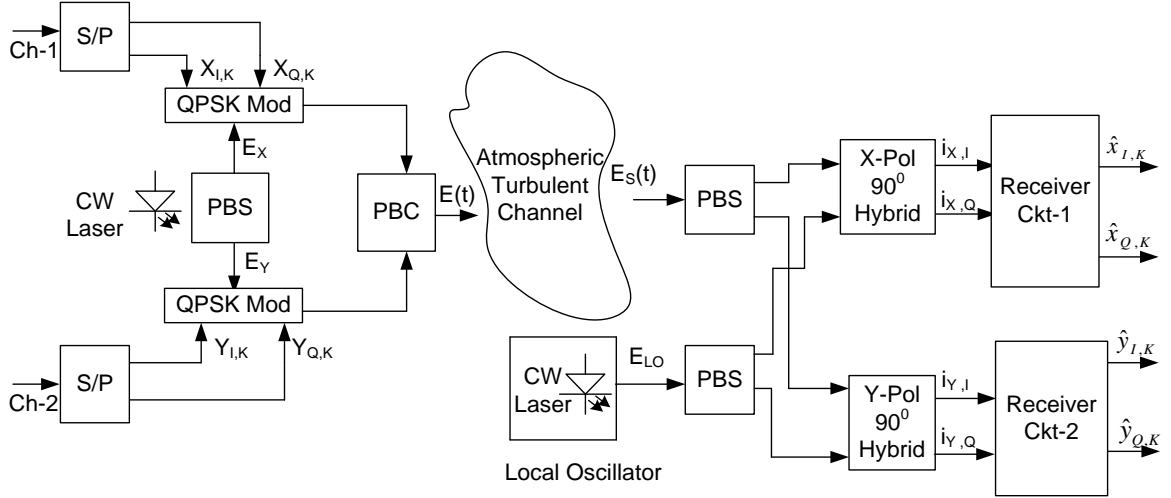
Fig. 3.4: Block Diagram of a Polarization Division Multiplexing coherent DQPSK Free Space Optical link.

3.3.2 Error probabilities analysis

3.3.2.1 Analysis of the transmitted signal

The electric field of the resultant optical signal from the output of the PBC and input to the atmospheric channel can be represented as [56]-

$$E(z,t) = \sqrt{\frac{E_s}{T_s}} \sum_k \sum_p \sum_m S_{m,p,k} \, p(t - kT_s) \, e^{(\omega_0 t + \phi_s(t))}$$

(3.4)

where, m denotes I or Q which is representing in-phase and quadrature phase respectively, p denotes X or Y which is representing horizontal and vertical polarization respectively and the symbol period, $T_s = 2T_b$, T_b represents the bit duration and symbol energy, $E_s = 2E_b$, E_b

representing the bit energy, *p(t)* representing the pulse shape function, optical carrier frequency represented by ω_0 and Φ_s is the laser phase noise.

3.3.2.2 Analysis of the received signal

The input signal to the PBS is represented as [56]-

$$\vec{E}_S(t) = E_{S,X}(t)\hat{x} + E_{S,Y}(t)\hat{y} \tag{3.5}$$

where,

$$E_{S,X}(t) = E_{X,I}(t)\cos[\omega_0 t + \phi_{X,I}(t)] - E_{X,Q}(t)\sin[\omega_0 t + \phi_{X,Q}(t)]$$

$$E_{S,Y}(t) = E_{Y,I}(t)\cos[\omega_0 t + \phi_{Y,I}(t)] - E_{Y,Q}(t)\sin[\omega_0 t + \phi_{Y,Q}(t)]$$

The detail of 90^0 hybrid with receiver circuit used in Fig. 3.4 is shown in Fig. 3.5.
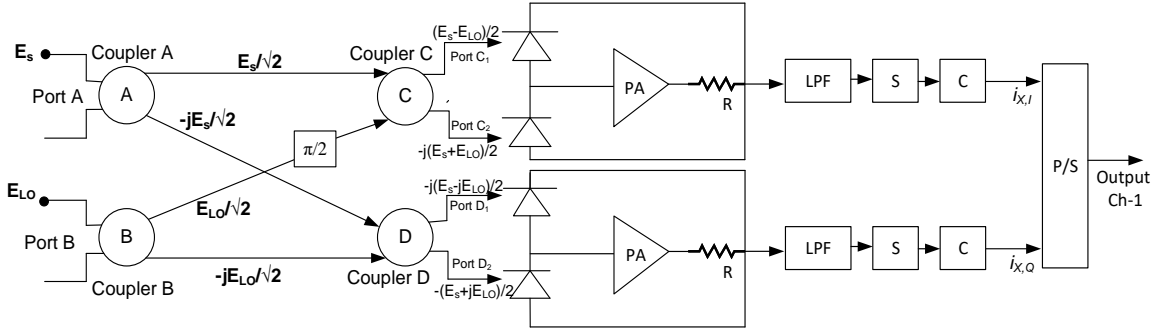
Fig. 3.5: Diagram of a 90^0 Hybrid with receiver circuit for channel-1.

The local oscillator output signal which is the input of the X-Pol 90^0 hybrid can be expressed as [56]-

$$E_{LO,X}(t) = E_{LO,X}\cos\omega_0 t \tag{3.6}$$

The sub channels random rotation due to the presence of turbulence, the signal suffered fading and crosstalk. The state of polarizations at the PBS, the input signal of the X-Pol 90^0 hybrid can be expressed as [56]-

$$E'_{S,X}(t) = \varepsilon_F E_{S,X}(t) + \varepsilon_X E_{S,Y}(t) \tag{3.7}$$

where, ε_F is the coefficient of complex fading due to X-polarization and ε_X is the complex crosstalk coefficient due to Y-polarization. The magnitude of these coefficient can be written as [55, 146]-

$$|\varepsilon_F| = \cos\theta \text{ and } |\varepsilon_X| = \sin\theta \tag{3.8}$$

The instantaneous output at the port C_1 of the X-Pol 90^0 hybrid, after neglecting common losses can be expressed as-

$$\begin{aligned}
E_{X,C_1}(t) &= E'_{S,X}(t) - E_{LO,X}(t) \\
&= \varepsilon_F E_{S,X}(t) + \varepsilon_X E_{S,Y}(t) - E_{LO,X}(t)
\end{aligned}$$

$$\begin{aligned}
\left|E_{X,C_1}(t)\right|^2 &= \left|\varepsilon_F E_{S,X}(t) + \varepsilon_X E_{S,Y}(t) - E_{LO,X}(t)\right|^2 \\
&= \varepsilon_F^2 \left|E_{X,I}(t)\cos[\omega_0 t + \phi_{X,I}(t)] - E_{X,Q}(t)\sin[\omega_0 t + \phi_{X,Q}(t)]\right|^2 \\
&\quad + \varepsilon_X^2 \left|E_{Y,I}(t)\cos[\omega_0 t + \phi_{Y,I}(t)] - E_{Y,Q}(t)\sin[\omega_0 t + \phi_{Y,Q}(t)]\right|^2 + \left|E_{LO,X}\cos\omega_0 t\right|^2 \\
&\quad + 2\varepsilon_F \varepsilon_X \left(E_{X,I}(t)\cos[\omega_0 t + \phi_{X,I}(t)] - E_{X,Q}(t)\sin[\omega_0 t + \phi_{X,Q}(t)]\right). \\
&\quad \left(E_{Y,I}(t)\cos[\omega_0 t + \phi_{Y,I}(t)] - E_{Y,Q}(t)\sin[\omega_0 t + \phi_{Y,Q}(t)]\right) \\
&\quad - 2\varepsilon_F E_{LO,X}\cos\omega_0 t \left(E_{X,I}(t)\cos[\omega_0 t + \phi_{X,I}(t)] - E_{X,Q}(t)\sin[\omega_0 t + \phi_{X,Q}(t)]\right) \\
&\quad - 2\varepsilon_X E_{LO,X}\cos\omega_0 t \left(E_{Y,I}(t)\cos[\omega_0 t + \phi_{Y,I}(t)] - E_{Y,Q}(t)\sin[\omega_0 t + \phi_{Y,Q}(t)]\right)
\end{aligned} \tag{3.9}$$

Neglecting the optical frequency term as well as the *sine* and *quadrature* terms because they will not generate any in-phase signal, the resultant signal can be written as [56]-

$$\begin{aligned}
\left|E_{X,C_1}(t)\right|^2 &= \varepsilon_F^2 \left[\frac{E_{X,I}^2}{2} + \frac{E_{X,Q}^2}{2}\right] + \varepsilon_X^2 \left[\frac{E_{Y,I}^2}{2} + \frac{E_{Y,Q}^2}{2}\right] + \frac{E_{LO,X}^2}{2} \\
&\quad + \varepsilon_F \varepsilon_X E_{X,I} E_{Y,I}\cos(\phi_{X,I} - \phi_{Y,I}) - \varepsilon_F E_{LO,X} E_{X,I}\cos(\phi_{X,I}) \\
&\quad - \varepsilon_X E_{LO,X} E_{Y,I}\cos(\phi_{Y,I})
\end{aligned} \tag{3.10}$$

After neglecting the time dependence and multiplying with conversion parameter K, the output power can be expressed for the port C_1 is [56],

$$P_{X,C_1} = K|E_{X,C_1}|^2 = \frac{K}{2}\varepsilon_F^2\left[|E_{X,I}|^2 + |E_{X,Q}|^2\right] + \frac{K}{2}\varepsilon_X^2\left[|E_{Y,I}|^2 + |E_{Y,Q}|^2\right]$$

$$+ \frac{K}{2}|E_{LO,X}|^2 + 2\varepsilon_F\varepsilon_X\sqrt{\frac{K}{2}}E_{X,I}\sqrt{\frac{K}{2}}E_{Y,I}\cos(\phi_{X,I} - \phi_{Y,I})$$

$$- 2\varepsilon_F\sqrt{\frac{K}{2}}E_{LO,X}\sqrt{\frac{K}{2}}E_{X,I}\cos(\phi_{X,I}) - 2\varepsilon_X\sqrt{\frac{K}{2}}E_{LO,X}\sqrt{\frac{K}{2}}E_{Y,I}\cos(\phi_{Y,I}) \quad (3.11)$$

$$= \varepsilon_F^2 P_{S,X} + \varepsilon_X^2 P_{S,Y} + P_{LO,X} + 2\varepsilon_F\varepsilon_X\sqrt{P_{X,I}P_{Y,I}}\cos(\phi_{X,I} - \phi_{Y,I})$$

$$- 2\varepsilon_F\sqrt{P_{X,I}P_{LO,X}}\cos(\phi_{X,I}) - 2\varepsilon_X\sqrt{P_{Y,I}P_{LO,X}}\cos(\phi_{Y,I})$$

Similarly, the power at port C_2,

$$P_{X,C_2} = \varepsilon_F^2 P_{S,X} + \varepsilon_X^2 P_{S,Y} + P_{LO,X} + 2\varepsilon_F\varepsilon_X\sqrt{P_{X,I}P_{Y,I}}\cos(\phi_{X,I} - \phi_{Y,I})$$

$$+ 2\varepsilon_F\sqrt{P_{X,I}P_{LO,X}}\cos(\phi_{X,I}) + 2\varepsilon_X\sqrt{P_{Y,I}P_{LO,X}}\cos(\phi_{Y,I}) \quad (3.12)$$

The differential photocurrents from the output port C_1 and C_2 are written by-

$$i_{X,C} = i_{X,C_2} - i_{X,C_1}$$

$$= 4\varepsilon_F R_d\sqrt{P_{X,I}P_{LO,X}}\cos\phi_{X,I} + 4\varepsilon_X R_d\sqrt{P_{Y,I}P_{LO,X}}\cos\phi_{Y,I} \quad (3.13)$$

Now the signal terms after considering fading due to PBS misalignment and turbulence is-

$$i_{S,X,C} = 4\varepsilon_F R_d\sqrt{IP_{X,I}P_{LO,X}}\cos\phi_{X,I} \quad (3.14)$$

And the crosstalk terms due to X-Pol and turbulence is-

$$i_{Xtalk,X,C} = 4\varepsilon_X R_d\sqrt{IP_{Y,I}P_{LO,X}}\cos\phi_{Y,I} \quad (3.15)$$

3.3.2.3 Analysis of SNR and BER

The conditional signal to crosstalk plus noise ratio (SCNR) condition on turbulence and misalignment angle is represent as-

$$SCNR(\theta, I) = \frac{|i_{S,X,C}|^2}{|i_{Xtalk,X,C}|^2 + i_B^2 + \sigma_{th}^2 + \sigma_{sh}^2}$$

$$= \frac{16R_d^2 IP_{X,I}P_{LO,X}\cos^2\theta\cos^2\phi_{X,I}}{16R_d^2 IP_{Y,I}P_{LO,X}\sin^2\theta\cos^2\phi_{Y,I} + i_B^2 + \dfrac{4kTB}{R_L} + 2eBR_d(P_{X,I} + P_{LO,X})}$$

$$(3.16)$$

Now the conditional BER is given by-

$$BER_{cond}(\theta, I) = \frac{1}{2} erfc\left(\frac{\sqrt{SCNR(\theta, I)}}{2}\right)$$

(3.17)

The probability density function of turbulence induced fading I, is taken as log-normal distribution for weak atmospheric turbulence which is given by-

$$f_I(I) = \frac{1}{\sqrt{2\pi\sigma^2}I} e^{\frac{-(\ln(I)-\mu)^2}{2\sigma^2}} \quad ; I > 0$$

(3.18)

Finally, the BER average is given by [147]-

$$BER_{average} = \int_0^{\frac{\pi}{2}} \int_0^{\infty} BER_{cond.}(\theta, I).f_I(I).f_\theta(\theta)dI\ d\theta$$

(3.19)

Where, $f_\theta(\theta)$ represents the probability density function of random misalignment angle θ, which is modeled as Maxwellian distribution [56, 148]-

$$f_\theta(\theta) = \frac{32}{\pi^2\theta_m^3}\theta^2 e^{-\frac{(2\theta)^2}{\pi\theta_m^2}}$$

(3.20)

Where, θ_m represents the mean misalignment angle of the random rotations.

3.3.3 Results and discussion

Following the analytical approach, we determine the system BER performance of a FSO link considering polarization division multiplexing optical DQPSK modulation with coherent homodyne detection. Table-3.1 contains the parameters that are used for numerical simulation. In Fig. 3.6, the plots of bit error rate as a function of received optical signal power are depicted for different cases of without turbulence, with turbulence and without and with polarization induced crosstalk. Results show that system severely affected

in BER performance because of polarization induced crosstalk as well as atmospheric turbulence.

Table 3.1: List of parameters used for numerical simulation

Parameters	Values
PIN photodetector Responsivity, Rd	0.85
Characteristic of the MZ, V_0	500mV to 8V
Temperature, T	300K
Thermal Resistance, R_L	50Ω
Signal Bandwidth	10GHz
Laser wavelength, λ	1550nm
Power split ratio of two polarized Signals [15]	0.45
Local oscillator power split ratio	0.45
Link distance, L	Up to 3650m
Received power, Pr	-30 to 0 dBm
X-polarized signal phase, $\Phi_{X,I}$	45^0
Y-polarized signal phase, $\Phi_{Y,I}$	45^0
Structure parameter, C_n^2	$10^{-14}m^{-2/3}$
Background noise	10^{-8}watt

The effect of crosstalk and fading only due to the misalignment angle of the received signal is shown in Fig. 3.7. When atmospheric turbulence is added along with this effect, the resultant BER performance degrades severely which is shown in Fig. 3.8. Results show that degradation in BER performance and power penalty occurs significantly which is found to 8.2dB, 9.2dB and 12dB for mean misalignment angle of 4^0, 5^0 and 6^0 respectively at a BER of 10^{-10} for a FSO link with distance of 1000m considering a given turbulence parameter of $C_n^2 = 10^{-14}m^{-2/3}$.
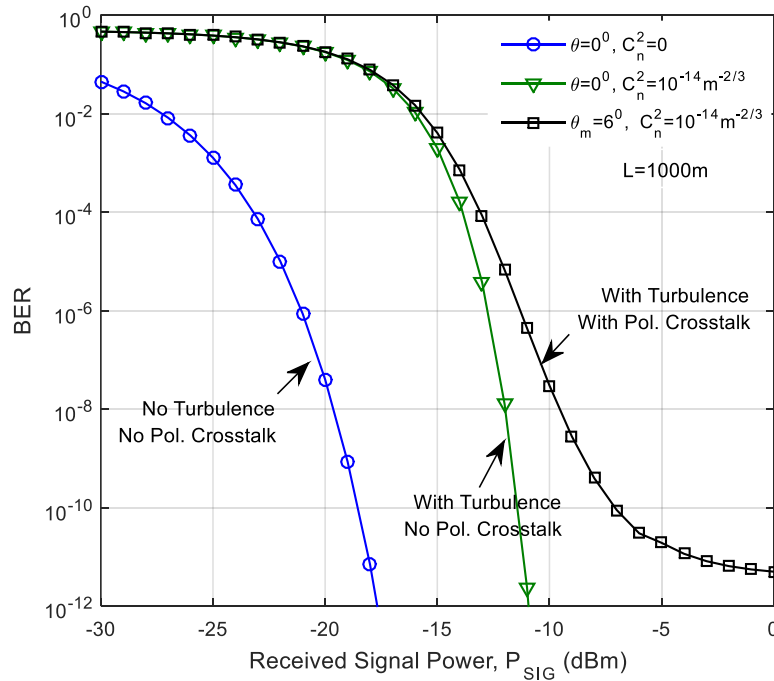
Fig. 3.6: BER performance curves with respect to received optical signal power with and without turbulence in presence and absence of crosstalk considering local oscillator power of 10mW.
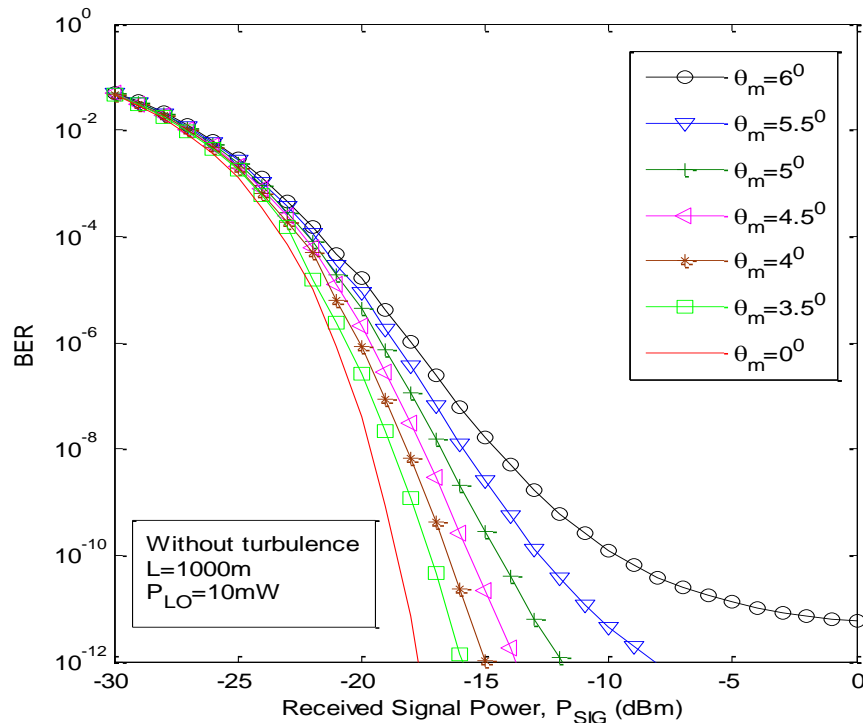
Fig. 3.7: BER performance curves for various value of mean misalignment angle in absence of atmospheric turbulence.
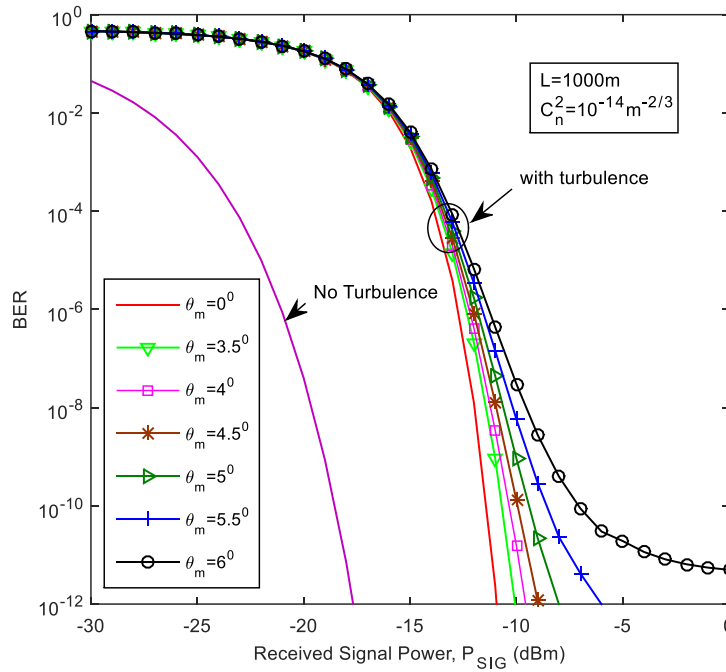
Fig. 3.8: BER performance curves for various value of mean misalignment angle in presence of atmospheric turbulence considering local oscillator power of 10 mW.

The system BER performance improvement due to the increase in local oscillator power is shown in Fig.3.9. When local oscillator power increases, it is in fact increases the signal to noise ratio of the received signal. So the bit error rate performance improves when local oscillator power increases. Result shows that almost 5.1dB improvement in receiver sensitivity occurs due to increase in the local oscillator power from 1mW to 10mW. The system BER performance with respect to received optical signal power under turbulent condition are provided in Fig. 3.10 with link distance as a parameter and considering mean misalignment angle of 4^0. As expected, the performance degrades due to the increase in link distance because it increases signal fading. It is also shown that the allowable link distance for proposed system is 3650m at a BER of 10^{-11} considering the mean misalignment angle is 4^0 because of the effect of atmospheric turbulence. The power penalty increases due to increase in the mean misalignment angle of the received signal as shown in Fig. 3.11 considering both with and without atmospheric turbulence at a BER of 10^{-10}.
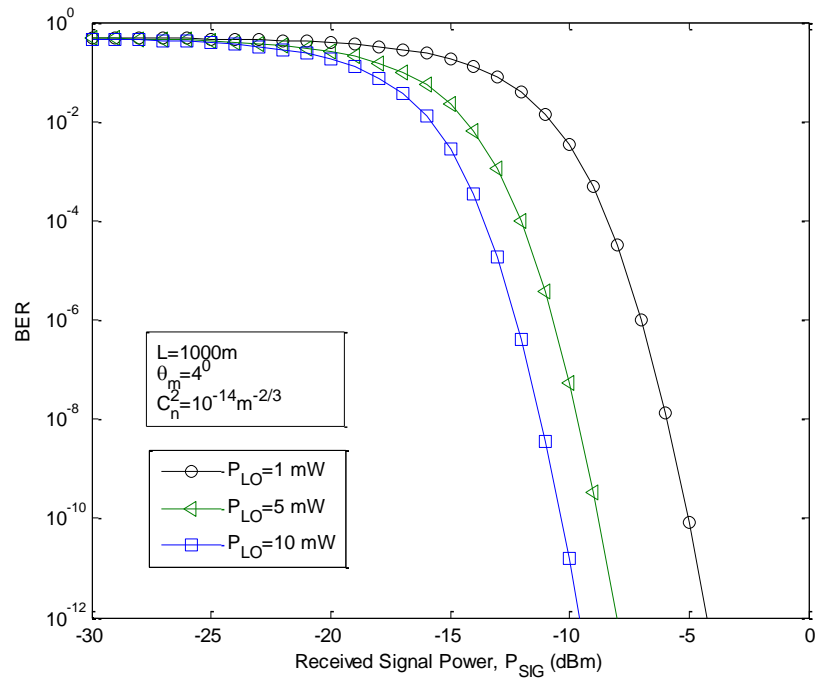
Fig.3.9: BER Performance for different Local oscillator power at a link distance of 1000m and mean misalignment angle of 4^0.
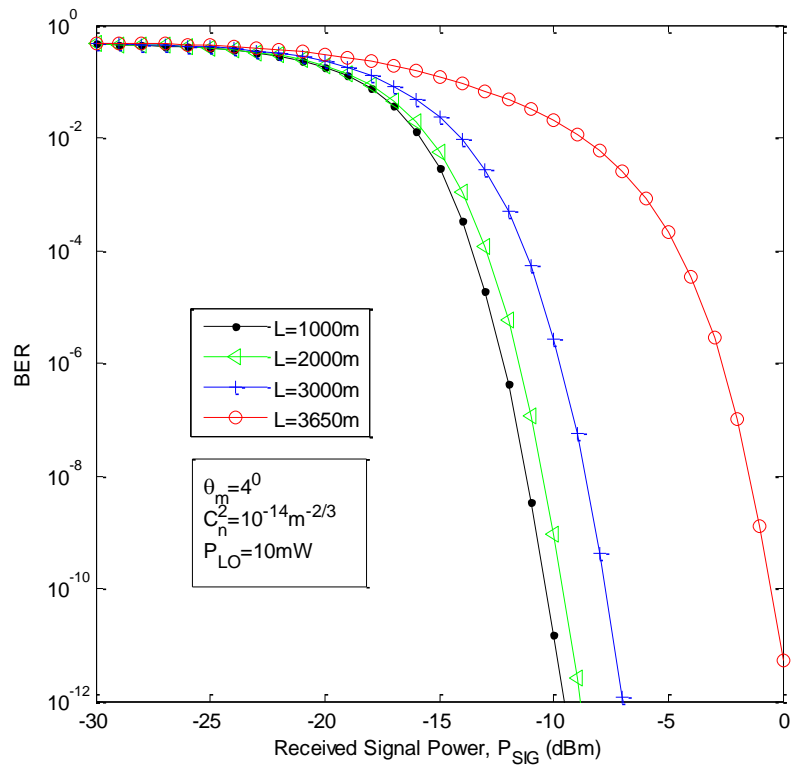
Fig. 3.10: BER performance for various link distances with turbulence and mean misalignment angle of 4^0.

It is noticed that signal suffers almost 7dB, 7.9dB, 9.7dB and 16.7dB more power penalty due to atmospheric turbulence for link distance of 1000m, 2000m, 3000m and 3650m respectively. The amount of penalties are found from the BER versus received optical power curves and provided in Table 3.2 and Table 3.3.

Table 3.2: Power penalties due to both polarization crosstalk and atmospheric turbulence when mean misalignment angle is an input variable at a BER of 10^{-10}.

Mean Misalignment Angle / Link Distance	0^0 (dB)	3.5^0 (dB)	4^0 (dB)	4.5^0 (dB)	5^0 (dB)	5.5^0 (dB)	6^0 (dB)
1000 m	7	8	8.3	8.7	9.3	10.2	11.7
2000 m	7.9	8.95	9.25	9.65	10.2	10.9	12.45
3000 m	9.7	10.7	11	11.45	12	12.5	13.85
3650m	16.7	17.7	18	18.4	19	19.5	20.5

Table 3.3: Power penalties due to both polarization crosstalk and atmospheric turbulence when link distance is an input variable at a BER of 10^{-10}.

Link Distance (m) / Mean Misalignment Angle	500 (dB)	1000 (dB)	1500 (dB)	2000 (dB)	2500 (dB)	3000 (dB)	3500 (dB)	3550 (dB)
4^0	3.3	3.5	3.8	4.2	5.1	6.1	9.1	13.3
5^0	4	4.2	4.5	5	5.8	6.7	9.5	14.5
6^0	5	5.25	5.6	6	6.7	7.7	10.3	14.8

Fig. 3.12 shows the plots of receiver sensitivity degradation for different values of mean angular misalignment to obtain a BER of 10^{-8} considering link distance as an input variable. This receiver sensitivity degradation curve is found from the system BER performance curves. Result shows as expected that when link distance increase the receiver sensitivity degradation is higher and also when mean misalignment angle increase the receiver sensitivity degradation is also higher.
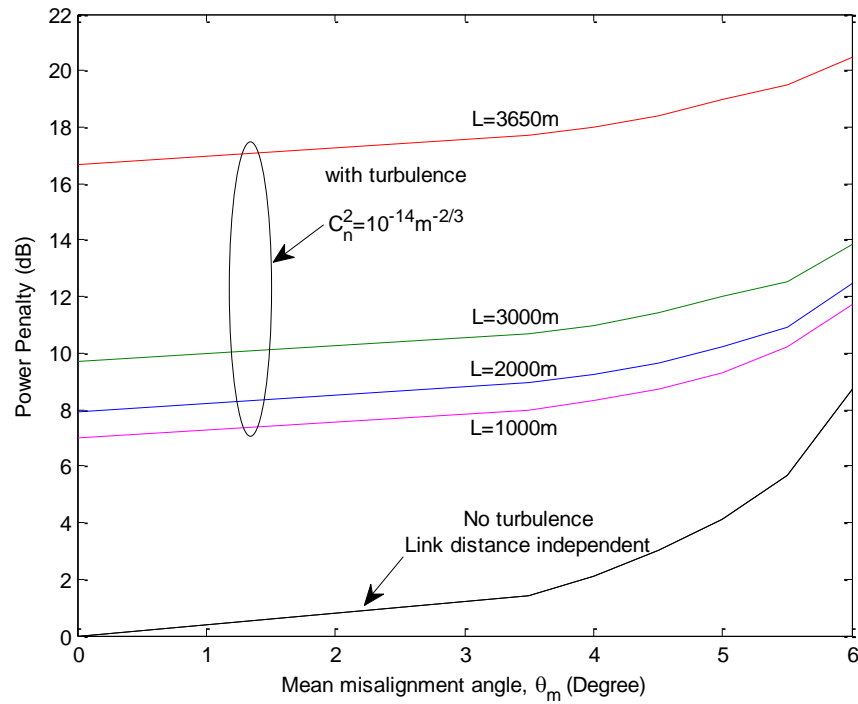
Fig. 3.11: Power penalty versus mean misalignment angle with and without atmospheric turbulence at a BER of 10^{-10}.
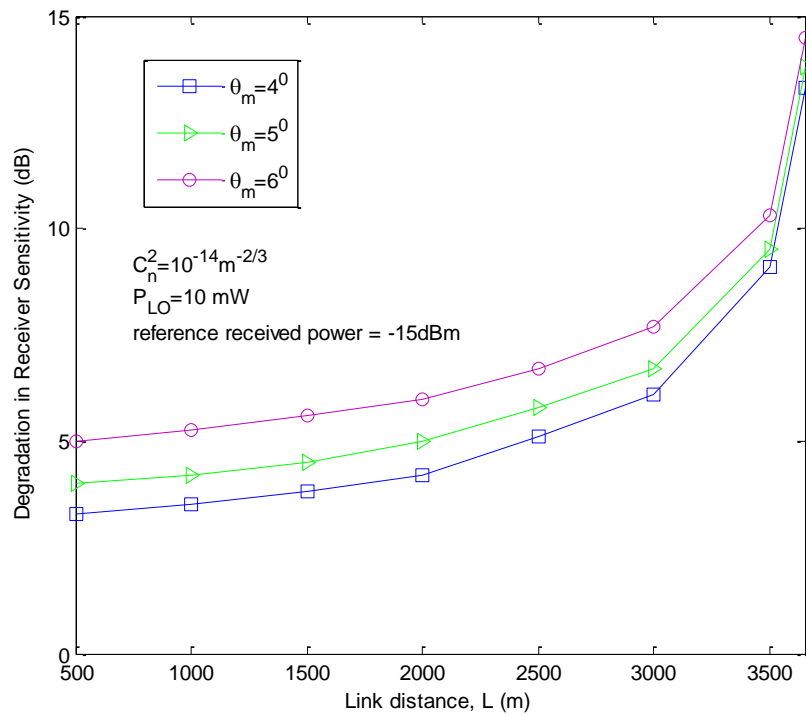
Fig. 3.12: Receiver sensitivity degradation curves for different mean misalignment angle considering link distance as an input parameter at a BER of 10^{-8}.
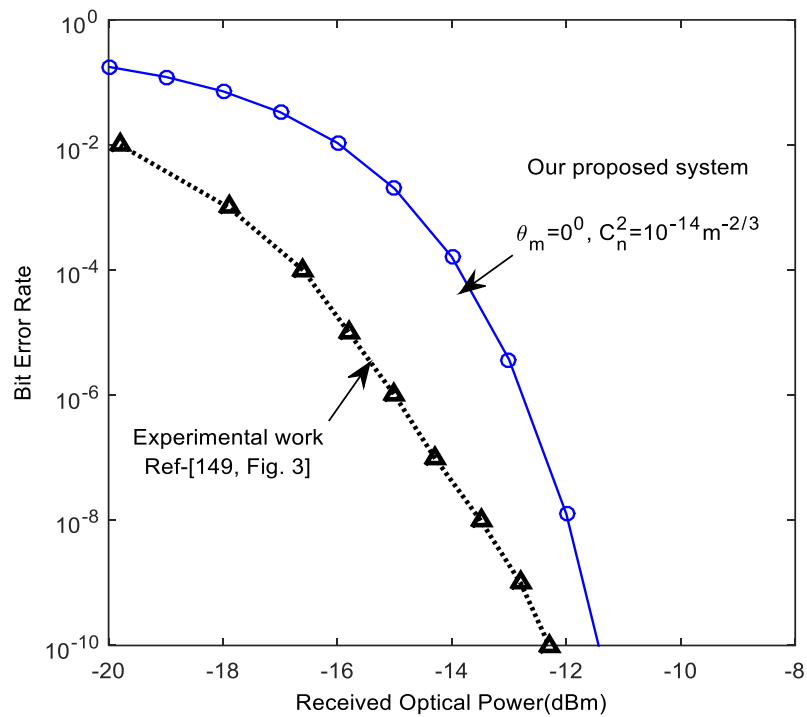
Fig. 3.13: Compare the results of our proposed work with the experimental results in reference [149].
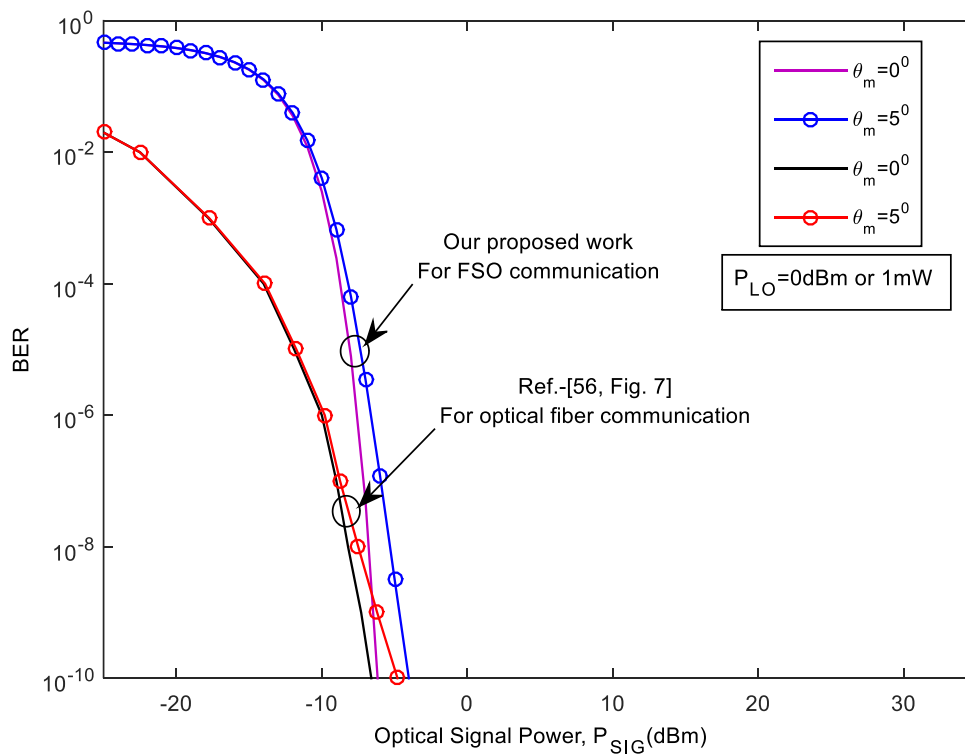
Fig. 3.14: Performance comparison curve between our proposed work (PDM FSO) and reference [56] which is PDM optical fiber communication.

Finally, results of our proposed analytical system is compared with the experimental results of reference [149] and also compared with the published work in reference [56] which is shown in Fig. 3.13 and Fig. 3.14 respectively. It is noticed that our results are in commensurate with the published results.

3.4 BER performance of a Coherent-optical OFDM FSO System with Polarization Diversity

3.4.1 System model

A complete block diagram representation of the proposed system is shown in Fig. 3.15. The complex signal from OFDM modulator is separated by a real-imaginary separator and fed into two different Dual Drive Mach-Zehnder Interferometer (DDMZI) for optical DQPSK modulation [45, 46, 48]. The horizontal and vertical polarized light from polarized beam splitter (PBS) act as a carrier for real and imaginary data respectively. The resultant two modulated signals are combined by a polarized beam combiner and passed through the open air. The received light is again splitted and fed into two different 90^0 hybrid circuit. Light from local oscillator also splitted and fed into the corresponding 90^0 hybrid circuit which is act as a reference light. Digital output is get from the receiver circuit. Reverse process is done for the rest part of the system and retrieve the transmitted bit stream.
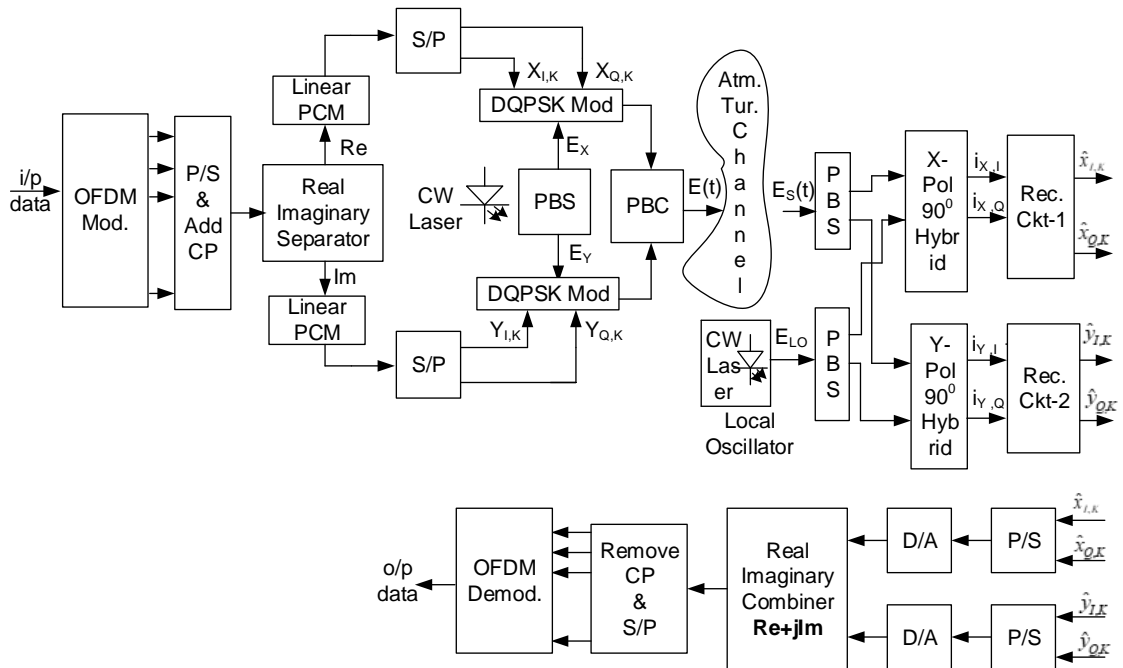
Fig. 3.15: System Block Diagram for OFDM optical differential QPSK modulated FSO system with Polarization Diversity.

3.4.2 Error probabilities analysis

3.4.2.1 Analysis of the transmitted signal

The complex envelop of the OFDM signal is expressed as [42]-

$$v(t) = \sqrt{\frac{2E_s}{T_s}} \sum_{k=0}^{\infty} \sum_{n=0}^{N-1} x_{k,n}(t)\,\varphi_n(t - kT) \quad ; \quad T = NT_s \qquad (3.21)$$

where, $x_{k,n}$ carries the information to be sent over the k*th* symbol interval and n*th* sub band (n=0,1,2,3.............N-1). E_s, T_s and N represent the symbol energy, symbol period and the number of OFDM subcarrier respectively. The complex orthonormal waveform, $\{\varphi_n(t)\}_{n=0}^{N-1}$ is represented as-

$$\varphi_n(t) = \begin{cases} e^{j2\pi(n-\frac{N-1}{2})t/T} & ; \quad t\,\varepsilon\,[0,T] \\ 0 & ; \quad otherwise \end{cases}$$

$$(3.22)$$

The n*th* subcarrier frequency is $f_c + \dfrac{2n - (N-1)}{2T}$. Setting k=0 for simplicity, for first symbol interval, $t \, \epsilon \, (0, T)$ in equation (3.21) we get,

$$v(t) = \sqrt{\frac{2E_s}{T_s}} \sum_{n=0}^{N-1} x_{0,n} \, e^{j\frac{2\pi nt}{NT_s}} \, e^{\frac{-j\pi(N-1)t}{NT_s}} \, ; \quad 0 \le t \le NT_s \tag{3.23}$$

Where, the term, $e^{\frac{-j\pi(N-1)t}{NT_s}}$ is not a function of n, so we can combine it with the carrier term, $e^{j2\pi f_c t}$. Now the equation (3.23) is written by-

$$v(t) = \sqrt{\frac{2E_s}{T_s}} \sum_{n=0}^{N-1} x_{0,n} \, e^{j\frac{2\pi nt}{NT_s}} \quad ; \qquad 0 \le t \le NT_s \tag{3.24}$$

The real and imaginary separator separate the signal, *v(t)* and the output from linear quantized PCM can be expressed as-

$$v_R(t) = \text{Re}\left\{ \sqrt{\frac{2lE_b}{lT_b}} \sum_{n=0}^{N-1} x_{0,n} \, e^{j\frac{2\pi nt}{NT_s}} \right\} \quad ; \qquad 0 \le t \le NT_s$$

$$= \sqrt{2P_b} \sum_{n=0}^{N-1} x_{0,n} \, \cos(\frac{2\pi nt}{NT_s})$$

$$where, \, E_s = lE_b \, , T_s = lT_b \, , l = \log_2 M \tag{3.25}$$

In equation (3.25), *M* and *l* represents the quantization level and number of bits required for different level of quantization respectively and E_b and T_b represents the bit energy and bit period respectively.

The continuous wave input optical signal from laser source can be written as-

$$\vec{E}_{In} = \vec{E}_{Xin} + \vec{E}_{Yin}$$

$$= A_x e^{j(\omega_c t + \varphi_x(t))}.\hat{x} + A_y e^{j(\omega_c t + \varphi_y(t))}.\hat{y} \tag{3.26}$$

where, A_x and A_y are the magnitudes and φ_x and φ_y are the phase of *x* and *y* components respectively.

Now the output light from DDMZI is represented as-

$$E_{out} = E_{Xin}\left[\cos\left(\pi\frac{V_R(t)}{V_\pi}\right) + \cos\left(\pi\frac{\widetilde{V_R}(t)}{V_\pi}\right)e^{\frac{j\pi}{2}}\right] \tag{3.27}$$

The resultant transmitted signals electric field can be represented as-

$$\vec{E}(t) = E_x(t)\hat{x} + E_y(t)\hat{y}$$

$$= A_x e^{j(\omega_c t+\varphi_x(t))}\left[\cos\left(\pi\frac{V_R(t)}{V_\pi}\right) + j\cos\left(\pi\frac{\widetilde{V_R}(t)}{V_\pi}\right)\right]\hat{x}$$

$$+A_y e^{j\left(\omega_c t+\varphi_y(t)\right)}\left[\cos\left(\pi\frac{V_{In}(t)}{V_\pi}\right) + j\cos\left(\pi\frac{\widetilde{V_{In}}(t)}{V_\pi}\right)\right]\hat{y} \tag{3.28}$$

$$E_x(t) = A_x e^{j(\omega_c t+\varphi_x(t))}\left[\cos\left(\pi\frac{V_R(t)}{V_\pi}\right) + j\cos\left(\pi\frac{\widetilde{V_R}(t)}{V_\pi}\right)\right]$$

$$= A_x e^{j(\omega_c t+\varphi_x(t))}\left(\cos\delta + j\cos\tilde{\delta}\right)$$

$$= A_x\sqrt{\cos^2\delta + \cos^2\tilde{\delta}}\ e^{j\left\{\omega_c t+\varphi_x(t)+\tan^{-1}\frac{\cos\tilde{\delta}}{\cos\delta}\right\}}$$

$$\cong A_x\sqrt{2 - \delta^2 - \tilde{\delta}^2}\ e^{j\{\omega_c t+\varphi_x(t)+\alpha_x\}}\ where, \sin\delta \approx \delta, \sin\tilde{\delta} \approx \tilde{\delta},\ \alpha_x = \tan^{-1}\frac{\cos\tilde{\delta}}{\cos\delta}$$

$$\cong A_x\sqrt{2 - \frac{\pi^2 V_R^2(t)}{V_\pi^2} - \frac{\pi^2\widetilde{V}_R^2(t)}{V_\pi^2}}\ e^{j\{\omega_c t+\varphi_x(t)+\alpha_x\}}$$

$$\cong A_x\sqrt{2 - \frac{\pi^2}{N^2 V_\pi^2}\left(\frac{2E_b}{T_b} + \frac{2E_b}{T_b}\right)}\ e^{j\{\omega_c t+\varphi_x(t)+\alpha_x\}}$$

$$\cong A_x\sqrt{2 - \frac{4\pi^2 P_b}{N^2 V_\pi^2}}\ e^{j\{\omega_c t+\varphi_x(t)+\alpha_x\}} \tag{3.29}$$

So the resultant transmitted signal can be written as-

$$\vec{E}(t) = A_x\sqrt{2 - \frac{4\pi^2 P_b}{N^2 V_\pi^2}}\ e^{j\{\omega_c t+\varphi_x(t)+\alpha_x\}}.\hat{x} + A_y\sqrt{2 - \frac{4\pi^2 P_b}{N^2 V_\pi^2}}\ e^{j\{\omega_c t+\varphi_y(t)+\alpha_y\}}.\hat{y} \quad 3.30)$$

3.4.2.2 Analysis of the received signal

The signal from local oscillator at the input of the X-Pol 90^0 hybrid is expressed as-

$$E_{LO,X}(t) = E_{LO,X} \cos \omega_c t \tag{3.31}$$

Random rotations of the sub channel due to the presence of turbulence, the signal suffered fading and crosstalk. The state of polarizations at the PBS, the input signal at the input of the X-Pol 90^0 hybrid is written by-

$$E'_x(t) = \varepsilon_F E_x(t) + \varepsilon_X E_y(t) \tag{3.32}$$

where, ε_F represents complex fading coefficient due to X-polarization and ε_X is the complex crosstalk coefficient due to Y-polarization. The magnitude of these coefficients is provided in equation (3.8).

The probability density function of random misalignment angle is considered as Maxwellian distribution which is shown in equation (3.20).

For strong atmospheric turbulence, Gamma-Gamma model can be considered and the probability density function of I can be modeled as [140, 150]-

$$P(I) = \frac{2(\alpha\beta)^{(\alpha+\beta)/2}}{\Gamma(\alpha)\Gamma(\beta)} I^{\frac{(\alpha+\beta)}{2}-1} K_{(\alpha-\beta)}(2\sqrt{\alpha\beta I}), I > 0 \tag{3.33}$$

After avoiding common losses, the instantaneous output of the port C_1 of the X-Pol 90^0 hybrid is-

$$E_{x,C_1}(t) = E'_x(t) - E_{LO,X}(t)$$
$$= \sqrt{I}\varepsilon_F E_x(t) + \sqrt{I}\varepsilon_X E_y(t) - E_{LO,X}(t)$$

$$\left| E_{x,C_1}(t) \right|^2 = \left| \varepsilon_F E_x(t) + \varepsilon_X E_y(t) - E_{LO,X}(t) \right|^2$$

$$= I\varepsilon_F^2 \left| E_x(t) \right|^2 + I\varepsilon_x^2 \left| E_y(t) \right|^2 + \left| E_{LO,X} \right|^2$$

$$+ 2I\varepsilon_F \varepsilon_x \left| E_x(t) \right| \left| E_y(t) \right| - 2\sqrt{I}\varepsilon_F \left| E_x(t) \right| \left| E_{LO,X} \right|$$

$$- 2\sqrt{I}\varepsilon_x \left| E_y(t) \right| \left| E_{LO,X} \right|$$

$$= I\varepsilon_F^2 A_x^2 (2 - \frac{4\pi^2 P_b}{N^2 V_\pi^2}) + I\varepsilon_x^2 A_y^2 (2 - \frac{4\pi^2 P_b}{N^2 V_\pi^2}) + P_{LO,X}$$

$$+ 2I\varepsilon_F \varepsilon_x (2 - \frac{4\pi^2 P_b}{N^2 V_\pi^2}) - 2\varepsilon_F A_x \sqrt{I(2 - \frac{4\pi^2 P_b}{N^2 V_\pi^2}) P_{LO,x}}$$

$$- 2\varepsilon_x A_y \sqrt{I(2 - \frac{4\pi^2 P_b}{N^2 V_\pi^2}) P_{LO,x}}$$

$$(3.34)$$

Now the output power for the port C_1 is represented as-

$$P_{X,C_1} = \varepsilon_F^2 I A_x^2 (2 - \frac{4\pi^2 P_{b,X}}{N^2 V_\pi^2}) + \varepsilon_X^2 I A_y^2 (2 - \frac{4\pi^2 P_{b,Y}}{N^2 V_\pi^2}) + P_{LO,X}$$

$$+ 2\varepsilon_F \varepsilon_X I A_x A_y \sqrt{(2 - \frac{4\pi^2 P_{b,X}}{N^2 V_\pi^2})(2 - \frac{4\pi^2 P_{b,Y}}{N^2 V_\pi^2})} \cos(\theta_x + \theta_y)$$

$$- 2\varepsilon_F A_x \sqrt{I(2 - \frac{4\pi^2 P_{b,X}}{N^2 V_\pi^2}) P_{LO,X}} \cos\theta_x - 2\varepsilon_X A_y \sqrt{I(2 - \frac{4\pi^2 P_{b,Y}}{N^2 V_\pi^2}) P_{LO,X}} \cos\theta_y$$

$$(3.35)$$

Similarly, the power at port C_2,

$$P_{x,C_2} = \varepsilon_F^2 I A_x^2 (2 - \frac{4\pi^2 P_{b,X}}{N^2 V_\pi^2}) + \varepsilon_X^2 I A_y^2 (2 - \frac{4\pi^2 P_{b,Y}}{N^2 V_\pi^2}) + P_{LO,X}$$

$$+ 2\varepsilon_F \varepsilon_X I A_x A_y \sqrt{(2 - \frac{4\pi^2 P_{b,X}}{N^2 V_\pi^2})(2 - \frac{4\pi^2 P_{b,Y}}{N^2 V_\pi^2})} \cos(\theta_x + \theta_y)$$

$$+ 2\varepsilon_F A_x \sqrt{I(2 - \frac{4\pi^2 P_{b,X}}{N^2 V_\pi^2}) P_{LO,X}} \cos\theta_x$$

$$+ 2\varepsilon_X A_y \sqrt{I(2 - \frac{4\pi^2 P_{b,Y}}{N^2 V_\pi^2}) P_{LO,X}} \cos\theta_y$$

$$(3.36)$$

The differential photocurrent between the port C_1 and C_2 is written by-

$$i_{x,C} = i_{x,C_2} - i_{x,C_1}$$

$$= 4\varepsilon_F R_d A_x \sqrt{I(2 - \frac{4\pi^2 P_{b,X}}{N^2 V_\pi^2}) P_{LO,X}} \cos\theta_x$$

$$+ 4\varepsilon_X R_d A_y \sqrt{I(2 - \frac{4\pi^2 P_{b,Y}}{N^2 V_\pi^2}) P_{LO,X}} \cos\theta_y$$

(3.37)

Now the signal terms after considering fading due to PBS misalignment and turbulence is-

$$i_{x,C} = 4\varepsilon_F R_d A_x \sqrt{I(2 - \frac{4\pi^2 P_{b,X}}{N^2 V_\pi^2}) P_{LO,X}} \cos\theta_x$$

(3.38)

And the crosstalk terms due to X-Pol and turbulence is-

$$i_{Xtalk,C} = 4\varepsilon_X R_d A_y \sqrt{I(2 - \frac{4\pi^2 P_{b,Y}}{N^2 V_\pi^2}) P_{LO,X}} \cos\theta_y$$

(3.39)

3.4.2.3 Analysis of SNR and BER

The conditional signal to noise plus crosstalk ratio (SNCR) condition on turbulence and misalignment angle is represent as-

$$SNCR(\theta, I) = \frac{|i_{X,C}|^2}{|i_{Xtalk,C}|^2 + i_B^2 + \sigma_{th}^2 + \sigma_{sh}^2}$$

$$= \frac{16 R_d^2 I A_x^2 (2 - \frac{4\pi^2 P_{b,X}}{N^2 V_\pi^2}) P_{LO,X} \cos^2\theta \cos^2\theta_x}{[16 R_d^2 I A_y^2 (2 - \frac{4\pi^2 P_{b,Y}}{N^2 V_\pi^2}) P_{LO,X} \sin^2\theta \cos^2\theta_y}$$

$$\overline{} \quad + i_B^2 + \frac{4kTB}{R_L} + 2eBR_d(P_{b,X} + P_{LO,X})]$$

(3.40)

Now, the conditional BER of the system is written by-

$$BER_{cond.}(\theta, I) = \frac{1}{2} erfc\left(\frac{\sqrt{SNCR(\theta, I)}}{2}\right)$$

(3.41)

So, the system average BER can be represented as [147]-

$$BER_{average} = \int_0^{\frac{\pi}{2}} \int_0^{\infty} BER_{cond.}(\theta, I).P(I).P(\theta)dI\ d\theta$$

(3.42)

Now we can simplify the equation (3.42) by taking some necessary steps. Firstly, we rewrite the equation (3.40) as-

$$SNCR(\theta, I_{res}) = \frac{C_1 I \cos^2 \theta}{C_2 I \sin^2 \theta + N_0}$$

(3.43)

where,　　$C_1 = 16R_d^2 A_x^2 (2 - \frac{4\pi^2 E_b}{N^2 V_\pi^2 T_b})P_{LO,X} \cos^2 \theta_x$

$$C_2 = 16R_d^2 A_y^2 (2 - \frac{4\pi^2 E_b}{N^2 V_\pi^2 T_b})P_{LO,X} \cos^2 \theta_y$$

$$N_0 = i_B^2 + \frac{4kTB}{R_L} + 2eBR_d(P_{b,X} + P_{LO,X})$$

Substituting equations (3.20) and (3.41) into (3.42), then we found the average BER equation as-

$$BER_{average} = \int_0^{\infty} \int_0^{\frac{\pi}{2}} \left[\frac{1}{2} - \frac{1}{2} erf\left(\frac{\sqrt{SNCR(\theta, I)}}{2} \right) \right] \frac{32}{\pi^2 \theta_m^3} \theta^2 e^{-\frac{(2\theta)^2}{\pi \theta_m^2}} f(I)\ d\theta\ dI$$

(3.44)

To eliminate the error function associated in equation (3.44), we can invoke equation (3.321.1) reported in [151] and the resultant average BER expression is then-

$$BER_{average} = \int_0^{\infty} \int_0^{\frac{\pi}{2}} \left[\frac{1}{2} - \frac{1}{\sqrt{\pi}} \sum_{q=0}^{\infty} \frac{(-1)^q \left[\frac{\sqrt{SNCR(\theta, I)}}{2} \right]^{2q+1}}{q!(2q+1)} \right] \frac{32}{\pi^2 \theta_m^3} \theta^2 e^{-\frac{(2\theta)^2}{\pi \theta_m^2}} f(I)\ d\theta\ dI$$

(3.45)

To reduce the integral number involved in (3.45), we can invoke equation (3.326.2) reported in [151] and assumed only signal to crosstalk ratio when averaging over Maxwellian distribution to get the more simplified form of the average BER. The final expression of the average BER is -

$$BER_{average} = \frac{32}{\pi^2 \theta_m^3} \int_0^\infty \left[\frac{\Gamma\left(\frac{3}{2}\right)}{4\left(\frac{\pi\theta_m^2}{4}\right)^{\frac{3}{2}}} - \frac{1}{\sqrt{\pi}} \sum_{q=0}^{\infty} \frac{(-1)^q \left[\sqrt{\frac{A_1 I}{4A_2 I + 4N_0}}\right]^{2q+1} \Gamma\left(\frac{-2q+2}{2}\right)}{q!(2q+1)\times 2\left(\frac{\pi\theta_m^2}{4}\right)^{\frac{-2q+2}{2}}} \right] f(I)\,dI \qquad (3.46)$$

3.4.3   Results and Discussion

The system parameters that are used for numerical computations are listed in Table-3.4. Following the analytical approach, the BER performance results are evaluated numerically for different system parameters.

Table 3.4: System Parameters used for simulation results

Parameters	Values
Photodetector Responsivity, Rd	0.85
Characteristic of the MZ, V_0	500mV to 8V
Temperature, T	300K
Thermal Resistance, R_L	50Ω
Signal Bandwidth	10GHz
Laser wavelength, λ	1550nm
Link distance, L	Up to 3650m
Received power, Pr	-70 to -25 dBm
Local Oscillator power	1 mW
Phase of the X-polarized signal, $\Phi_{X,I}$	45^0
Phase of the Y-polarized signal, $\Phi_{Y,I}$	45^0
Structure parameter, C_n^2	$10^{-14}\text{m}^{-2/3}$
Background noise	10^{-8}watt

The system BER versus received optical power curves for without polarization and atmospheric turbulence, with turbulence but without polarization and with turbulence with polarization are shown in Fig. 3.16. It is noticeably shown in Fig. 3.16 that, the system requires almost 7dB more power due to mitigate the combined effect of turbulence and polarization induced crosstalk to achieve a BER of 10^{-12}.
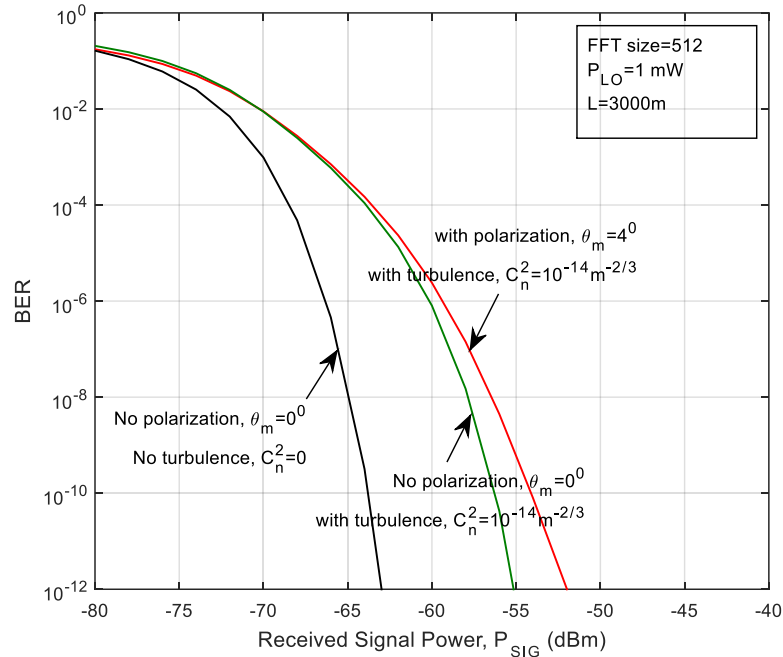
Fig. 3.16: Effect of turbulence and polarization induced crosstalk on the system BER performance considering link loss coefficient is zero.

Fig. 3.17 provides the impact of increasing mean misalignment angle on system power requirements. The system power requirements increase with increasing crosstalk and the maximum allowable mean misalignment angle is 7^0 to maintain a BER of 10^{-6}. Fig. 3.18 shows that the system power requirements decrease with increasing number of OFDM carrier which is expected as OFDM performs best against frequency selective fading channel. When the number of OFDM carrier increase the bandwidth per channel is reduce, so the noise per channel is also reduce. By increasing local oscillator power, the system BER performance can improve which is shown in Fig. 3.19. Due to increases local oscillator power, it increases the signal to noise ratio of the received signal. Result shows that when the local oscillator power increases from 1mW to 10mW it decreases the system power requirements almost 10dB at a BER of 10^{-12}.
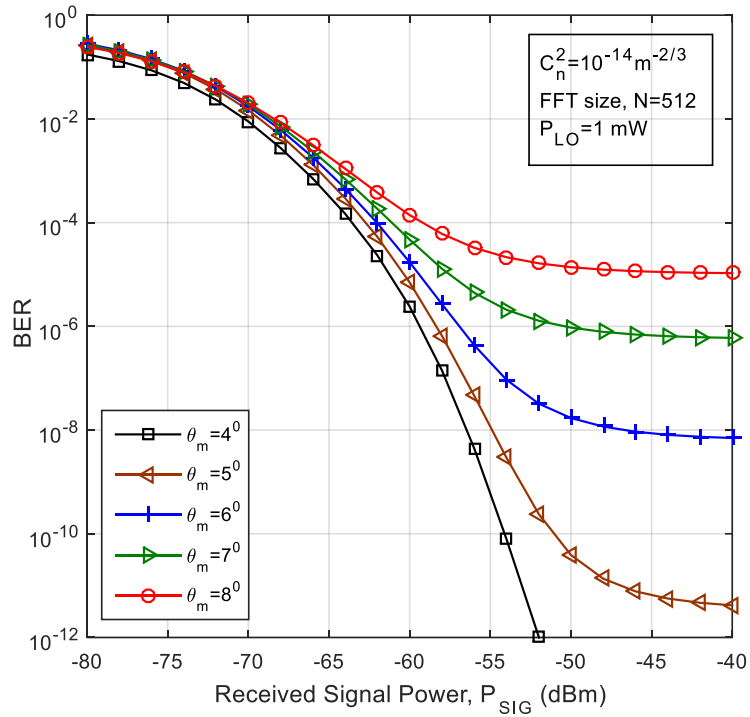
Fig.3.17: BER performance curves for different mean misalignment angle due to strong turbulence considering link loss coefficient is zero.
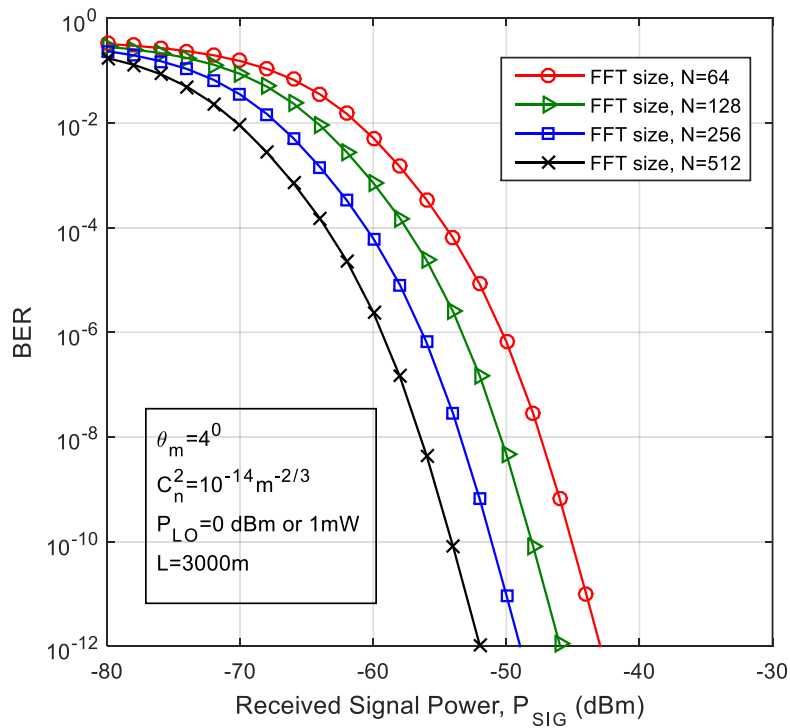
Fig. 3.18: Effect of increasing number of OFDM carrier on system BER performance over turbulence with polarization induced crosstalk considering link loss coefficient is zero.
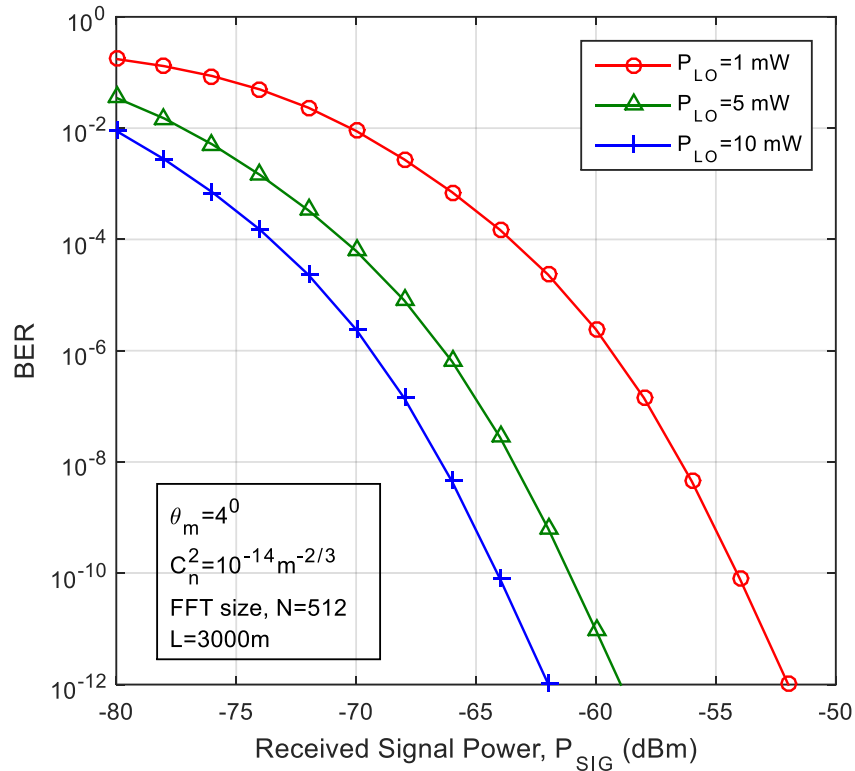
Fig. 3.19: Impact of increasing local oscillator power on BER performance over turbulence with polarization induced crosstalk considering link loss coefficient is zero.

The change in system BER performance with increasing link distance is shown in Fig. 3.20 and it is found that the system allowable link distance is 3650m. When the mean misalignment angle increases beyond 7^0, the system became link distance independent at a BER of 10^{-6} which is shown in Fig. 3.21. Receiver sensitivity due to the increasing OFDM carrier is provided in Fig 3.22. Results shows that, the receiver sensitivity improves when the number of OFDM carrier increase. Fig. 3.23 shows that the power penalty increase due to increasing the mean misalignment angle of the received signal which in fact increase the signal crosstalk and power penalty is found to 9.5dB, 12dB and 21dB for mean misalignment angle of 4^0, 5^0 and 6^0 respectively at a BER of 10^{-8} for a FSO link distance of 2000m with turbulence variance $10^{-14}m^{-2/3}$. The amount of penalties found from the BER versus received optical power curves and provided in Table 3.5.
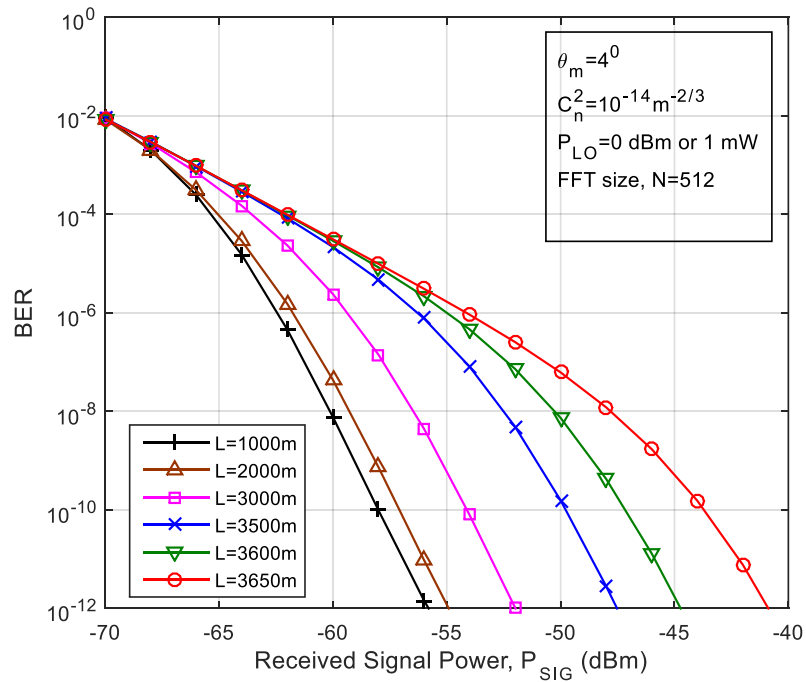
Fig. 3.20: Impact of increasing link distance on system BER performance curve when both turbulence and polarization crosstalk presence considering link loss coefficient is zero.
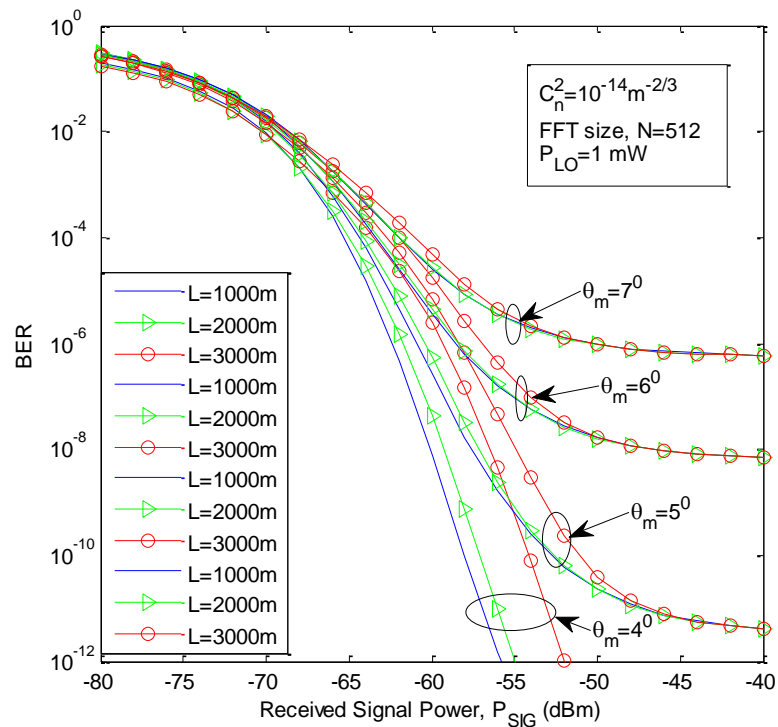
Fig.3.21: BER Performance curve for different mean misalignment angle with different Link distance in presence of turbulence considering link loss coefficient is zero.
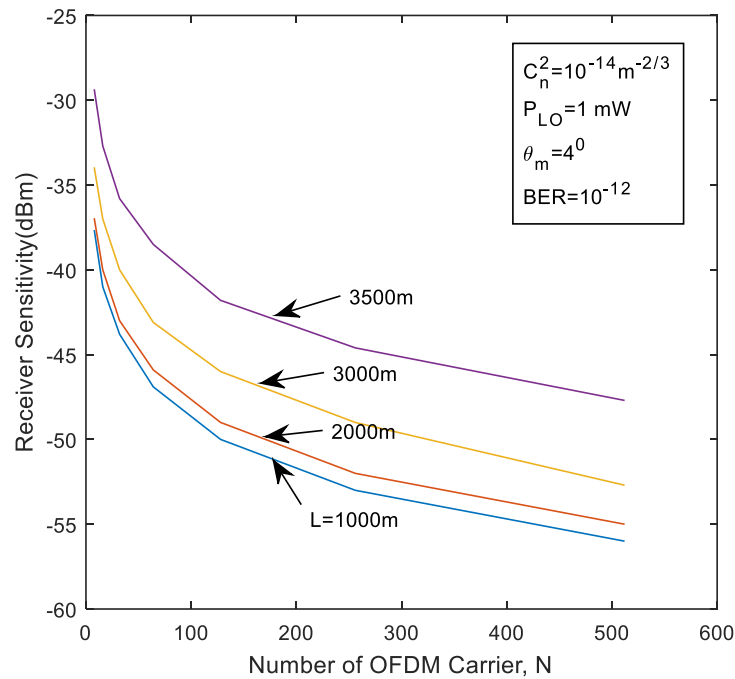
Fig. 3.22: Receiver sensitivity versus number of OFDM carrier for different Link distance when both turbulence and polarization crosstalk presence considering link loss coefficient is zero.

Table 3.5: Power penalties for different mean misalignment angle at a BER of 10^{-8}

Mean Misalignment Angle / Link Distance	4^0 (dB)	4.5^0 (dB)	5^0 (dB)	5.5^0 (dB)	6^0 (dB)
1000 m	9	10	11.5	14	21
2000 m	9.5	10.5	12	14	21
3000 m	11.5	12	13	14.6	21
3500m	15.5	16.3	17	18.1	21

It is clearly found that the significant amount of power penalties reduces when the OFDM carrier increase from 64 to 512 and the amount is almost 9dB at a BER of 10^{-9} for mean misalignment angle of 4^0 with turbulence variance $10^{-14}m^{-2/3}$ which depicted in Fig. 3.24 for a link distance 3000m.
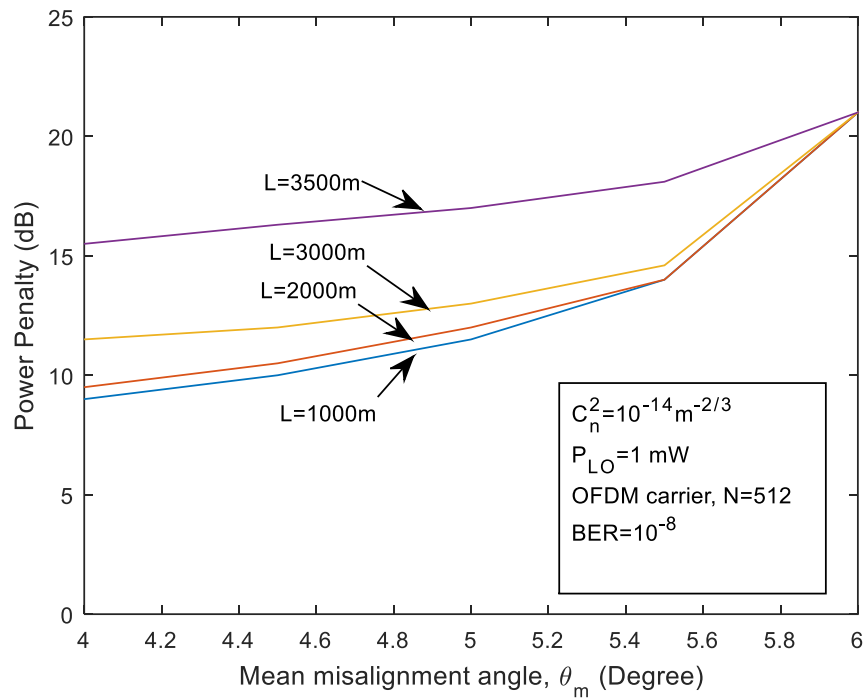
Fig.3.23: Power penalty versus mean misalignment angle for different Link distance in presence of turbulence considering link loss coefficient is zero.
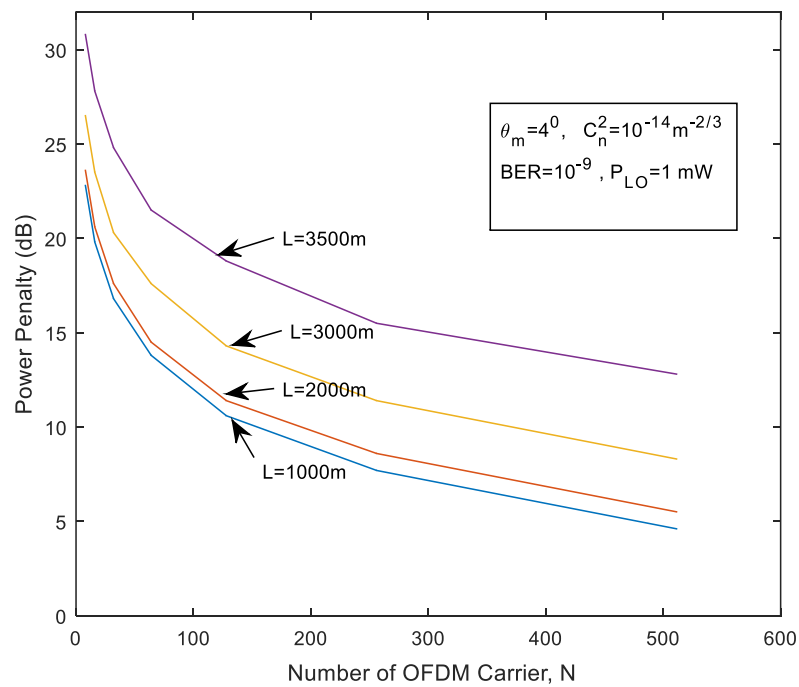
Fig. 3.24: Power penalty versus number of OFDM carrier for different Link distance when both turbulence and polarization crosstalk presence considering link loss coefficient is zero.
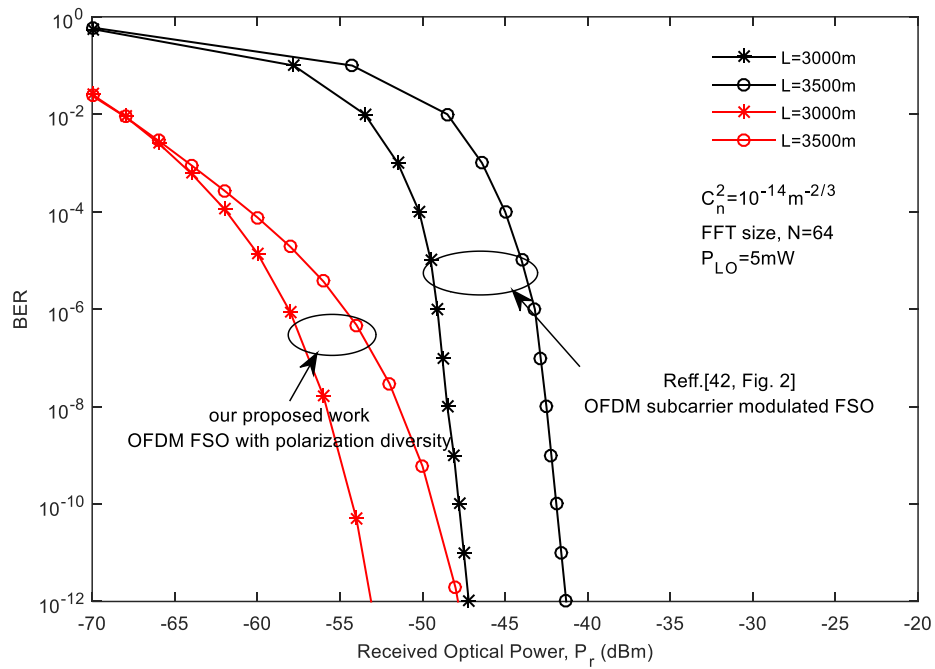
Fig. 3.25: Compare the BER performance of our proposed work with the work in reference [42].
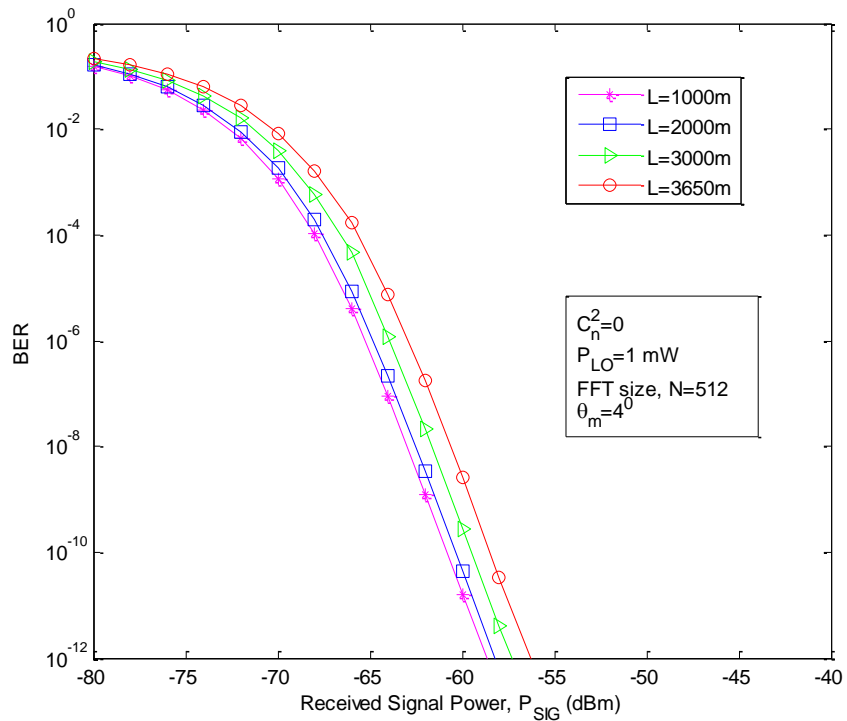
Fig. 3.26: Impact of increasing link distance on system BER performance curve when there is no turbulence but in presence of polarization induced crosstalk considering link loss coefficient is 0.17X10^{-12} m^{-1}.

Our proposed work is compared with one earlier published work and found that almost 6dB improvement in receiver sensitivity for using polarization diversity which is shown in Fig. 3.25. The effect of increasing link distance on system BER performance in absence of atmospheric turbulence considering link loss per meter with mean misalignment angle of 4^0 is shown in Fig. 3.26. It is clearly found that the system suffers more power penalty due to increase the system link distance.

The system BER performance for all weather conditions for different mean misalignment angles are provided in Fig. 3.27. The allowable link distance versus number of OFDM subcarriers is provided in Fig. 3.28. Results show that, for the same system's constraints, the allowable link distance is higher for weak turbulence regime and the allowable link distance is decreasing with increasing turbulences, the change of allowable link distance with number of OFDM subcarrier is also less for weak turbulence and the change increasing with increasing turbulences.
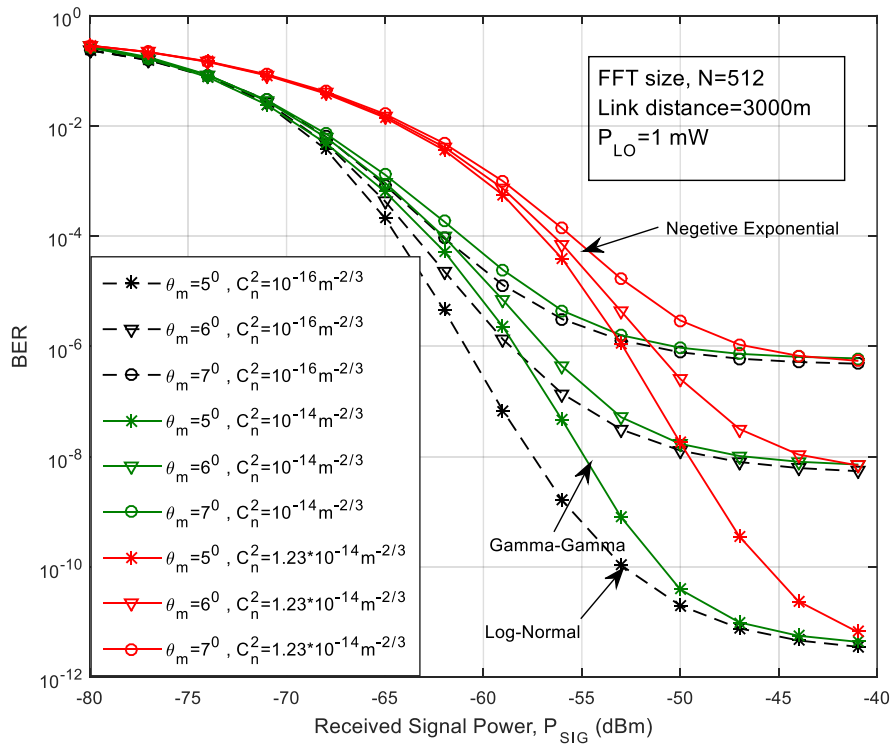
Fig. 3.27: Effect of increasing random mean angular misalignment angle on system's BER performance considering different atmospheric turbulence condition.
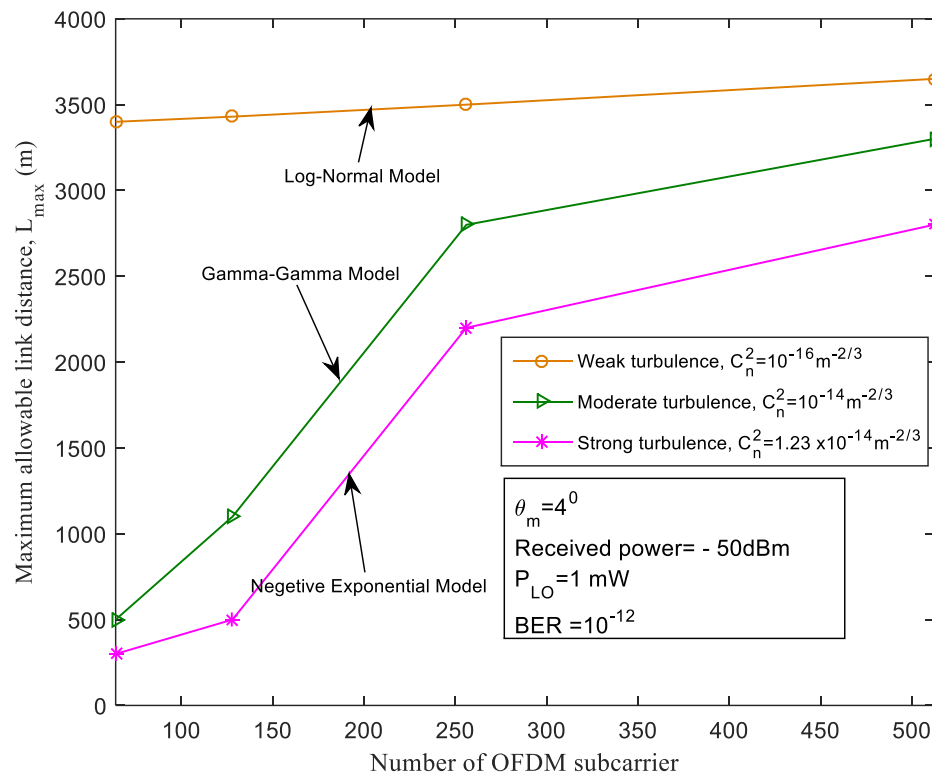
Fig.3.28: Maximum allowable system link distance versus number of OFDM subcarrier for a fixed BER of 10^{-12} and a constant received optical power of -50dBm.

3.5 Aperture Averaged BER Performance of an OFDM FSO System with Polarization Diversity

3.5.1 Aperture averaging

At the receiver side, when the high and low intensity peaks of the received beam are outside the receiver aperture for a point receiver due to turbulence, signal fading results in. Aperture averaging technique reduces fading due to atmospheric turbulence by increasing the diameter of the receiver aperture which actually decreases the relatively fast fluctuations due to small-scale eddies. The key parameter that quantifies the reduction of fading due to aperture averaging is known as aperture averaging factor. It is the ratio of two variances and given by [134]-

$$A = \frac{\sigma_l^2(D)}{\sigma_l^2(0)} \tag{3.47}$$

where, $\sigma_I^2(0)$ is the variance for a very small receiver aperture known as point receiver and $\sigma_I^2(D)$ the variance for a receiver aperture with diameter D. The parameter *A* represents the aperture averaging factor. When the aperture diameter is $D \langle\langle \sqrt{\lambda L}$, then *D* is called the diameter of a point receiver, where λ is for laser wavelength and *L* is the link distance. The values of aperture averaging factor for different receiver aperture diameters used in our simulation are from [134, Fig. 3] and listed in Table 3.6.

Table 3.6: Calculated value of aperture averaging factor [134, Fig. 3].

Aperture Diameter (D)	Aperture Averaging Factor (A)
0.5 mm	0.85
0.8mm	0.71
1mm	0.58
1.5mm	0.39
2mm	0.27
3mm	0.15
4mm	0.08

3.5.2 Analysis of SNR and BER

The system model shown in Fig. 3.15 is considered here and the channel model is considered for weak turbulence condition which is log-normal model. For cross polarization induced crosstalk, the random angular misalignment angle is Maxweillian distributed. The equation (3.40) and (3.46) is used for SNR and average BER respectively where aperture averaging factor is multiplied with the variance of point receiver.

3.5.3 Results and discussion

To perform analytical simulation process, we considered different values of system parameters (listed in Table 3.7). Analysis is carried out to investigate the impact of aperture averaging on the system BER performance. Considering weak atmospheric turbulence, the BER performance versus received signal power for two different link distances with different receiver aperture diameters are depicted in Fig. 3.29. Results clearly point out that the receiver sensitivity improves 3.2dB, 4.9dB and 5.8dB for aperture diameter of 0.5mm, 0.8mm and 1mm respectively with respect to point receiver for link distance of 3500m at a

BER of 10^{-12}. In Fig. 3.30, the BER performance for different aperture diameters considering transmitted beam width is an input variable is provided. It is clearly seen that the BER performance improves due to increase in aperture diameter up to a certain value of transmitted beam width.

Table 3.7: List of the parameters value used for analytical simulation.

Parameters	Values
Characteristic of the MZ, V_0	500mV to 8V
Temperature, T	300K
Thermal Resistance, R_L	50Ω
FFT size, N	512
Laser wavelength, λ	1550nm
Responsivity, R_d	0.85
Detector aperture radius, D	0- 4mm
Received power, Pr	-70 to -45dBm
Mean misalignment angle, θ_m	4^0
Local Oscillator Power, P_{LO}	0dBm or 1mW
Transmitted Beam Width, W_0	0-4mm
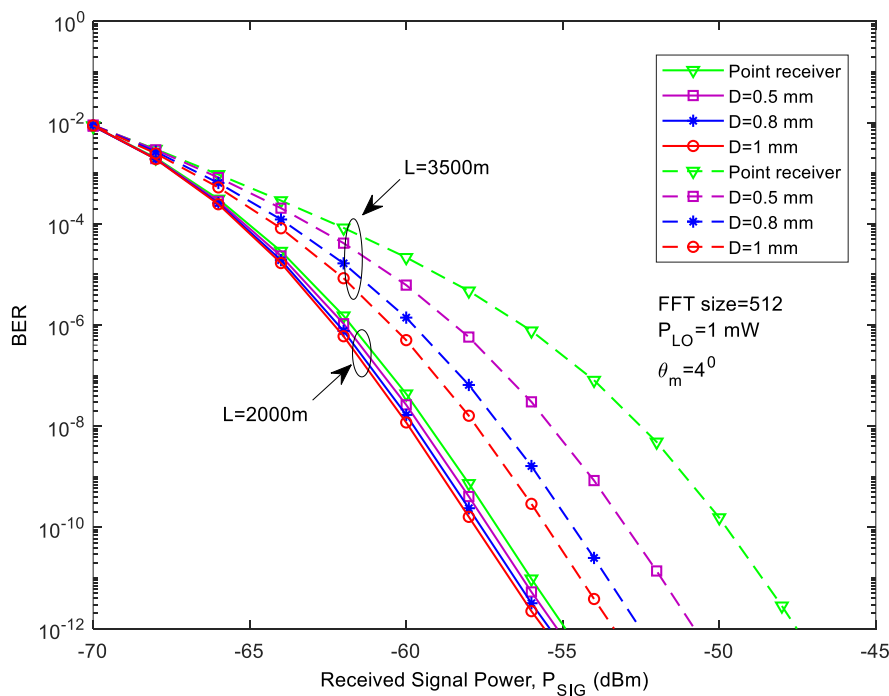
Fig. 3.29: BER performance for different aperture diameters.
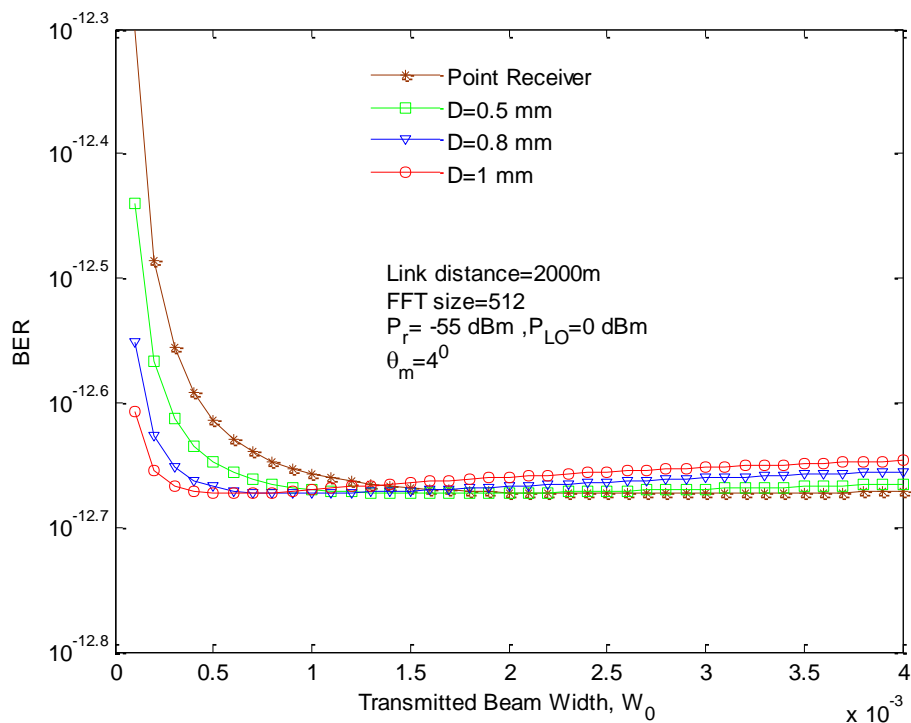
Fig. 3.30: BER versus transmitted beam width for different aperture diameters.
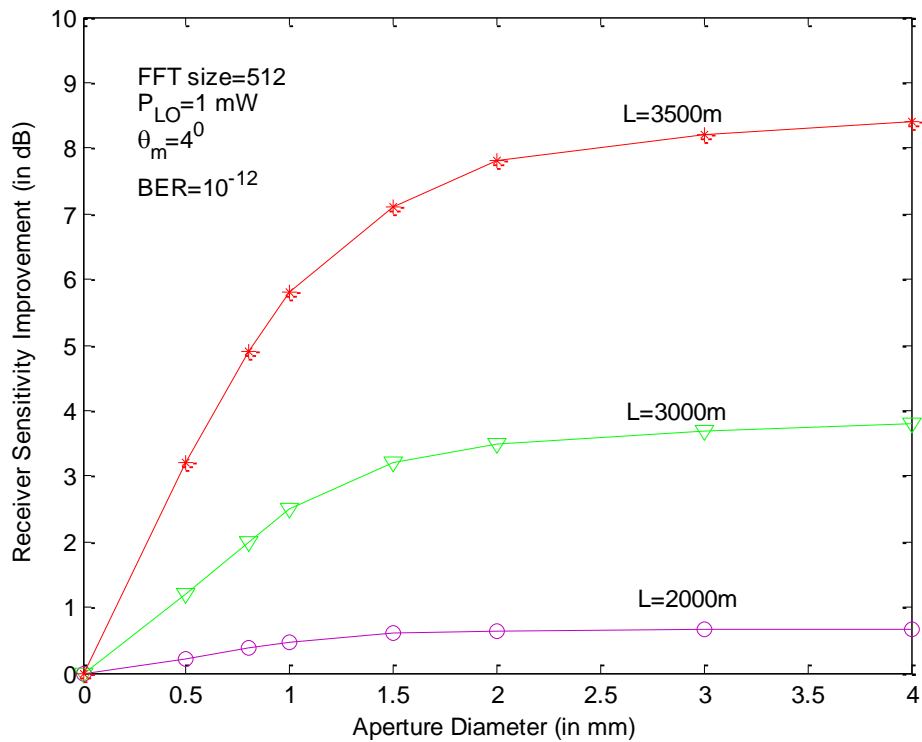
Fig. 3.31: Receiver sensitivity improvement versus aperture diameter for different link length at a BER of 10^{-12}.

The receiver sensitivity improvement versus aperture diameter curves considering three different link distances is given in Fig. 3.31. The receiver sensitivity improvement is found to almost 0.48dB, 2.5dB and 5.8dB for link length of 2000m, 3000m and 3500m respectively for an aperture diameter of 1mmat a BER of 10^{-12}.

3.6 Summary

The system performance degrades significantly because of crosstalk from the X-Pol due to induced random misalignment angle caused by the existence of strong atmospheric turbulence. Results are evaluated numerically taking into account the probability density function of the polarization fluctuation to be Maxwellian distribution. It is found that, when increasing the mean misalignment angle beyond 7^0 the system BER performance falls severely. It is also noticed that significant amount of receiver sensitivity improvement occurs when local oscillator power and number of OFDM carrier increase. The results may be used to find application in design of PDM optical FSO link over turbulent channel.

Chapter 4

Space Frequency Block Coded OFDM FSO System

Chapter-4

SPACE FREQUENCY BLOCK CODED OFDM FSO SYSTEM

4.1 Introduction

Spatial diversity is considered as a promising solution to combat atmospheric turbulences. By using multiple apertures at the transmitter and/or the receiver sides, spatial diversity has the potential to mitigate atmospheric turbulence effects, enhances the performance of the FSO links and overcomes the limitations on the transmit optical power.

Two spatial diversity techniques are generally considered for FSO systems. Namely, repetition codes (RCs) and orthogonal space time/frequency block codes (OSTBCs). Conventional OSTBCs, as used in RF systems, should be modified to deal with IM/DD techniques because the output of the transmitter must be unipolar.

The application of FSO communication is increasing day by day to mitigate the public increasing demand of high data rate. Space frequency block coding (SFBC) technology can help the FSO communication system by enhancing its capacity. SFBC can also be effectively used with OFDM to reduce the frequency selective fading effect of the channel.

4.2 Space Frequency Block Coding (SFBC)

Another important spatial diversity technique is space frequency block coding for multipath environment using the concept of Alamoti's space time block coding scheme. To obtain SFBC in microwave communication reconfigurable antennas are needed. But in FSO communication it is difficult to perform SFBC scheme, so we consider RF modulation for frequency diversity. The *[2 × 2]* SFBC illustration is shown in Fig. 4.1.
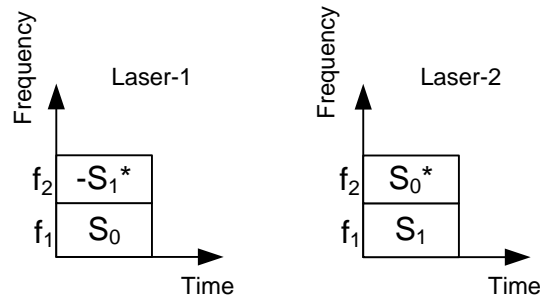
Fig. 4.1: SFBC illustrations for two transmit and two receive antennas.

4.2.1 SFBC Encoder

A detail description of the SFBC encoder is shown in Fig. 4.2 where serial input bit streams are mapping according to Alamoti's scheme. Then two different radio frequencies are considered to modulate data at electrical domain and two laser sources to represent space at optical domain. Two symbols S_0 and S_1 are modulated by frequency f_1, at the same time complex conjugate of S_0 and negative complex conjugate of S_1 are modulated by frequency f_2. Then, the first laser transmits S_0 and negative complex conjugate of S_1, whereas the second laser transmits S_1 and complex conjugate of S_0 during the same time according to the SFBC illustration.
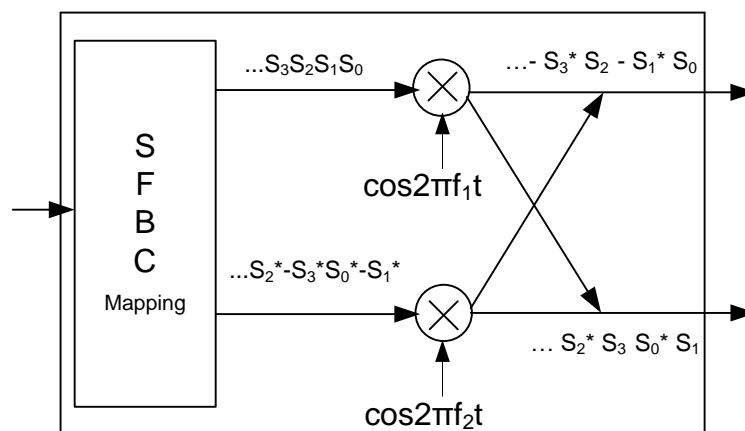
Fig. 4.2: 2 X 2 SFBC encoder.

4.2.2 SFBC Decoder

A detail description of the SFBC decoder is shown in Fig. 4.3 where the incoming bit streams remapped first. Then the same radio-frequencies are used to demodulate the corresponding incoming data. Finally, after de-mapping resultant demodulated data we get our original bit streams.
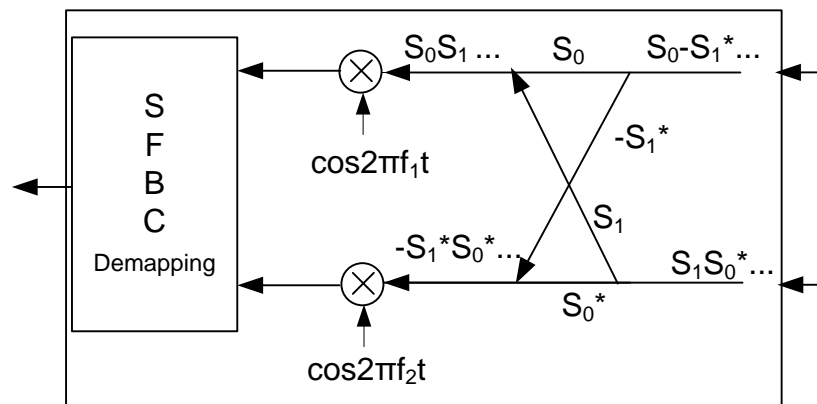
Fig. 4.3: 2X2 SFBC decoder.

4.3 Performance Analysis of an Optical Link considering SFBC

4.3.1 System model

In Fig. 4.4, the full block diagram of SFBC-coherent optical OFDM followed by DQPSK FSO system with polarization diversity is shown. After OFDM modulator, the resultant complex signal is mapped according to the SFBC encoding technique. To perform optical differential quadrature phase shift keying (DQPSK) modulation, we separate the resultant SFBC encoded complex signal first by using a real-imaginary separator and put them as the in-phase and quadrature phase inputs of the two different Dual Drive Mach-Zehnder Interferometers (DDMZI). A polarized beam splitter (PBS) is used to generate the horizontal and vertical polarized lights which are then used as the light carrier for real and imaginary data respectively. After DQPSK modulation, a polarized beam combiner (PBC) is required to combine the two resultant modulated signals and then transmit through the

atmospheric channel in presence of strong turbulence. At the receiver end, a PBS is used to separate the horizontal and vertical light from the received light and put them as the input of two different 90^0 hybrid circuit. For coherent detection, local oscillator's light used as the reference light which is also splitted. The splitted horizontal and vertical lights of the local oscillator act as another input for the corresponding 90^0 hybrid circuit. The output current from 90^0 hybrid circuit is passed through a receiver circuit from which we get the digital output. Finally, to achieve the original transmitted bit stream the reverse process must be done for the remaining part of the proposed system.
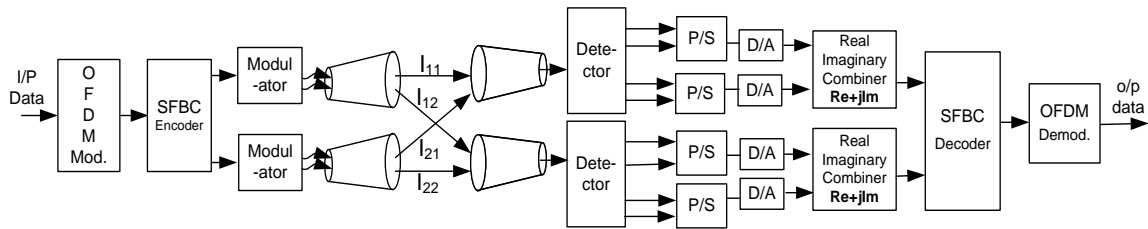
Fig. 4.4: Complete Block Diagram for SFBC-coherent optical OFDM followed by DQPSK FSO system with Polarization Diversity.

4.3.2 Error probability estimation

4.3.2.1 Analysis of the transmitted signal

The OFDM signal which is complex-valued can be expressed as -

$$v(t) = \sqrt{\frac{2E_s}{T_s}} \sum_{k=0}^{\infty} \sum_{n=0}^{N-1} x_{k,n}(t) \, \varphi_n(t-kT) \quad ; \quad T = NT_s \tag{4.1}$$

where, $x_{k,n}$ represents the message of k*th* symbol interval and n*th* sub band (n=0,1,2,3……….N-1). N is representing the OFDM subcarrier number and $\{\varphi_n(t)\}_{n=0}^{N-1}$ is represented as the complex orthonormal waveform. E_s and T_s represents the symbol energy and symbol time respectively.

The resultant output from SFBC encoder is written as-

$$v(t) = \sqrt{\frac{2E_s}{T_s}} \sum_{k=0}^{\infty} \left\{ \sum_{n=0}^{\frac{N}{2}-1} x_{k,2n}(t) \phi_n(t-kT) \cos 2\pi f_1 t + \sum_{n=0}^{\frac{N}{2}-1} -x_{k,2n+1}^*(t) \phi_n(t-kT) \cos 2\pi f_2 t \right\}$$

(4.2)

where, f_1 and f_2 represents the radio frequency used for SFBC.

The digital output signal of linear quantized pulse code modulator (PCM) can be written as-

$$v_R(t) = \text{Re}\{v(t)\}; \qquad 0 \le t \le NT_s$$

(4.3)

The continuous light beam from laser source which is used for light carrier can be represent

as- $\vec{E}_{In} = \vec{E}_{Xin} + \vec{E}_{Yin} = A_x e^{j(\omega_c t + \varphi_x(t))}.\hat{x} + A_y e^{j(\omega_c t + \varphi_y(t))}.\hat{y}$

(4.4)

where, φ_x and φ_y are the phase and A_x and A_y are the magnitudes of x and y components respectively. The continuous wave laser light frequency is ω_c. The equation of the output light of DDMZI is written by -

$$E_{out} = E_{Xin} \left[\cos\left(\pi \frac{V_R(t)}{V_\pi} \right) + \cos\left(\pi \frac{\widetilde{V_R}(t)}{V_\pi} \right) e^{\frac{j\pi}{2}} \right]$$

(4.5)

where, V_π represents the characteristics of the MZI. Now, the resultant electric field of the transmitted signals can be expressed as-

$$\vec{E}(t) = E_x(t)\hat{x} + E_y(t)\hat{y} = A_x e^{j(\omega_c t + \varphi_x(t))} \left[\cos\left(\pi \frac{V_R(t)}{V_\pi} \right) + j\cos\left(\pi \frac{\widetilde{V_R}(t)}{V_\pi} \right) \right] \hat{x}$$

$$+ A_y e^{j(\omega_c t + \varphi_y(t))} \left[\cos\left(\pi \frac{V_{In}(t)}{V_\pi} \right) + j\cos\left(\pi \frac{\widetilde{V_{In}}(t)}{V_\pi} \right) \right] \hat{y}$$

(4.6)

$$E_x(t) = A_x e^{j(\omega_c t + \varphi_x(t))} \left[\cos\left(\pi \frac{V_R(t)}{V_\pi} \right) + j\cos\left(\pi \frac{\widetilde{V_R}(t)}{V_\pi} \right) \right]$$

$$= A_x e^{j(\omega_c t + \varphi_x(t))} [\cos\delta + j\cos\tilde{\delta}]$$

$$\cong A_x \sqrt{\cos^2\delta + \cos^2\tilde{\delta}} e^{j\left(\omega_c t + \varphi_x(t) + \tan^{-1}\frac{\cos\tilde{\delta}}{\cos\delta} \right)}$$

$$\cong A_x \sqrt{2 - \delta^2 - \tilde{\delta}^2} e^{j(\omega_c t + \varphi_x(t) + \alpha_x)}$$

$$\cong A_x \sqrt{2 - \frac{\pi^2 v_R^2(t)}{V_\pi^2} - \frac{\pi^2 \tilde{v}_R^2(t)}{V_\pi^2}} e^{j(\omega_c t + \varphi_x(t) + \alpha_x)}$$

$$\cong A_x\sqrt{2 - \frac{8\pi^2 E_b}{N^2 V_\pi^2 T_b}(cos^2 2\pi f_1 t + cos^2 2\pi f_2 t)}e^{j(\omega_c t + \varphi_x(t) + \alpha_x)} \qquad (4.7)$$

where, E_b and T_b are representing the bit energy and bit duration respectively. Now, we can write the resultant signal as-

$$\vec{E}(t) = A_x\sqrt{2 - \frac{8\pi^2 E_b}{N^2 V_\pi^2 T_b}(cos^2 2\pi f_1 t + cos^2 2\pi f_2 t)}e^{j(\omega_c t + \varphi_x(t) + \alpha_x)}.\hat{x} +$$

$$A_y\sqrt{2 - \frac{8\pi^2 E_b}{N^2 V_\pi^2 T_b}(cos^2 2\pi f_1 t + cos^2 2\pi f_2 t)}e^{j(\omega_c t + \varphi_y(t) + \alpha_y)}.\hat{y} \qquad (4.8)$$

4.3.2.2 Analysis of the received signal

The signal suffered fading due to the presence of strong atmospheric turbulence and crosstalk due to presence of cross polarization. The details description of a 90^0 hybrid circuit followed by a receiver circuit is provide in Fig. 4.5. A 90^0 hybrid circuit is consists by a balance detection circuit with four coupler. In receiver circuit, the differential current from balance detection circuit is passed through a low pass filter. Then by using a sampler and a comparator we get the digital data.
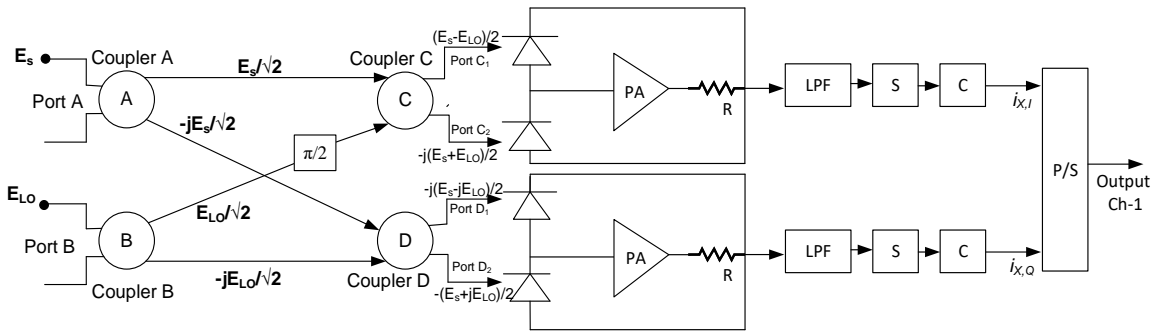
Fig. 4.5: Details representation of a 90^0 Hybrid circuit followed by a receiver circuit.

At the PBS, the polarizations state of the input signal of the X-Pol 90^0 hybrid is represent by-

$$E_x'(t) = \varepsilon_F E_x(t) + \varepsilon_X E_y(t) \qquad (4.9)$$

where, $\mathcal{E}_F$ and $\mathcal{E}_X$ represents the complex fading coefficient and the complex crosstalk coefficient respectively. X-polarization adds signals fading whereas Y-polarization introduces crosstalk. We can write the equations to measure the value of these coefficients as-

$$|\varepsilon_F| = \cos\theta \text{ and } |\varepsilon_X| = \sin\theta \tag{4.10}$$

where, θ is the random angular misalignment angle. Now, we consider Maxwellian distribution for representing the probability density function of random misalignment angle, whose equation is given below-

$$P(\theta) = \frac{32}{\pi^2\theta_m^3}\theta^2 e^{-\frac{(2\theta)^2}{\pi\theta_m^2}} \tag{4.11}$$

where, θ_m is the mean misalignment angle.

To account the effect of strong atmospheric turbulence, we considered the Gamma-Gamma distribution model for the probability density function of channel irradiance *I*, which is modeled as-

$$P(I) = \frac{2(\alpha\beta)^{(\alpha+\beta)/2}}{\Gamma(\alpha)\Gamma(\beta)}I^{\frac{(\alpha+\beta)}{2}-1}K_{(\alpha-\beta)}(2\sqrt{\alpha\beta I}), I > 0 \tag{4.12}$$

where, *I* is for optical signal intensity, the second kind of the modified Bessel function is represented by $K_{\alpha-\beta}$ where $\alpha-\beta$ is its order and symbol Γ is the gamma function. The small-scale and large-scale eddies are represented by α and β respectively. The expression of α and β are expressed as-

$$\alpha = [\exp\{\frac{o.49\sigma_l^2}{(1+1.11\sigma_l^{\frac{12}{5}})^{\frac{7}{6}}}\}-1]^{-1} \qquad and \qquad \beta = [\exp\{\frac{o.51\sigma_l^2}{(1+0.69\sigma_l^{\frac{12}{5}})^{\frac{5}{6}}}\}-1]^{-1}$$

where, σ_l^2 represents the Rytov variance. It is a variance of log-intensity function, its expression is as-

$$\sigma_l^2 = 0.5 \times C_n^2 \times k^{7/6} \times L^{11/6} \tag{4.13}$$

where, $C_n{}^2$ represents refractive index structure parameter, k represents the wave-number and L is the link distance.

To calculate the turbulence, Hufnagel–Velley model is considered usually to find the profile model of $C_n{}^2$ as a function of height, h [140].

$$C_n^2(h) = 0.00594\left(\frac{w}{27}\right)^2 (10^{-5} h)^{10} \exp\left(-\frac{h}{1000}\right) + 2.7 \times 10^{-16} \exp\left(-\frac{h}{1500}\right)$$
$$+ C_n^2(0)\exp\left(-\frac{h}{1000}\right)$$

(4.14)

$$w = \left[\frac{1}{15 \times 10^3} \int_{5 \times 10^3}^{20 \times 10^3} \left\{w_s h + w_g + 30\exp\left(-\left(\frac{h-9400}{4800}\right)^2\right)\right\}^2 dh\right]^{\frac{1}{2}}$$

where, w is the rms wind speed, $C_n{}^2(0)$ is the ground level value of $C_n{}^2$, w_s and w_g represents the beam slew rate and ground level wind speed respectively.

For 2 X 2 SFBC, the probability density function of the resultant channel irradiance can be expressed as [34]-

$$P(I_{res}) = P(I_{11}) \otimes P(I_{12}) \otimes P(I_{21}) \otimes P(I_{22})$$

(4.15)

where, I_{11}, I_{12}, I_{21} and I_{22} represents the channel irradiance for laser-1 to photodetector-1, laser-1 to photodetector-2, laser-2 to photodetector-1 and laser-2 to photodetector-2 respectively. The resultant channel irradiance can be expressed as [152]-

$$\boldsymbol{I}_{res} = \frac{1}{\boldsymbol{M}_T \boldsymbol{R}_C} \sum_{j=1}^{M_R} \sum_{i=1}^{M_T} \left|\boldsymbol{I}_{j,i}\right|^2$$

(4.16)

Where M_T, M_R and R_c represents number of transmitters, receiver and SFBC code rate respectively. After avoiding common losses, the instantaneous output of the port C_1 of the X-polarization 90^0 hybrid is-

$$E_{x,C_1}(t) = E'_x(t) - E_{LO,X}(t)$$
$$= \sqrt{I_{res}}\,\varepsilon_F E_x(t) + \sqrt{I_{res}}\,\varepsilon_X E_y(t) - E_{LO,X}(t)$$

(4.17)

The expression of the output power at the port C_1 is expressed as-

$$P_{X,C_1} = \varepsilon_F^2 I_{res} A_x^2 (2 - \frac{8\pi^2 E_b}{N^2 V_\pi^2 T_b}(\cos^2 2\pi f_1 t + \cos^2 2\pi f_2 t)) + \varepsilon_X^2 I_{res} A_y^2 (2 - \frac{8\pi^2 E_b}{N^2 V_\pi^2 T_b}(\cos^2 2\pi f_1 t + \cos^2 2\pi f_2 t)) + P_{LO,X}$$

$$+ 2\varepsilon_F \varepsilon_X I_{res} A_x A_y \sqrt{(2 - \frac{8\pi^2 E_b}{N^2 V_\pi^2 T_b}(\cos^2 2\pi f_1 t + \cos^2 2\pi f_2 t))(2 - \frac{8\pi^2 E_b}{N^2 V_\pi^2 T_b}(\cos^2 2\pi f_1 t + \cos^2 2\pi f_2 t))} \cos(\theta_x + \theta_y)$$

$$- 2\varepsilon_F A_x \sqrt{I_{res}(2 - \frac{8\pi^2 E_b}{N^2 V_\pi^2 T_b}(\cos^2 2\pi f_1 t + \cos^2 2\pi f_2 t))P_{LO,X}} \cos\theta_x - 2\varepsilon_X A_y \sqrt{I_{res}(2 - \frac{8\pi^2 E_b}{N^2 V_\pi^2 T_b}(\cos^2 2\pi f_1 t + \cos^2 2\pi f_2 t))P_{LO,X}} \cos\theta_y$$

$$(4.18)$$

where, $P_{LO,X}$ represents the local oscillator power for X-polarization 90^0 hybrid. Output power at port C_2 can write similarly. Now, the output differential photocurrent of the balanced photodetector between the port C_1 and C_2 is represented by-

$$i_{x,C} = i_{x,C_2} - i_{x,C_1} = 4\varepsilon_F R_d A_x \sqrt{I_{res}(2 - \frac{8\pi^2 E_b}{N^2 V_\pi^2 T_b}(\cos^2 2\pi f_1 t + \cos^2 2\pi f_2 t))P_{LO,X}} \cos\theta_x$$

$$+ 4\varepsilon_X R_d A_y \sqrt{I_{res}(2 - \frac{8\pi^2 E_b}{N^2 V_\pi^2 T_b}(\cos^2 2\pi f_1 t + \cos^2 2\pi f_2 t))P_{LO,X}} \cos\theta_y$$

$$(4.19)$$

Now the first part and second part of equation (4.19) represents the signal terms and crosstalk terms respectively due to PBS misalignment and turbulence.

4.3.2.3 SNR and BER Analysis

For the proposed system we calculate the signal to noise plus crosstalk ratio (SNCR) instead of signal to noise ratio (SNR). By putting condition on turbulence and misalignment angle, the conditional SNCR can be written as-

$$SNCR(\theta, I_{res}) = \frac{|i_{X,C}|^2}{|i_{Xtalk,C}|^2 + i_B^2 + \sigma_{th}^2 + \sigma_{sh}^2}$$

$$= \frac{16 R_d^2 I_{res} A_x^2 (2 - \frac{8\pi^2 E_b}{N^2 V_\pi^2 T_b}(\cos^2 2\pi f_1 t + \cos^2 2\pi f_2 t)) P_{LO,X} \cos^2\theta \cos^2\theta_x}{[16 R_d^2 I_{res} A_y^2 (2 - \frac{8\pi^2 E_b}{N^2 V_\pi^2 T_b}(\cos^2 2\pi f_1 t + \cos^2 2\pi f_2 t)) P_{LO,X} \sin^2\theta \cos^2\theta_y}$$

$$+ i_B^2 + \frac{4kTB}{R_L} + 2eBR_d(P_{b,X} + P_{LO,X})]$$

$$(4.20)$$

The conditional BER of the system is written by -

$$BER_{cond.}(\theta, I_{res}) = \frac{1}{2} erfc\left(\frac{\sqrt{SNCR(\theta, I_{res})}}{2}\right) \tag{4.21}$$

Finally, we can express the average BER by averaging the conditional BER over two different individual probability density function which is written by -

$$BER_{average} = \int_0^{\frac{\pi}{2}}\int_0^{\infty} BER_{cond.}(\theta, I_{res}).P(I_{res}).P(\theta)dI_{res} \, d\theta \tag{4.22}$$

To simplify the equation (4.22), we first rearrange the equation (4.20) as-

$$SNCR(\theta, I_{res}) = \frac{A_1 I_{res} \cos^2 \theta}{A_2 I_{res} \sin^2 \theta + N_0} \tag{4.23}$$

where,

$$A_1 = 16R_d^2 A_x^2 (2 - \frac{8\pi^2 E_b}{N^2 V_\pi^2 T_b}(\cos^2 2\pi f_1 t + \cos^2 2\pi f_2 t))P_{LO,X} \cos^2 \theta_x$$

$$A_2 = 16R_d^2 A_y^2 (2 - \frac{8\pi^2 E_b}{N^2 V_\pi^2 T_b}(\cos^2 2\pi f_1 t + \cos^2 2\pi f_2 t))P_{LO,X} \cos^2 \theta_y$$

$$N_0 = i_B^2 + \frac{4kTB}{R_L} + 2eBR_d(P_{b,X} + P_{LO,X})$$

Substituting (4.11) and (4.21) into (4.22), we get the BER equation as-

$$BER_{average} = \int_0^{\infty}\int_0^{\frac{\pi}{2}}\left[\frac{1}{2} - \frac{1}{2}erf\left(\frac{\sqrt{SNCR(\theta, I_{res})}}{2}\right)\right]\frac{32}{\pi^2 \theta_m^3}\theta^2 e^{-\frac{(2\theta)^2}{\pi\theta_m^2}} P(I_{res}) \, d\theta \, dI_{res} \tag{4.24}$$

The error function is eliminated from (4.24) by invoking equation (3.321.1) reported in [151], now the BER expression is-

$$BER_{average} = \int_0^\infty \int_0^{\frac{\pi}{2}} \left[\frac{1}{2} - \frac{1}{\sqrt{\pi}} \sum_{q=0}^{\infty} \frac{(-1)^q \left[\frac{\sqrt{SNCR(\theta,I_{res})}}{2} \right]^{2q+1}}{q!(2q+1)} \right] \frac{32}{\pi^2 \theta_m^3} \theta^2 e^{-\frac{(2\theta)^2}{\pi \theta_m^2}} P(I_{res}) \, d\theta \, dI_{res}$$

(4.25)

Multiple integrals involved in (4.25) can be reduced by invoking equation (3.326.2) reported in [151] and taking only signal to crosstalk ratio when averaging over Maxwellian distribution to obtain the simplified expression of the average BER as-

$$BER_{average} = \frac{32}{\pi^2 \theta_m^3} \int_0^\infty \left[\frac{\Gamma\left(\frac{3}{2}\right)}{4\left(\frac{\pi \theta_m^2}{4}\right)^{\frac{3}{2}}} - \frac{1}{\sqrt{\pi}} \sum_{q=0}^{\infty} \frac{(-1)^q \left[\sqrt{\frac{A_1 I_{res}}{4 A_2 I_{res} + 4 N_0}} \right]^{2q+1} \Gamma\left(\frac{-2q+2}{2}\right)}{q!(2q+1) \times 2\left(\frac{\pi \theta_m^2}{4}\right)^{\frac{-2q+2}{2}}} \right] P(I_{res}) \, dI_{res}$$

(4.26)

4.3.3   Results and discussion

Table-4.1 provides the values of the important system parameters that we considered for numerical computations. Following the analytical model, we evaluate the system BER performance results numerically considering both with and without turbulence for without SFBC with polarization diversity, with SFBC with polarization diversity and without diversity and the results are provide in Fig. 4.6. In Fig. 4.6, it is noticeable that, the proposed system requires almost 7.5dB less power due to applying SFBC coding and also shown that the receiver sensitivity improves almost 38dB due to polarization diversity to achieve a BER of 10^{-12} considering local oscillator power is 5mW and link distance is 2000m.

Table 4.1: The list of the system parameters values used for simulation process

Parameters	Values
Photodetector Responsivity, Rd	0.85
Characteristic of the MZ, V_π	500mV to 8V
Temperature, T	300K
Thermal Resistance, R_L	50Ω
Signal Bandwidth	10GHz
Laser wavelength, λ	1550nm
Link distance, L	Up to 3600m
Received power, Pr	-90 to -50 dBm
Local Oscillator power	5 mW
Phase of the X-polarized signal, $\Phi_{X,I}$	45^0
Phase of the Y-polarized signal, $\Phi_{Y,I}$	45^0
Structure parameter, C_n^2	$10^{-14}m^{-2/3}$
Background noise	10^{-8}watt
Radio frequency	1GHz and 1.2 GHz
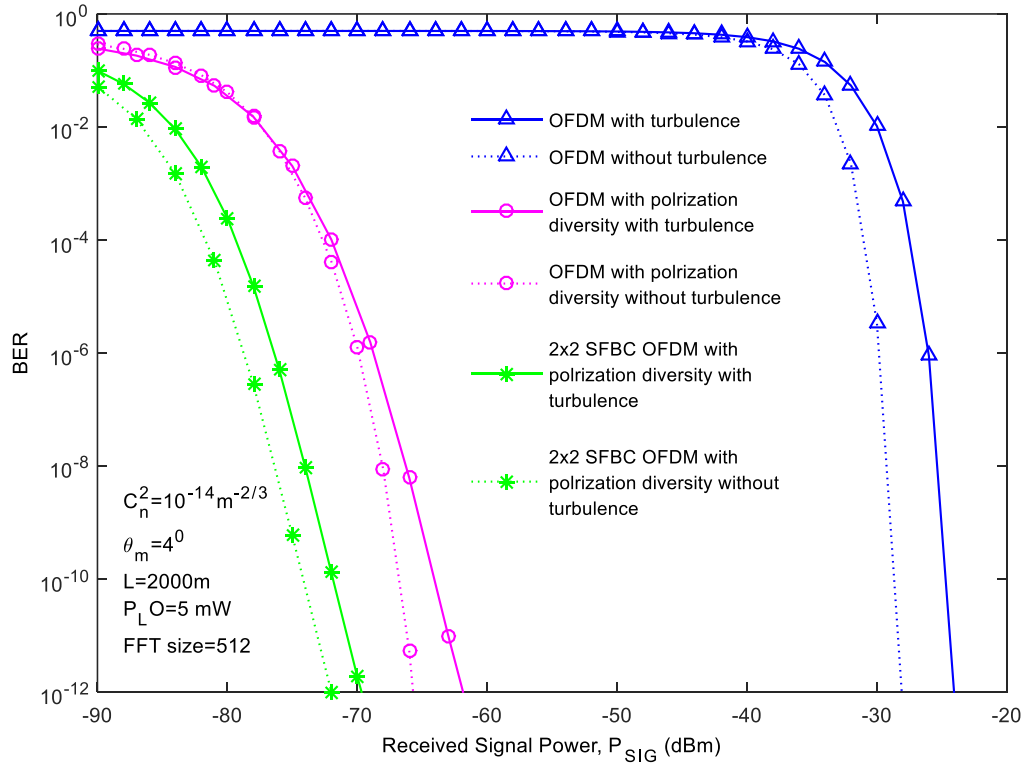
Fig. 4.6: BER performance comparison curves between with and without turbulence for OFDM with polarization diversity with and without SFBC.
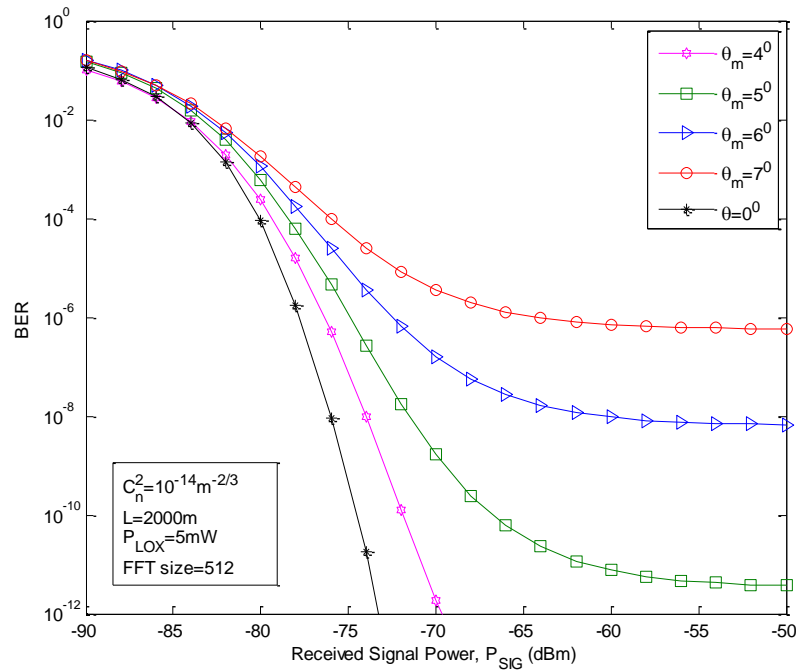
Fig. 4.7: Impact of increasing number of mean angular misalignment on 2X2 SFBC OFDM with polarization diversity system BER performance.

When the mean angular misalignment angle increases which actually increases the crosstalk, the BER performance falls drastically which are clearly depicted in Fig. 4.7. When crosstalk increases, the power requirements of the system also increase as expected and we found that, the maximum possible mean misalignment angle for the proposed system is 7^0 at a BER of 10^{-6}. But when the number of OFDM subcarrier increases which in fact reduces the per channel bandwidth, the BER performance of our system improves significantly, that is clearly depicted in Fig. 4.8. In Fig. 4.9, we found that when we increase the local oscillator power, it also improves our system performance because when local oscillator power increase, its increase the SNR of the received light signal. The system required almost 10 dB less power due to the increase of local oscillator power from 1mW to 10mW at a BER of 10^{-12}. The system power penalty curves considering angular mean misalignment angle and number of OFDM subcarrier as a variable are provided in Fig. 4.10 and Fig. 4.11 respectively. The amount of penalties found from the BER versus received optical power and provided in Table 4.2 and Table 4.3 respectively.
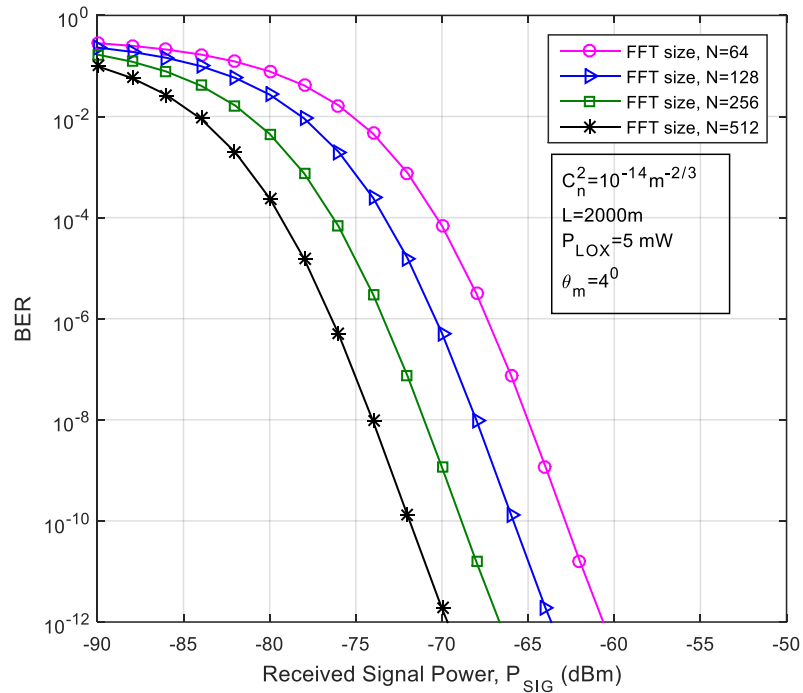
Fig. 4.8: 2X2 SFBC OFDM with polarization diversity system BER performance comparison curves for different number of OFDM subcarrier.
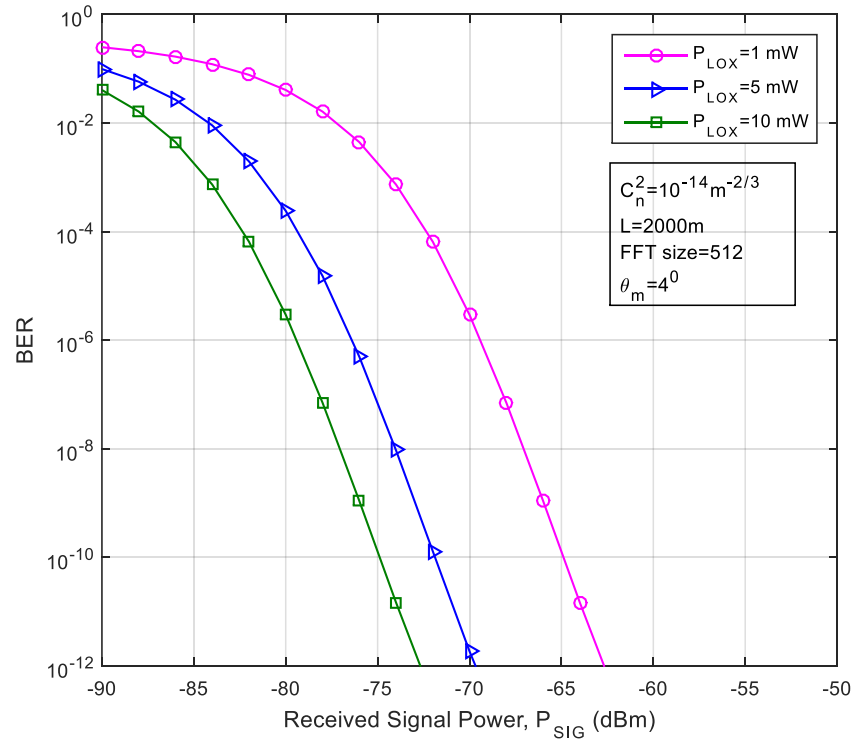
Fig. 4.9: 2X2 SFBC OFDM with polarization diversity system BER performance comparison curves for different local oscillator power.

Table 4.2: Power penalties for different mean misalignment angles at a BER of 10^{-8}

Mean Misalignment Angle / Link Length	0^0 (dB)	4^0 (dB)	4.5^0 (dB)	5^0 (dB)	5.5^0 (dB)	6^0 (dB)
2000 m	0	0.9	1.5	2.9	4.95	12.8
3000 m	0	1.2	1.7	3	5	12.8

Table 4.3: Power penalties for different number of OFDM subcarriers at a BER of 10^{-12}

Number of OFDM Subcarrier / Link Length	8 (dB)	16 (dB)	32 (dB)	64 (dB)	128 (dB)	256 (dB)	512 (dB)
2000 m	23.2	20.3	17.3	14	11.7	8	5.3
3000 m	25.2	22	19	16.2	13	10	7.2

In Fig. 4.10, we found that almost 9dB power penalties reduces when the OFDM carrier number increase from 64 to 512 considering the value of refractive index structure parameter is $10^{-14}\text{m}^{-2/3}$, the link distance is 3600m and the mean misalignment angle is 4^0 at a BER of 10^{-12}. Power penalty is also found to 1.8dB and 11.6dB more when we considered mean misalignment angle of 5^0 and 6^0 respectively with respect to 4^0 at a BER of 10^{-8} considering link distance of 3600m with refractive index structure parameter is $10^{-14}\text{m}^{-2/3}$ which provides in Fig. 4.11. Finally, the effect of different atmospheric turbulent condition on system BER performance is also given in Fig.4.12.
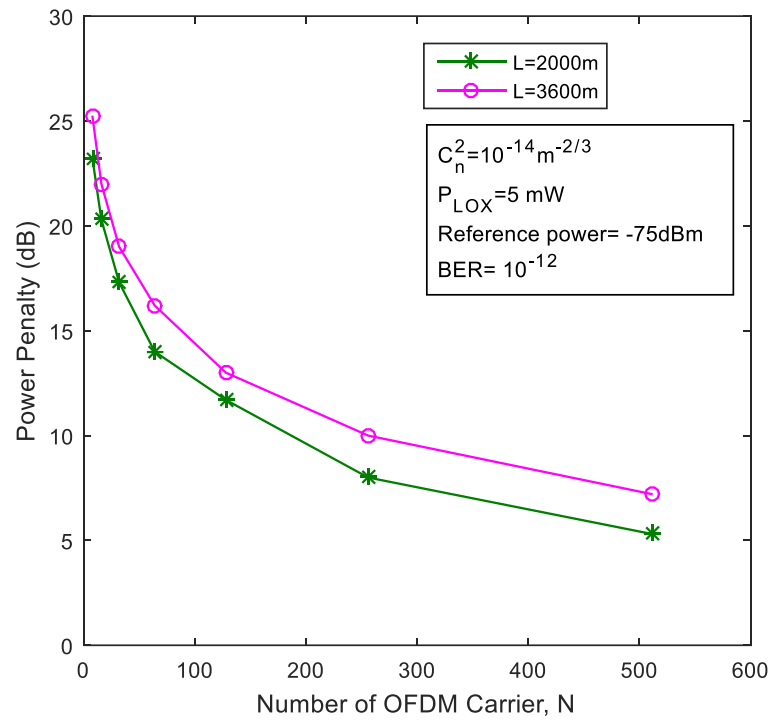
Fig. 4.10: Power penalty curves of 2X2 SFBC OFDM with polarization diversity system for two different link distance considering number of OFDM subcarrier as a variable.
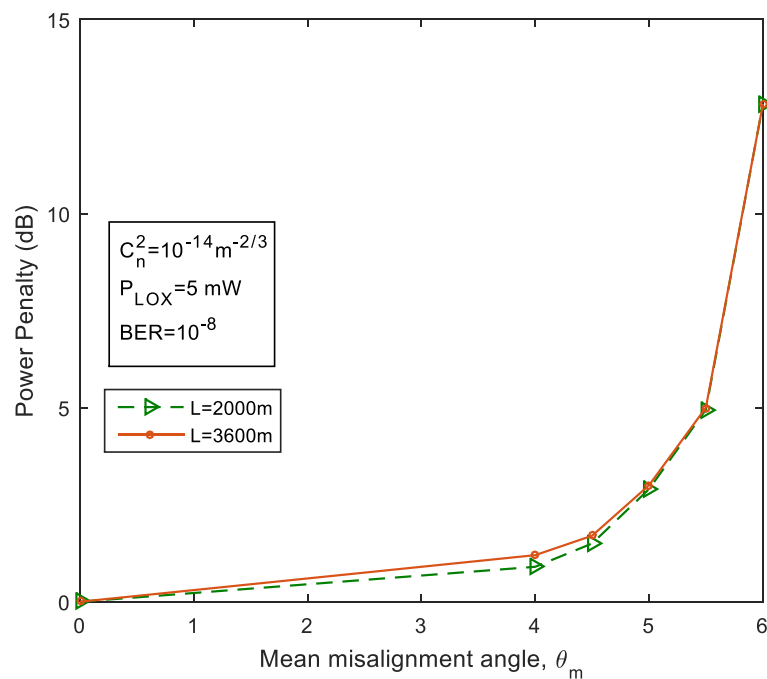
Fig. 4.11: Power penalty curves of 2X2 SFBC OFDM with polarization diversity system for two different link distances considering mean angular misalignment as a variable.
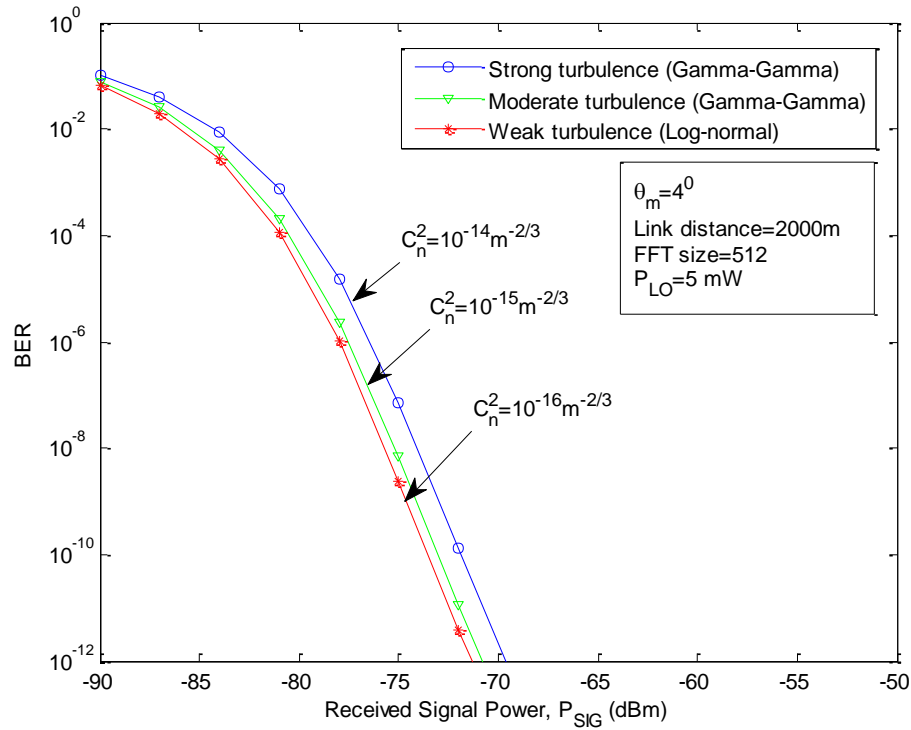
Fig. 4.12: Impact of different weather condition on BER performance of 2X2 SFBC OFDM system with polarization diversity.

4.4 Summary

In this chapter, an analytical model is proposed for the SFBC non-Hermitian coherent optical OFDM FSO system followed by DQPSK with polarization diversity. Analytical expressions are developed for output current of the balanced photodetector and the signal to noise plus cross talk ratio in presence of strong atmospheric turbulence. It is noticed that system suffer power penalty because of crosstalk induced by cross polarization. Finally, it is found that, the system bit error rate performance improves significantly due to space frequency block code along with polarization diversity.

Chapter 5

Comparative Performance Analysis between SFBC and STBC Coding

Chapter-5

COMPARATIVE PERFORMANCER ANALYSIS BETWEEN SFBC AND STBC CODING

5.1 Introduction

Alamouti STBC [153] known as the full spatial diversity scheme is very simple symbol wise decoding scheme. This simplest orthogonal STBC is considered for MIMO system with very low hardware complexity. For non-flat fading channels, effective performance was reported [154] when STBC coding was used with OFDM. The BER performance of a STBC coded non-Hermitian coherent-optical OFDM FSO system followed by DQPSK with polarization diversity is evaluated and compared with the same system with SFBC coded.

5.2 Space Time Block Coding (STBC)

Space-time block coding is a simple and ingenious transmit diversity technique. Alamouti proposed [153] a simple scheme for a *[2 × 2]* MIMO system that achieves a full diversity gain with a simple maximum likelihood decoding algorithm. It also satisfies for higher-order diversity systems involving a large number of antennas, and whose basic approach is also available.

The information bits are first modulated using an *M*-ary modulation scheme. The encoder then takes a block of two modulated symbols s_0 and s_1 in each encoding operation and gives it to the transmit antennas according to the code matrix,

$$S = \begin{bmatrix} s_0 & -s_1^* \\ s_1 & s_0^* \end{bmatrix} \tag{5.1}$$

In eq. (5.1), the first column represents the first transmission period and the second column the second transmission period. The first row corresponds to the symbols transmitted from the first antenna and the second row corresponds to the symbols transmitted from the second antenna. During the first symbol period, the first antenna transmits s_0 and the

second antenna transmits s_1. In second symbol period, the first antenna transmits $-s_1^*$ and the second antenna transmit s_0^*. This implies that symbols are both transmitted in space (across two antennas) and time (two transmission intervals) as shown in Fig 5.1. This is space - time block coding.
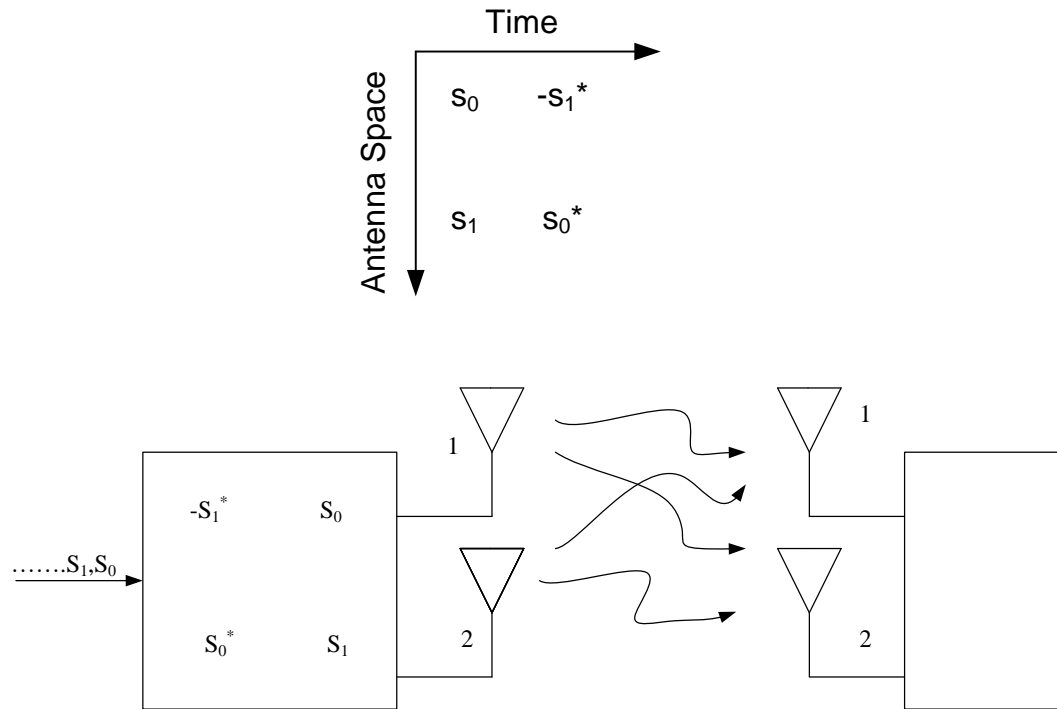
Fig. 5.1: Two transmit two receive antenna Alamouti STBC Block Diagram.

5.3 Alamouti-type STBC for FSO communication system [155]

Proposed Alamouti STBC was absolutely suitable for complex valued data for microwave MIMO channel. But for FSO communication, data through the optical links are considered to be intensity modulated. That is the reason why complex valued data would not be able to transmit through the FSO channel in the same manner as conventional Alamouti STBC. A new scheme has been proposed by Simon *et al.* considering real valued data only, named after Alamouti as Alamouti-type STBC for FSO channel.
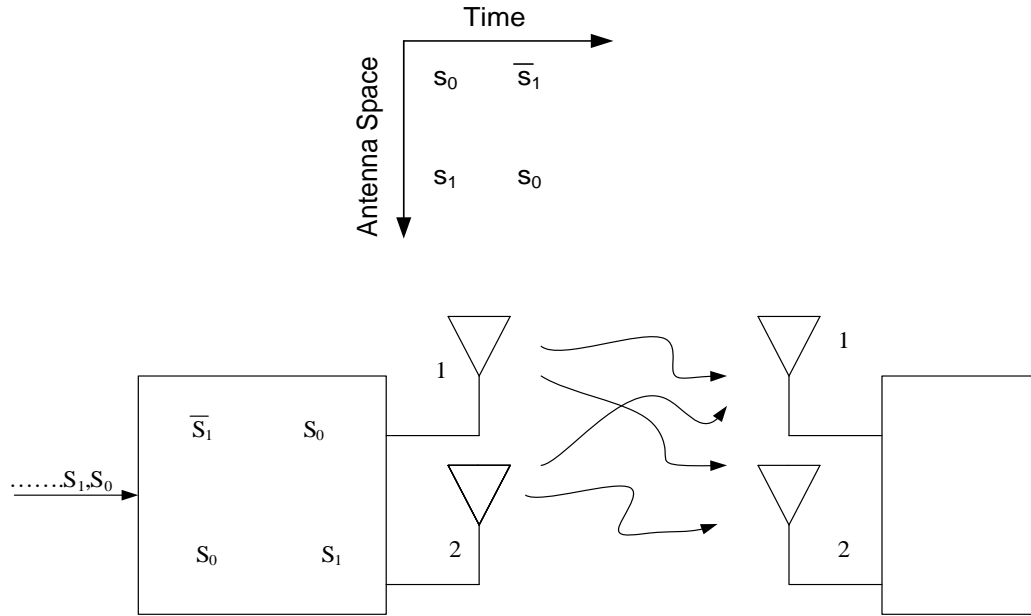
Fig. 5.2: Two transmit two receive antenna Alamouti-type STBC.

5.4 Comparative Performance Analysis between SFBC and STBC Coding

5.4.1 System model

A detail block diagram of the proposed system is presented in Fig. 5.3(a), details of modulator and detector are provided in Fig. 5.3(b). According to Alamouti's STBC coding, the resultant OFDM modulated signal is mapped and the illustration of Alamouti's STBC is shown in Fig. 5.3(c). At first time slot, laser-1 transmits S_0 and laser-2 transmits S_1 but in second time slot, laser-1 transmits the negative complex conjugate of S_1 and laser-2 transmits complex conjugate of S_0. Now for differential quadrature phase shift keying (DQPSK) modulation, first we separate the complex-valued STBC coded signal by the help of a real-imaginary separator and then used as the inputs for two different Dual Drive Mach-Zehnder Interferometers (DDMZI). By using a polarized beam splitter (PBS), a continuous wave laser light signal is splitted into a horizontal and a vertical polarized light beam. These lights signal which are 90^0 out of phase are considered for the carrier signal, one for real data and another for imaginary data respectively. Each modulator modulates the laser output for X and Y polarizations with in-phase (I) and quadrature phase (Q) data represented by $S_{I,k,x}$, $S_{Q,k,x}$, $S_{I,k,y}$ and $S_{Q,k,y}$ respectively. For simplicity, we set k=0 in the Fig. 5.3(b) to represents the first symbol. Then, a polarized beam combiner (PBC)

combines the resultant two DQPSK modulated signals and passed through the strong turbulent channel. The received signal is separated into horizontal and vertical light by a PBS and fed them into two different 90^0 hybrid circuit. To perform optical coherent detection, local oscillator's is required. The light beam from local oscillator is splitted into horizontal and vertical light beam and act as the reference light beam for corresponding 90^0 hybrid circuits. A balance detection technique is used in 90^0 hybrid circuit. For the first symbol, the both in-phase and quadrature phase current for X and Y polarization from the balanced detection circuit are indexed by $i_{I,0,x}$, $i_{Q,0,x}$, $i_{I,0,y}$ and $i_{Q,0,y}$ respectively and given in Fig. 5.3(b). By using balance detector circuit with a receiver circuit, we achieved the resultant digital output. Finally, to retrieve the transmitted message data, the reverse process is required for the rest part of the proposed system.
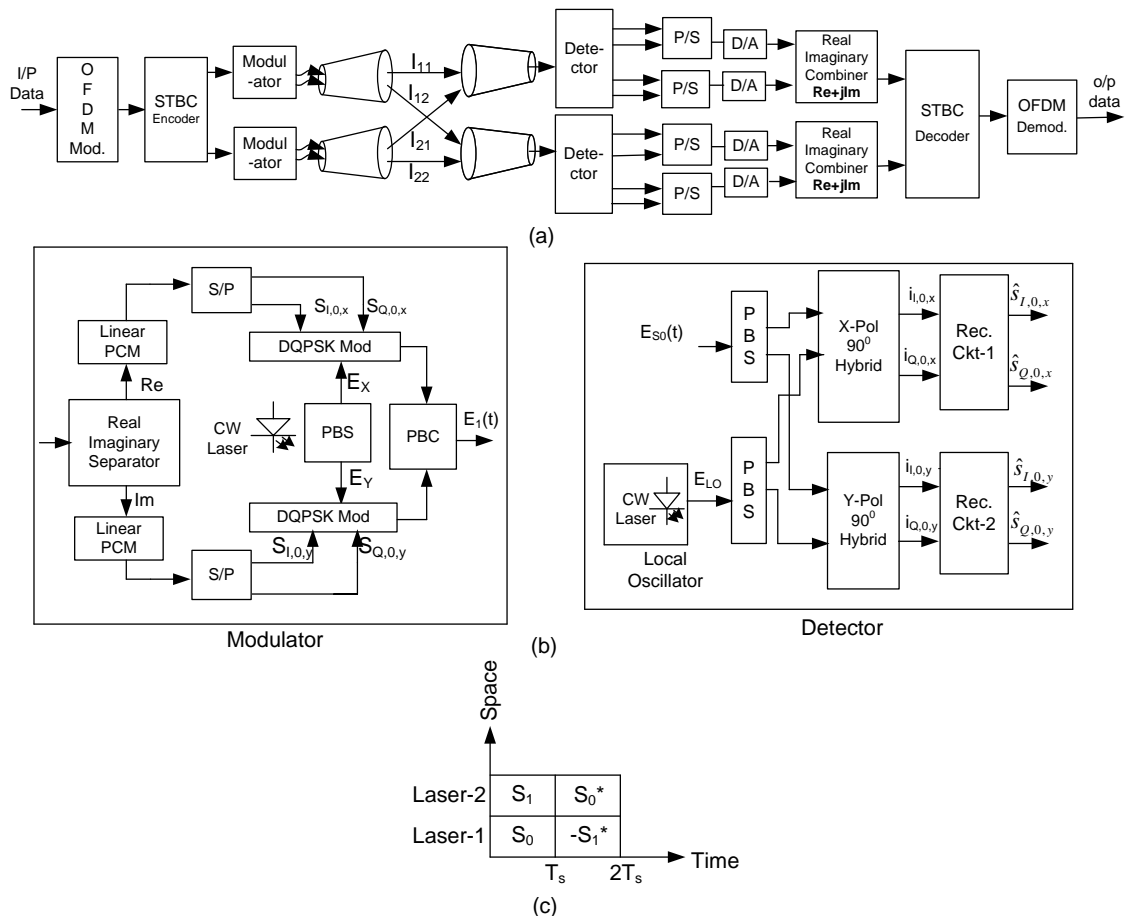
Fig. 5.3: (a) The whole system's block diagram is represented, (b) Details block diagram of modulator and detector and (c) 2 X 2 illustration of STBC.

5.4.2 Error Rate Estimation

5.4.2.1 Analysis of the transmitted signal considering STBC coding

The output equations for two laser sources after STBC encoding can be expressed as-

For laser-1,

$$v_1(t) = \sqrt{\frac{2E_s}{T_s}} \sum_{k=0}^{\infty} \left\{ \sum_{n=0}^{\frac{N}{2}-1} s_{k,2n}(t)\phi_{2n}(t-kT) + \sum_{n=0}^{\frac{N}{2}-1} -s_{k,2n+1}^*(t)\phi_{2n+1}(t-kT) \right\} \qquad (5.2)$$

For laser-2,

$$v_2(t) = \sqrt{\frac{2E_s}{T_s}} \sum_{k=0}^{\infty} \left\{ \sum_{n=0}^{\frac{N}{2}-1} s_{k,2n+1}(t)\phi_{2n+1}(t-kT_s) + \sum_{n=0}^{\frac{N}{2}-1} s_{k,2n}^*(t)\phi_{2n}(t-kT) \right\} \qquad (5.3)$$

Finally, the resultant transmitted signals electric field is written by-

$$\vec{E}(t) = E_x(t)\hat{x} + E_y(t)\hat{y} = A_x e^{j(\omega_c t + \varphi_x(t))} \left[\cos\left(\pi \frac{v_R(t)}{V_\pi}\right) + j\cos\left(\pi \frac{\widetilde{v_R}(t)}{V_\pi}\right) \right] \hat{x}$$

$$+ A_y e^{j(\omega_c t + \varphi_y(t))} \left[\cos\left(\pi \frac{V_{In}(t)}{V_\pi}\right) + j\cos\left(\pi \frac{\widetilde{V_{In}}(t)}{V_\pi}\right) \right] \hat{y}$$

$$E_x(t) = A_x e^{j(\omega_c t + \varphi_x(t))} \left[\cos\left(\pi \frac{v_R(t)}{V_\pi}\right) + j\cos\left(\pi \frac{\widetilde{v_R}(t)}{V_\pi}\right) \right]$$

$$= A_x e^{j(\omega_c t + \varphi_x(t))} \left[\cos\delta + j\cos\tilde{\delta} \right]$$

$$\cong A_x \sqrt{\cos^2\delta + \cos^2\tilde{\delta}} \, e^{j\left(\omega_c t + \varphi_x(t) + \tan^{-1}\frac{\cos\tilde{\delta}}{\cos\delta}\right)}$$

$$\cong A_x \sqrt{2 - \delta^2 - \tilde{\delta}^2} \, e^{j(\omega_c t + \varphi_x(t) + \alpha_x)}$$

$$\cong A_x \sqrt{2 - \frac{\pi^2 v_R^2(t)}{V_\pi^2} - \frac{\pi^2 \tilde{v}_R^2(t)}{V_\pi^2}} \, e^{j(\omega_c t + \varphi_x(t) + \alpha_x)}$$

$$\cong A_x \sqrt{2 - \frac{16\pi^2 E_b}{N^2 V_\pi^2 T_b}} \, e^{j(\omega_c t + \varphi_x(t) + \alpha_x)} \qquad (5.4)$$

where, E_b is the bit energy and T_b is the bit duration. Similarly, we get $E_y(t)$ and get the resultant electric field as-

$$\vec{E}(t) = A_x \sqrt{2 - \frac{16\pi^2 E_b}{N^2 V_\pi^2 T_b}} \; e^{j\{\omega_c t + \varphi_x(t) + \alpha_x\}}.\hat{x} + A_y \sqrt{2 - \frac{16\pi^2 E_b}{N^2 V_\pi^2 T_b}} \; e^{j\{\omega_c t + \varphi_y(t) + \alpha_y\}}.\hat{y} \qquad (5.5)$$

5.4.2.2 Analysis of the received signal considering STBC coding

By neglecting common losses, we can write the instantaneous output from the port C_1 of the X-polarization 90^0 hybrid circuit as-

$$E_{x,C_1}(t) = E_x'(t) - E_{LO,X}(t)$$
$$= \sqrt{I_{res}}\, \varepsilon_F E_x(t) + \sqrt{I_{res}}\, \varepsilon_X E_y(t) - E_{LO,X}(t)$$

The output power equation from the port C_1 can be represented as-

$$P_{X,C_1}(t) = \varepsilon_F^2 I_{res} A_x^2 (2 - \frac{16\pi^2 E_b}{N^2 V_\pi^2 T_b}) + \varepsilon_X^2 I_{res} A_y^2 (2 - \frac{16\pi^2 E_b}{N^2 V_\pi^2 T_b}) + P_{LO,X}$$
$$+ 2\varepsilon_F \varepsilon_X I_{res} A_x A_y \sqrt{(2 - \frac{16\pi^2 E_b}{N^2 V_\pi^2 T_b})(2 - \frac{16\pi^2 E_b}{N^2 V_\pi^2 T_b})} \cos(\theta_x + \theta_y) \qquad (5.6)$$
$$- 2\varepsilon_F A_x \sqrt{I_{res}(2 - \frac{16\pi^2 E_b}{N^2 V_\pi^2 T_b}) P_{LO,X}} \cos\theta_x - 2\varepsilon_X A_y \sqrt{I_{res}(2 - \frac{16\pi^2 E_b}{N^2 V_\pi^2 T_b}) P_{LO,X}} \cos\theta_y$$

where, $P_{LO,X}$ is the required power for the local oscillator for X-polarization. Similarly, we can find the output power for port C_2. Now, the resultant differential photocurrent from the balanced photodetector can be expressed as-

$$i_{x,C} = i_{x,C_2} - i_{x,C_1} = 4\varepsilon_F R_d A_x \sqrt{I_{res}(2 - \frac{16\pi^2 E_b}{N^2 V_\pi^2 T_b}) P_{LO,X}} \cos\theta_x$$
$$+ 4\varepsilon_X R_d A_y \sqrt{I_{res}(2 - \frac{16\pi^2 E_b}{N^2 V_\pi^2 T_b}) P_{LO,X}} \cos\theta_y \qquad (5.7)$$

In equation (5.32), the first part is the signal terms and the second part is the crosstalk terms.

5.4.2.3 Analysis of the SNR and BER considering STBC coding

The conditional signal to noise plus crosstalk ratio (SNCR) conditioned on a given value of misalignment angle and turbulence is expressed as-

$$
SNCR(\theta, I_{res}) = \frac{\left|i_{X,C}\right|^2}{\left|i_{Xtalk,C}\right|^2 + i_B^2 + \sigma_{th}^2 + \sigma_{sh}^2}
$$

$$
= \frac{16 R_d^2 I_{res} A_x^2 (2 - \dfrac{16\pi^2 E_b}{N^2 V_\pi^2 T_b}) P_{LO,X} \cos^2\theta \cos^2\theta_x}{16 R_d^2 A_y^2 (2 - \dfrac{16\pi^2 E_b}{N^2 V_\pi^2 T_b}) P_{LO,X} \sin^2\theta \cos^2\theta_y + i_B^2 + \dfrac{4kTB}{R_L} + 2eBR_d (P_{b,X} + P_{LO,X})}
$$

$$(5.8)$$

After finding the conditional SNCR, we get the conditional BER of the proposed system by using the following equation -

$$
BER_{cond.}(\theta, I_{res}) = \frac{1}{2} erfc\left(\frac{\sqrt{SNCR(\theta, I_{res})}}{2} \right)
$$

$$(5.9)$$

By averaging the conditional BER over two earlier mentioned probability density functions, we get the average BER and the expression is -

$$
BER_{average} = \int_0^{\frac{\pi}{2}} \int_0^{\infty} BER_{cond.}(\theta, I_{res}) . P(I_{res}) . P(\theta) dI_{res} \, d\theta
$$

$$(5.10)$$

By invoking equation (3.326.2) reported in [151], we can reduce the number of integrals involved in equation (5.10) and assuming only signal to crosstalk ratio at the time of averaging over Maxwellian distribution to obtain the final simplified expression of the average BER of our proposed system. And the final expression is represented as-

$$
BER_{average} = \frac{32}{\pi^2 \theta_m^3} \int_0^{\infty} \left[\frac{\Gamma\left(\dfrac{3}{2}\right)}{4\left(\dfrac{\pi\theta_m^2}{4}\right)^{\frac{3}{2}}} - \frac{1}{\sqrt{\pi}} \sum_{q=0}^{\infty} \frac{(-1)^q \left[\sqrt{\dfrac{A_1 I_{res}}{4A_2 I_{res} + 4N_0}} \right]^{2q+1} \Gamma(-q+1)}{q!(2q+1) \times 2\left(\dfrac{\pi\theta_m^2}{4}\right)^{-q+1}} \right] P(I_{res}) \, dI_{res}
$$

$$(5.11)$$

5.4.3 Comparative results and discussion

Table-5.1 contains the required system parameters values that are used in numerical computations. The results are compared with the results of without polarization diversity, with polarization diversity without STBC, and also compared with the system where SFBC is considered instead of STBC with polarization diversity and the whole comparison are provided in a single figure, Fig. 5.4.

Table 5.1: System's parameters list with required values for analytical simulation

Parameters	Values
Photodetector Responsivity, Rd	0.85
Characteristic of the MZI, V_π	500mV to 8V
Temperature, T	300K
Thermal Resistance, R_L	50Ω
Signal Bandwidth	10GHz
Structure parameter, $C_n{}^2$	$10^{-14}m^{-2/3}$
Link distance, L	2000m
Local Oscillator power	1 mW
Received power, Pr	-90 to -50 dBm
Phase of the X-polarized signal, $\Phi_{X,I}$	45^0
Phase of the Y-polarized signal, $\Phi_{Y,I}$	45^0
Laser wavelength, λ	1550nm
Background noise	$10^{-8}watt$

It is clearly visible in Fig. 5.4 that, our proposed system improves 4.5dB receiver sensitivity which actually the coding gains for using STBC with respect to the same system without STBC. But when compare with SFBC, it shows that 3dB more receiver sensitivity is achievable if we consider 2X2 SFBC instead of 2X2 STBC coding at a BER of 10^{-12}.

System BER is increasing with the angular misalignment angle which leads to system performance degradation. From Fig 5.5, it is noticed that system BER is increased 10^{-12} to 10^{-6} when angular misalignment angle increased from 4º to 7º for both STBC and SFBC techniques.
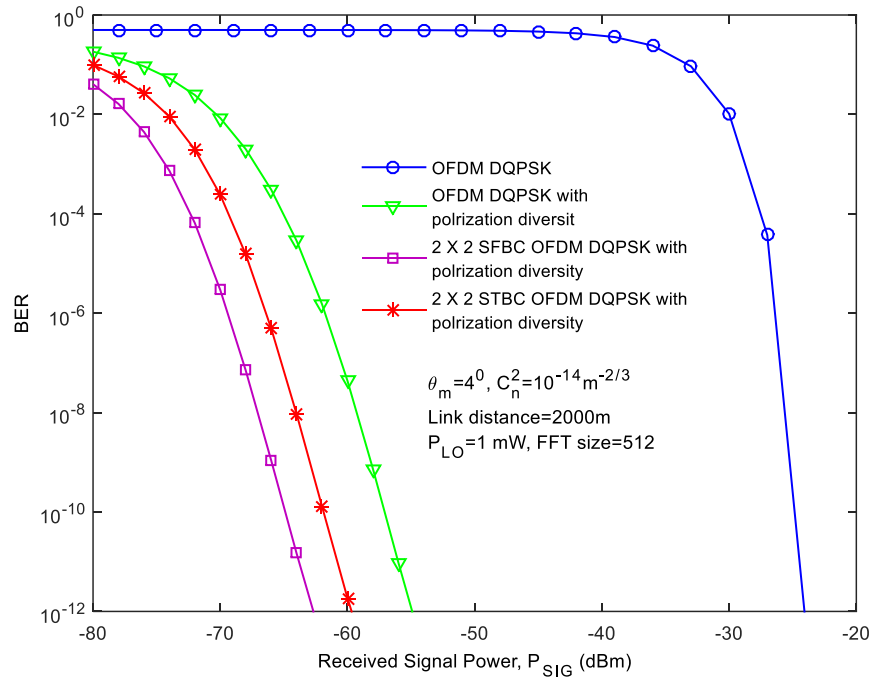
Fig. 5.4: BER curves for 2X2 STBC OFDM FSO system with polarization diversity, 2X2 SFBC OFDM FSO system with polarization diversity, OFDM FSO system with polarization diversity and only OFDM FSO system.
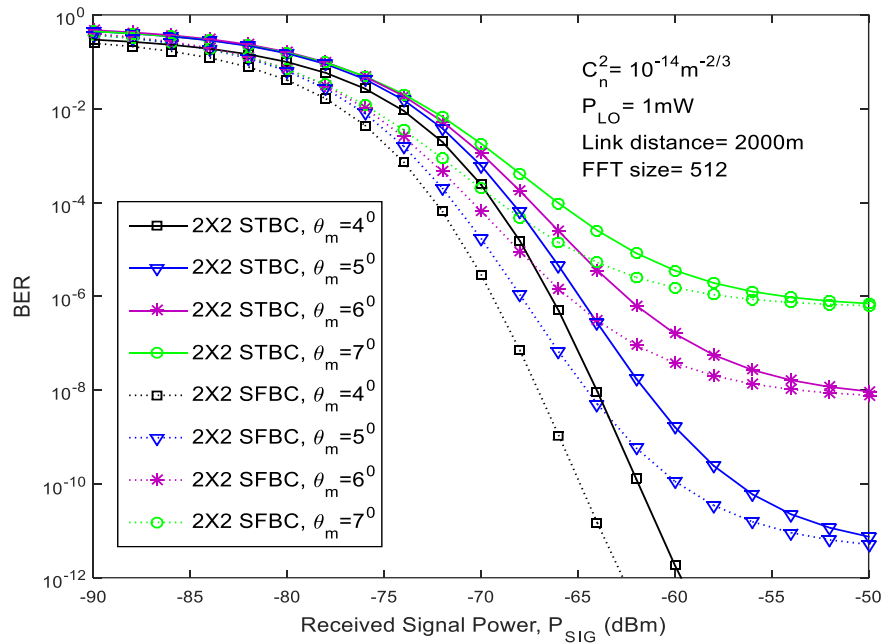
Fig. 5.5: Impact due to change of mean misalignment angle on BER performances for both 2X2 STBC and 2X2 SFBC OFDM FSO system with polarization diversity in presence of strong atmospheric turbulence.

Result shows that the SFBC coding performs better than STBC coding technique. The signal to crosstalk ratio can be improved if we increased the local oscillator power, due to this, system performance is improved which is clearly shown in Fig. 5.6.

For different local oscillator power, almost 3dB improvement in receiver sensitivity is found due to using SFBC instead of STBC coding. Power penalty curves for both space frequency diversity and space time diversity considering number of OFDM subcarrier and random angular mean misalignment angle as an input variable are provided in Fig. 5.7 and Fig. 5.8 respectively. When OFDM subcarrier increases, it is actually decrease the bandwidth of per channel, so the power penalty of the system reduces considerably.
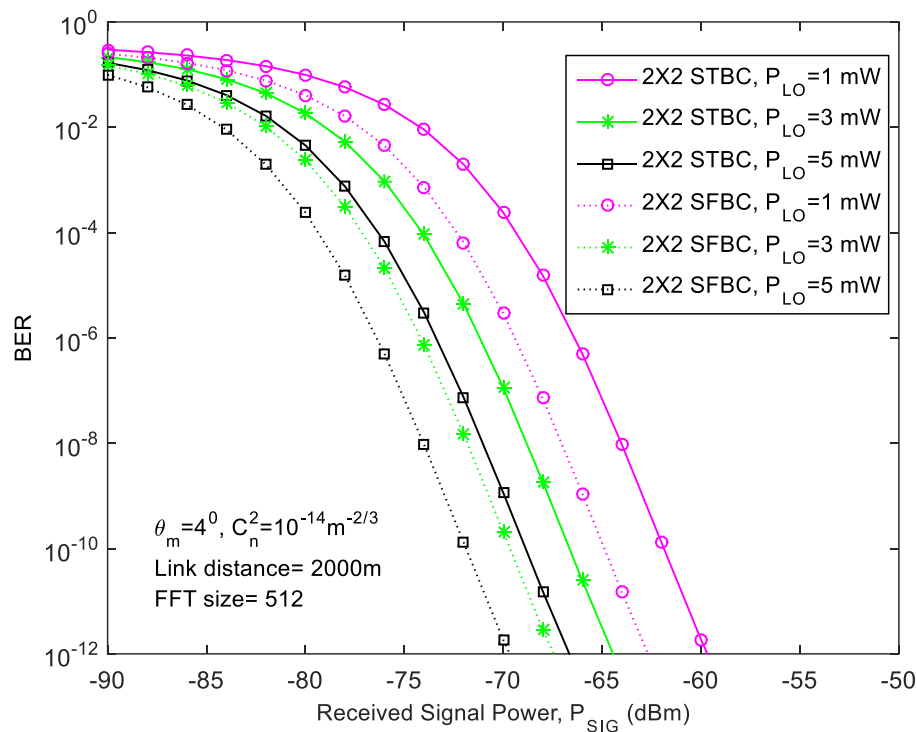
Fig.5.6: The effect on system BER performance for different local oscillator power for both 2X2 STBC and 2X2 SFBC OFDM FSO system with polarization diversity in presence of strong atmospheric turbulence.

In Fig. 5.7, power penalties reduce almost 8.5dB for STBC and 9.4dB for SFBC when OFDM subcarrier increases from 64 to 512 assuming the turbulence variance is $10^{-14} m^{-2/3}$ at link distance of 2000m and the random mean misalignment is 4^0 at a BER of 10^{-12}. The amount of penalties found from the BER versus received optical power curves shown earlier and provided in Table 5.2 and Table 5.3.

Table 5.2: Power penalties for different mean misalignment angles at a BER of 10^{-6}

Mean Misalignment Angle Block Coding	0^0 (dB)	4^0 (dB)	4.5^0 (dB)	5^0 (dB)	5.5^0 (dB)	6^0 (dB)	6.5^0 (dB)	7^0 (dB)
2 X 2 SFBC	0	0.7	1.3	2.1	3	4.5	7	12.5
2 X 2 STBC	0	3.3	4	5	6.2	7.5	10	15

Table 5.3: Power penalties for different number of OFDM subcarriers at a BER of 10^{-12}

Number of OFDM Subcarrier Block Coding	8 (dB)	16 (dB)	32 (dB)	64 (dB)	128 (dB)	256 (dB)	512 (dB)
2 X 2 SFBC	25.5	22.2	19.2	16.2	13.2	10.2	6.8
2 X 2 STBC	28.3	25	22	19	16.1	13.2	10.5
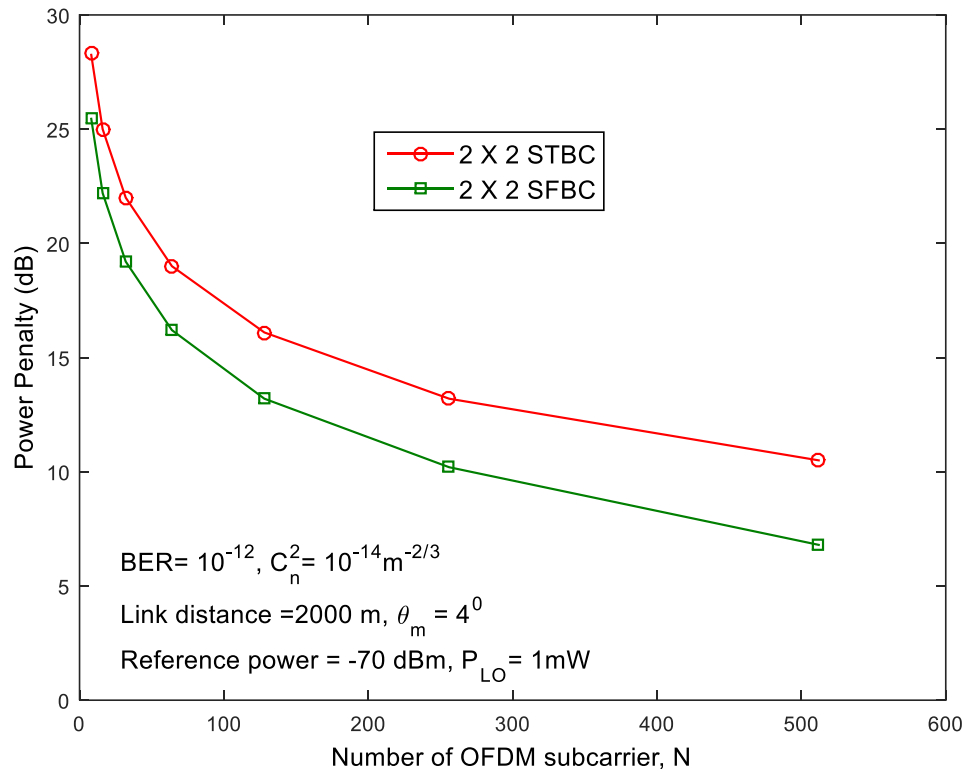
Fig.5.7: Power penalty comparison curves of both 2X2 STBC and 2X2 SFBC OFDM system with polarization diversity assuming input variable is the OFDM subcarrier number in presence of strong atmospheric turbulence.

For STBC, power penalty increases 11.7dB and 11.8dB for SFBC when random mean misalignment angle increases from 4^0 to 7^0 at a BER of 10^{-6} assuming link length of 2000m, number of OFDM carrier is 512 and the turbulence variance is $10^{-14}m^{-2/3}$ which given in Fig. 5.8.
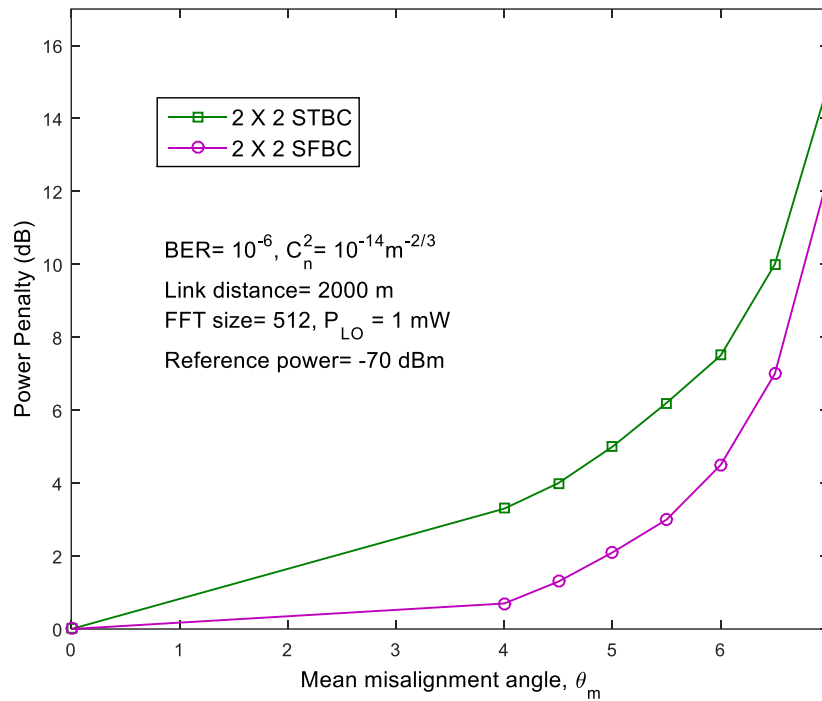
Fig. 5.8: Power penalty comparison curves of 2X2 STBC and 2X2 SFBC OFDM FSO system with polarization diversity assuming random mean angular misalignment as an input variable in presence of strong atmospheric turbulence.

5.5 Summary

The BER performance of space time block coded OFDM FSO system is compared with the same system considering space frequency block coding. BER results for both coding scheme are observed by varying local oscillator power, number of OFDM subcarrier and mean angular misalignment angle. By observing the results, it is found that system suffers more power penalty in case of STBC coding compared to SFBC coding. Finally, we conclude that, the system with SFBC coding performs better than STBC coding due to robustness of SFBC coding against frequency selective fading channel.

Chapter 6

CONCLUSIONS AND FUTURE WORKS

Chapter-6

CONCLUSIONS AND FUTURE WORKS

6.1 Conclusions

FSO communication system is an emerging technology for future broadband communication network. In FSO communication system, there is no need of license for frequency bandwidth which is very costly nowadays. Due to some lucrative features like very high data rate, unlimited bandwidth, simple hardware architecture, very low cost, easy to deployment, full duplex communication etc. FSO communication system is another appropriate technology which may act along with existing microwave communication system to meet up the upcoming high data rate demand.

In 6G mobile communication systems, the access technology is orthogonal frequency division multiplexing (OFDM). OFDM technology is very robust against frequency selective fading channel. By considering OFDM technology, the system's reliability and capacity are both increases. OFDM act as a special case of multiple subcarrier modulation in FSO communication system. In our proposed FSO system model, we implement non-Hermitian OFDM instead of transmitting only real parts considering Hermitian symmetry.

As FSO communication system is a line of sight technology, atmospheric turbulence is the main challenge for its performance. It degrades the system's performance by adding phase distortion and intensity fading to the incoming light beam. Aperture averaging technique is one of the most popular techniques which mitigate the fading associated due to atmospheric turbulence. Polarization diversity technique is also can be considered for fading mitigation. In case of polarization diversity, there is a possibility of cross polarization induced crosstalk. We found that, the improvement due to polarization diversity is more significant than the performance degradation due to cross polarization induced crosstalk.

Another fading mitigation technique is spatial diversity scheme like space time/frequency block coding. Space frequency block coding performs best due to its robustness against frequency selective fading channel. SFBC coding also increases system's redundancy and capacity.

6.2 Summary of the Major Contributions

The summary of the major contributions of my research works are listed below-

i.   An analytical approach is presented to evaluate the BER performance of a FSO system considering non-Hermitian orthogonal frequency division multiplexing (OFDM) modulation followed by optical differential quadrature phase shift keying (DQPSK) modulation. Analytical approach is developed to find the expressions for output current and signal to noise ratio (SNR) in presence of atmospheric turbulence. The conditional BER for a given turbulence-induced fading is also derived. Average SNR and BER are obtained considering the turbulence-induced fading to be log-normal distribution. It is noticed that the proposed OFDM FSO system suffers 4dB and1.4dB power penalty at a BER of 10^{-12} due to the effect of atmospheric turbulence and background radiation respectively for 512 numbers of OFDM subcarriers and a link distance of 2000 m.

ii.   An analytical approach is presented to evaluate the effect of pointing error on the performance of an orthogonal frequency division multiplexed (OFDM) optical differential quadrature phase shift keying (DQPSK) modulated FSO system. Analytical approach is developed to find the expressions for output current and SNR in presence of strong atmospheric turbulence with pointing error. The conditional bit error rate for a given turbulence induced fading and pointing error is also derived. Average BER is obtained by averaging the conditional BER over the pdf of pointing error along with the pdf of turbulence induced fading to be Gamma-Gamma distribution. It is clearly observed that the proposed system suffers almost 1.95dB and 1.25dB power penalty due to normalized pointing error standard deviation 2 and 1.5 respectively against strong turbulence and 1.7dB and 1.05dB power penalty due to normalized

pointing error standard deviation 2 and 1.5 respectively against weak turbulence at a BER of 10^{-9}.

iii. An analytical model for non-Hermitian OFDM based DQPSK FSO system is developed to account for the cross polarization induced crosstalk in the presence of strong atmospheric turbulence. The average BER is evaluated by averaging the conditional BER over the pdf of the turbulence considering Gamma–Gamma distribution and Maxwellian distribution for random angular misalignment. Results are evaluated in terms of BER and receiver sensitivity improvement due to polarization diversity. It is noticed that system BER performance degrades significantly and power penalty is found to almost 9.5dB, 12dB and 21dB for mean misalignment angle of 4^0, 5^0 and 6^0 respectively at a BER of 10^{-8} and a given turbulence parameter $C_n^2 = 10^{-14}$ m$^{-2/3}$ for a FSO link distance of 2000m.

iv. An analytical model is developed for a non-Hermitian coherent-optical OFDM FSO system with space frequency block code (SFBC) and polarization diversity. Analysis is carried out for a non-Hermitian OFDM FSO link with SFBC coding to evaluate the effect of cross polarization induced crosstalk in presence of channel impairments such as atmospheric turbulence. Expressions are developed for signal to noise plus crosstalk ratio for a given amount of polarization misalignment angle. Considering the probability density function of the misalignment angle to be Maxwellian distributed and Gamma–Gamma distribution for strong atmospheric turbulence, the average bit error rate (BER) is determined. Results show that, there is 38 dB improvement in receiver sensitivity due to polarization diversity without SFBC in presence of strong turbulence at a BER of 10^{-12} considering local oscillator power is 5 mW and link distance is 2000 m. At a given BER of 10^{-12}, penalty due to crosstalk is found to be 3.3 dB for mean misalignment angle of 4^0 when link distance is 2000m. Finally, it is noticed that, the amount of coding gain due to SFBC is found to be 7.5 dB at a BER of 10^{-12}.

v. An analytical model for a non-Hermitian orthogonal frequency division modulation (OFDM) system considering space time block coding (STBC) with polarization diversity in presence of strong atmospheric turbulence and compare

the bit error rate (BER) performance with the same system considering space frequency block coding (SFBC). We developed this analytical model to calculate the impact of crosstalk and fading on system performance due to cross polarization and strong atmospheric turbulence respectively. The analytical expressions for signal to noise plus crosstalk ratio are derived for a certain amount of random misalignment angle. The average BER is found by averaging the conditional BER over this two probability density functions. It is noticed that, receiver sensitivity improvement due to STBC coding is almost 4.5dB at a BER of 10^{-12} compare to 7.5dB due to SFBC coding.

6.3 Scopes of the future research works

Some possibilities to further extend of our research works are listed here-

i) Channel coding like Read Solomon code, convolutional code, low density parity check code etc. can be considered to reduce the fading effect.

ii) Optical MIMO OFDM FSO system with SFBC and polarization diversity can be implemented to extend the system capacity.

iii) In this research, only homodyne receiver is considered, researchers may also extend the work considering heterodyne receiver.

iv) Optical OFDM with WDM system may be considered to extend the system reliability and capacity also.

v) Effect of LASER Non-Linearity is not considered in my research work. Researchers may include this and get the more accurate results.

vi) To improve the system performance further, researchers may think about the different receiver diversity techniques like maximal ratio combining, equal gain combining, selection combining etc.

vii) By developing a probability density function for overall system's noise, the system's BER performance can be evaluated.

viii) To validate our analytical simulation results, researchers may consider numerical simulation and then compare with our results.

References

[1]   L. C. Andrews, R. Phillips, and C. Hopen, *Laser Beam Scintillation with Applications*. SPIE Press, 2001.

[2]   S. W. C. Vincent,"Free-Space Optical Communications" IEEE, Fellow, OSA Journal of Lightwave Technology, 24 (2006) 4750-4762.

[3]   S. V. Chinta, T. P. Kurzweg,D. S. Pfeil and K. R. Dandekar ,"4 X 4 space – time codes for free space optical interconnects", Photonics Packaging, Integration, and Interconnects. Proceedings of the SPIE, 7221 (2009) 722116-722116-8.

[4]   P. Wang, L. Zhang, L. Guo, F. Huang, T. Shang, R. Wang, and Y. Yang, "Average BER of subcarrier intensity modulated free space optical systems over the exponentiated Weibull fading channels," Opt. Express, 22(17), (2014).

[5]   K. Singh, C. Saleh, B. K. Sana, B. Feres, X. Ren, K. Hamadi, A. Grover and M. Singh "Investigations on mode-division multiplexed free-space optical transmission for inter-satellite communication link," Wireless Network, vol. 28, pp. 1003-1016, 2022.

[6]   E. Ebrahim Elsayed, B. B Yousif and M. Singh, "Performance enhancement of hybrid fiber wavelength division multiplexing passive optical network FSO systems using M-ary DPPM techniques under interchannel crosstalk and atmospheric turbulence," Optical and Quantum Electronics, Springer, vol. 54, no.116, 2022.

[7]   G. Z. Antonio, "Error Rate Performance for STBC in Free-Space Optical Communications through Strong Atmospheric Turbulence", IEEE Comm. Letters, 11 (2007) 390-392.

[8]   X. Zhu and J. M. Kahn, "Free-space optical communication through atmospheric turbulence channels," *IEEE Trans. Commun.*, 50 (2002) 1293–1300.

[9]   K. Sunilkumar, N. Anand, S. K. Satheesh, K. K. Moorthy, and G. Ilavazhagan, "Performance of free-space optical communication systems: effect of aerosol-induced lower atmospheric warming," Opt. Express 27, 11303-11311 (2019).

[10]   T. A. Bhuiyan, M. Z. Hassan, S. M. S. Tanzil, S. Hayder and S. P. Majumder, "Performance Improvement of IM-DD Free Space Optical CDMA with Maximal Ratio Combining", CICN '10 Proceedings of the 2010 International Conference on Computational Intelligence and Communication Networks IEEE Computer Society Washington, DC, USA, 2010.

[11]   W. Huang, J. Takayagi, T. Sakanaka and M. Nakagawa, "Atmospheric Optical Communication System Using Subcarrier PSK Modulation," IEEE International Conference, 3 (1993) 1597-1601.

[12]   Z. Ghassemlooy, W. O. Popoola, V. Ahmadi and E. Leitgeb, "MIMO Free-Space Optical Communication Employing Subcarrier Intensity Modulation in Atmospheric Turbulence Channels", Comm. Infrastructure. Systems and Applications in Europe, Springer-Verlag Berlin Heidelberg, 16 (2009) 61-74.

[13]   N. S. Kopeika and J. Bordogna, "Background noise in optical communication systems," *Proc. of the IEEE*, vol. 58, pp. 1571-1577, 1970.

[14]   A. A. Farid and S. Hranilovic, "Outage capacity optimization for free space optical links with pointing errors", LightwaveTechnol, vol. 25, no. 7, pp. 1702-1710, Jul 2007.

[15]   X. Song, F. Yang and J. Cheng, "Subcarrier intensity modulated optical wireless communications in atmospheric turbulence with pointing errors", *Opt. Comm. Netw*, vol. 5, no. 4, pp. 349-358, 2013.

[16]   M. Sheng, P. Jiang, Q. Hu, Q. Su and X. X. Xie, "End-to-end average BER analysis for multi-hop free-space optical communications with pointing errors", J Opt, vol. 15, no. 5, pp. 1-7, 2017.

[17]   F. Yang, J. Cheng and T. A. Tsiftsis, "Free-space optical communications with generalized pointing errors", IEEE ICC, vol. 9, no. 13, pp. 3943-3947, 2013.

[18]   N. A. Mohammed, A. S. El-Wakeel, and M. H. Aly, "Pointing Error in FSO Link under Different Weather Conditions," *International Journal of Video & Image Processing and Network Security (IJVIPNS-IJENS),* vol. 12, no. 1, pp. 6-9, 2012.

[19]   N. H. M. Noor, A. W. Naji, and W. Al-Khateeb, "Theoretical analysis of multiple transmitters/receivers on the performance of free space optics (FSO) link," IEEE International Conference on Space Science and Communication 2011, pp. 291-295, July 2011.

[20]   X. Zhu and J. M. Kahn, "Performance bounds for coded free-space optical communications through atmospheric turbulence channels," IEEE Transactions on Communications, vol. 51(8), pp. 1233-1239, August 2003.

[21]   A. Khatoon, W. G. Cowley, and N. Letzepis, "Channel measurement and estimation for free space optical communications," Australian Communications Theory Workshop (AusCTW) 2011, pp. 112-117, 2011.

[22]   N. Letzepis and A. G. i. Fabregas, "Outage probability of the Gaussian MIMO free-space optical channel with PPM," IEEE Transactions on Communications, vol. 57, pp. 3682-3690, 2009.

[23]   A. Molisch, "Statistical description of the wireless channel," in Wireless Communications - Edition 1: Wiley-IEEE Press, pp. 69-99, 2011.

[24]   N. Beaulieu, "An extended limit theorem for correlated lognormal sums," IEEE Transactions on Communications, vol. PP, pp. 1-4, 2011.

[25]   A. Harris, J. J. Sluss, H. H. Refai and P. G. Lopresti, "Analysis of beam steering tolerances and divergence for various long range FSO communication links", *Proc. SPIE, Digital Wireless Comm. VII and Space Comm. Tech*, vol. 5819, no. 455, 2005.

[26]   C. Abou-Rjeily and A. Slim, "Cooperative diversity for free-space optical communications: transceiver design and performance analysis," IEEE Transactions on Communications, vol. 59, pp. 658-663, 2011.

[27]   M. Uysal, L. Jing, and Y. Meng, "Error rate performance analysis of coded free-space optical links over gamma-gamma atmospheric turbulence channels," IEEE Transactions on Wireless Communications, vol. 5, pp. 1229-1233, June 2006.

[28]   G. R. Osche, *Optical detection theory for laser applications.* Wiley, New Jersey, 2002.

[29]   S. Karp, R. M. Gagliardi, S. E. Moran, and L. B. Stotts, Optical channels: fibers, cluds, water and the atmosphere. New York: Plenum Press, 1988.

[30]   L. C. Andrews and R. L. Phillips, *Laser beam propagation through random media*. Bellingham: WA: SPIE, 1998.

[31]   M. A. Khalighi, N. Schwartz, N. Aitamer and S. Bourennane, "Fading Reduction by Aperture Averaging and Spatial Diversity in Optical Wireless systems", Journal of Optical Communication and Networking, vol. 1, no. 6, pp. 580-593 (2006).

[32]   A. Belmonte and J. Kahn, "Field Conjugation Adaptive Arrays in Free Space Coherent Laser Communications", J. Opt. Comm. Networks, vol. 3, no. 11, pp. 830-838 (2011).

[33]   H. Yuksel, S. Milner and C. C. Davis, "Aperture averaging for optimizing receiver design and system performance on free-space optical communication links", J. Opt. Networks, vol. 4, no. 8, pp. 462-475 (2005).

[34]   M. Abtahi, P. Lemieux, W. Mathlouthi, and L. A. Rusch, "Suppression of turbulence-induced scintillation in free-space optical communication systems using saturated optical amplifiers," *Journal of Lightwave Technology,* vol. 24, p. 4966, December 2006.

[35]   X. Zhu, J. M. Kahn, and J. Wang, "Mitigation of turbulence-induced scintillation noise in free-space optical links using temporal-domain detection techniques," IEEE Photonics Technology Letters, vol. 15, pp. 623 - 625, April 2003.

[36]   A. Bekkali, C. B. Naila, K. Kazaura, K. Wakamori, and M. Matsumoto, "Transmission analysis of OFDM-based wireless services over turbulent radio-on-FSO links modeled by gamma-gamma distribution," *IEEE Photonics Journal,* vol. 2, pp. 510-520, 2010.

[37]   M. Z. Afgani, H. Hass, H. Elgala, and D. Knipp, "Visible light communication using OFDM", In Proc. TRIDENTCOM, 2006: 129-134.

[38]   T. Hwang, C. Yang, G. Wu, S. Li and G. Y. Li, "OFDM and Its Wireless Applications: A Survey", IEEE Transactions on Vehicular Technology, vol. 58(4), pp. 1673-1694, May-2009.

[39]   N. Cvijetic, D. Qian and T. Wang, "10 Gb/s Free-Space Optical Transmission using OFDM", IEEE conference of Optical Society of America, OFC/NFOEC (2008).

[40]   Y. Wang, D. Wang and J. Ma, "On the Performance of Coherent OFDM Systems in Free-space Optical Communications", IEEE Photonics Journal, vol. 7(4), August-2015.

[41]   M. Singh and J. Malhotra, "4×20Gbit/s-40GHz OFDM based Radio over FSO transmission link incorporating hybrid wavelength division multiplexing-mode division multiplexing of LG and HG modes with enhanced detection," Optoelectronics and Advanced Materials - Rapid Communications, vol. 14, no. 5-6, pp. 233-243, 2020.

[42]   Bobby Barua and S. P. Majumder, "Bit Error Rate Analysis of an OFDM Subcarrier Modulated FSO Link with Optical Intensity Modulated and a Direct Detection Receiver," International Journal of Optics and Photonic Engineering, UK, vol. 4(2018) 1-11.

[43]   R. Hui, B. Zhu, R. Huang, C. T. Allen, K. R. Demares, and D. Richards," Subcarrier multiplexing for high-speed optical transmission". J. Lightwave Technol., 2002; 20, 3: 417–427.

[44] W. O. Popoola and Z. Ghassemlooy, "BPSK Subcarrier Intensity Modulated Free Space Optical Communications in Atmospheric Turbulence", J. LightwaveTechnol., vol. 27(8), pp. 967-973, April-2009.

[45] T. Y. Liow, X. Tu, G. Q. Lo, D. L.Kwang, K. Goi, A. Oka, H.Kusaka, and K. Ogawa, "Silicon Quadrature Phase-Shift-Keying Modulator for 40- and 100-Gb/s Transmission", Fujikura Technical Review, 2014: 1-5.

[46] G. H. Smith and D. Novak, "Overcoming chromatic-dispersion effects in fiber-wireless systems incorporating external modulators. IEEE Trans", Microwave Theory Tech.1997; vol 45, pp1410-1415.

[47] A. H. Gnauck and P. J. Winzer, "Optical Phase Shift Keyed Transmission", J. of Lightwave Technology, vol. 23(1), Jan-2005.

[48] G. D Houser and E. Garmire, "Balanced detection technique to measure small changes in transmission", APPLIED OPTICS, vol. 33(6), pp. 1059-1062, 1994.

[49] S. A. J. Flrez, "Circular polarization and availability in free space optics (FSO) communication systems", IEEE Latin-American Conference on Communications (LATINCOM) (2010) 1-6.

[50] J. Grosinger, "Investigation of polarization modulation in optical free space communications through the atmosphere." vol. master: Technical University of Vienna, pp. 77, February 2008.

[51] G. D. Xie, F. X. Wang, A. Dang, and H. Guo, "A novel polarization-multiplexing system for free-space optical links," IEEE Photonics Technology Letters, 23 (2011) 1484-1486.

[52] S. P. Arun, M. G. Sumithra, K. Shankar, A. Grover, M. Singh and J. Malhotra, "Performance investigation of spectral-efficient high-speed inter-satellite optical wireless communication link incorporating polarization division multiplexing," Optical and Quantum Electronics, Springer, vol. 53, no. 270, 2021.

[53] M. M. Karbassian and H. Ghafouri-Shiraz, "Transceiver architecture for incoherent optical CDMA network based on polarization modulation," *Journal of Lightwave Technology,* vol. 26, pp. 3820-3828, 15 December 2008.

[54] X. Zhao, Y. Yao, Y. Sun, and C. Liu, "Circle polarization shift keying with direct detection for free-space optical communication," *IEEE/OSA Journal of Optical Communications and Networking* vol. 1, pp. 307-312, September 2009.

[55] J. Zhang, Z. Li and A. Dang, "Performance of Wireless optical communication systems under polarization effects over atmospheric turbulence" Journal of Optics Communication, ELSEVIER, 416 (2018) 207-213.

[56] K. A. Taher and S. P. Majumder, "Analytical Evaluation of the Effect of Cross-Polarization-induced Crosstalk on the BER Performance of a PDM-QPSK Coherent Homodyne Optical Transmission System", J. Opt. Comm., pp 1-10, (2016).

[57] Bobby Barua and S. P. Majumder, "Analytical performance evaluation of a STBC coded OFDM FSO communication system over turbulent atmospheric channel," Journal of Communication Technology and Electronics, 64(2019) 1101-1107.

[58] K. V. N. Kavitha, S. Ghos, A. Keetey and S. Khara, "Error rate analysis of a STBC-OFDM system with efficient channel coding technique at low SNR," International Journal of Applied Engineering Research, vol. 9(16), pp. 3481-3494, Jul-2014

[59]   A. F. Molisch, M. Z. Win, and J. H. Winters, "Space-time-frequency (STF) coding for MIMO-OFDM systems," *IEEE Commun. Lett.*, vol. 6, pp. 370–372, Sept. 2002.

[60]   H. B¨olcskei and A. J. Paulraj, "Space-frequency coded broadband OFDM systems," in *Proc. IEEE Wireless Commun. and Networking Conf. (WCNC'00)*, pp. 1–6.

[61]   N. Al-Dhahir, C. Fragouli, A. Stamoulis, W. Younis, and A. R. Calderbank, "Space-time processing for broadband wireless access," *IEEE Commun. Mag*, vol. 40, pp. 136–142, Sept. 2002.

[62]   M. Torabi and M. R. Soleymani "Space-time-frequency COFDM with power allocation for broadband wireless communications," in *Proc. 56thIEEE Vehicular Technology Conference (VTC-F'02)*, vol. 1, pp. 209–213.

[63]   G. Yi and K. B. Letaief, "An efficient space-frequency coded OFDM system for broadband wireless communications," *IEEE Trans. Commun.*, vol. 51, pp. 2019–2029, Dec. 2003

[64]   D. Huang, K. B. Letaief, and J. Lu, "A receive space diversity architecture for OFDM systems using orthogonal designs," *IEEE Trans. Wireless Commun.*, vol. 3, pp. 992–1002, May 2004.

[65]   K. F. Lee and D. B. Williams, "A space-frequency transmitter diversity technique for OFDM systems," in *Proc. IEEE Global Telecommunications Conference (Globecom'00)*, pp. 1473–1477.

[66]   W. Gappmair, S. Hranilovic, and E. Leitgeb, "OOK performance for terrestrial FSO links in turbulent atmosphere with pointing errors modeled by Hoyt distributions," *IEEE Communications Letters,* vol. 15, pp. 875-877, 2011.

[67]   R. R. Iniguez, S. M. Idrus, and Z. Sun, *Optical wireless communications - IR for wireless connectivity*. London: Taylor & Francis Group, LLC, 2008.

[68]   A. García-Zambrana, C. Castillo-Vázquez, and B. Castillo-Vázquez, "Rate adaptive FSO links over atmospheric turbulence channels by jointly using repetition coding and silence periods," *Optics Express,* vol. 18, pp. 25422-25440,2010.

[69]   C. B. Naila, A. Bekkali, K. Wakamori, and M. Matsumoto, "Performance analysis of CDMA-based wireless services transmission over a turbulent RF-on-FSO channel," *Journal of Optical Communications and Networking IEEE/OSA,* vol. 3, pp. 475-486, 2011.

[70]   Z. X. Wang, W. D. Zhong, S. N. Fu, and C. Lin, "Performance comparison of different modulation formats over free-space optical (FSO) turbulence links with space diversity reception technique," *IEEE Photonics Journal,* vol. 1, pp. 277-285, December 2009.

[71]   R. Gallager, "Low-density parity-check codes," *IRE Trans. Information Theory*, pp. 21-28, 1962.

[72]   B. Djordjevic, "LDPC-coded MIMO optical communication over the atmospheric turbulence channel using Q-ary pulse position modulation," *Opt. Express 16*, pp.10026-10032, 2007.

[73]   B. Djordjevic, B. Vasic and M. A. Niefeld, "Power efficient LDPC-coded modulation for free-space optical communication over the atmospheric turbulence channel," *in Proc. OFC 2007, Anaheim, CA, USA*, 2007.

[74]   Bobby Barua and S. P. Majumder, "BER Performance Analysis of an LDPC Coded OFDM Optical Wireless Communication System with Intensity Modulation and a Direct Detection Receiver," Advances in Wireless Communications and Networks, vol. 4, no.2, pp. 43-48, 2018.

[75]   T. Ohtsuki, "Turbo-coded atmospheric optical communication systems," *in IEEE International Conference on Communications (ICC) New York*, pp.2938-2942, 2002.

[76]   N. Kumar, V. Jain and S. Kar, "Evaluation of the performance of FSO system using OOK and M-PPM modulation schemes in inter-satellite links with Turbo codes," in *Proc. IEEE Int. Conf. Electr. And Comp. Techn*., pp. 59-63, 2011.

[77]   J. Hamkins, "Performance of binary turbo-coded 256-ary pulse position modulation", *TMO Progress Report*, pp. 42–138, Aug. 1999.

[78]   E. Forestieri, R. Gangopadhyay and G. Prati, "Performance of convolutional codes in a direct-detection optical PPM channel", *IEEE Transactions on Communications*, vol. 37, no. 12, pp. 1303– 1317, 1989.

[79]   M. K. K. Cheng, B. E. Moision, J. Hamkins and M. A. Nakashima, "Implementation of a coded modulation for deep space optical communications," in *Proc. IEEE, GLOBECOM* (San Francisco, CA), 2006.

[80]   J. Hamkins and B. E. Moision, "Performance of long block length REED Solomon codes with low-order pulse position modulation," *IEEE Trans. Comm*., 2005

[81]   X. Sun, D. R. Skillman, E. D. Holffman and D. Mao, "Free space laser communication experiments from earth to the lunar reconnaissance orbiter in lunar orbit" Opt. Exp., vol. 21, pp. 1865-1871, 2013.

[82]   A. G. Bell, "On the production and reproduction of sound by light," American Journal of Sciences, vol. Series 3, pp. 305 - 324, Oct. 1880.

[83]   D. Killinger, "Free space optics for laser communication through the air," Optics &Photonics News, vol. 13, pp. 36-42, Oct. 2002.

[84]   E. Ciaramella, Y. Arimoto, G. Contestabile, M. Presi, A. D'Errico, V. Guarino, and M. Matsumoto, "1.28 terabit/s (32x40 Gbit/s) WDM transmission system for free space optical communications," *IEEE Journal on Selected Areas inCommunications* vol. 27 pp. 1639 - 1645, 2009.

[85]   C. Long, "Optical communication for the amateur," in *'Amateur Radio' magazine*Melbourne: Wireless Institute of Australia, January 1979, pp. 7-14.

[86]   F. E. Goodwin, "A review of operational laser communication systems", *Proceedings of IEEE,* vol. 58, pp. 1746-1752, October 1970.

[87]   W. O. Popoola, "Subcarrier intensity modulated free space optical communication systems", in School of *Computing, Engineering and Information Sciences*, vol. Doctor of Philosophy Newcastle: University of Northumbria, 2009, p. 264.

[88]   H. Hemmati, "Interplanetary laser communications," Optics and Photonics News, vol. 18, pp. 22-27, Nov. 2007.

[89]   S. Hardy, "Free-space optics systems are finding their niches," Light wave pp. 33-36, Dec. 2005.

[90]   J. N. Pelton and A. U. M. Rae, "Global satellite communications technology and systems - an overview," *Journal Space Communications,* vol. 16, pp. 55-69, August 2000.

[91] N. D. Chatzidiamantis, H. G. Sandalidis, G. K. Karagiannidis, and M. Matthaiou, "Inverse gaussian modeling of turbulence-induced fading in free-space optical systems," *Journal of Lightwave Technology,* vol. 29, pp. 1590-1596, 2011.

[92] R. Mesleh, H. Elgala, and H. Haas, "Optical spatial modulation," *IEEE/OSA Journal of Optical Communications and Networking,* vol. 3, pp. 234-244, 2011.

[93] Y. Ma, S. C. Saha, A. L. Bernassau, and D. R. S. Cumming, "Terahertz free space communication based on acoustic optical modulation and heterodyne detection," *Electronics Letters,* vol. 47, pp. 868-870, 2011.

[94] C. P. Colvero, M. C. R. Cordeiro, G. V. d. Faria, and J. P. v. d. Weid, "Experimental comparison between far- and near infrared wavelengths in free space optical systems," *Microwave and Optical Technology Letters,* vol. 46, pp. 319-323, 20 August 2005.

[95] M. D'Amico, A. Leva, and B. Micheli, "Free-space optics communication systems: first results from a pilot field-trial in the surrounding area of Milan, Italy," *IEEE Microwave and Wireless Components Letters,* vol. 13, pp. 305-307, August 2003.

[96] E. Korevaar, I. I. Kim, and B. McArthur, "Atmospheric propagation characteristics of highest importance to commercial free space optics," *Proceeding of SPIE,* vol. 4976, pp. 1-12, 2003.

[97] D. Y. Song, J. W. Cho, Y. S. Hurh, J. H. Lim, D. W. Lee, and J. S. Lee, "4×10 Gb/s terrestrial optical free space transmission over 1.2 km using an EDFA preamplifier with 100 GHz channel spacing," *Optical Fiber Communication Conference, 2000,* vol. 3, pp. 142-144, 2000.

[98] A. Biswas and W. H. Farr, "Detectors for ground-based reception of laser communication from Mars. Lasers and electro-optics society," *The 17th Annual Meeting of the IEEE Lasers and Electro-Optics Society,* vol. 1, pp. 74-75, 7-11 November 2004.

[99] H. Tapse, D. K. Borah, and J. Perez-Ramirez, "Hybrid optical/RF channel performance analysis for Turbo codes," *IEEE Transactions on Communications,* vol. 59, pp. 1389-1399, 2011.

[100] N. D. Chatzidiamantis and G. K. Karagiannidis, "On the distribution of the sum of gamma-gamma variates and applications in RF and optical wireless communications," *IEEE Transactions on Communications,* vol. 59, pp. 1298-1308, 2011.

[101] M. Gregory and S. Badri-Hoeher, "Characterization of maritime RF/FSO channel," *International Conference on Space Optical Systems and Applications, (ICSOS) 2011,* pp. 21-27, 2011.

[102] P. Y. Zhou and F. Khan, "An introduction to millimeter-wave mobile broadband systems," *IEEE Communications Magazine,* vol. 49, pp. 101-107, June 2011.

[103] I. I. Kim, B. McArthur, and E. Korevaar, "Comparison of laser beam propagation at 785 nm and 1550 nm in fog and haze for optical wireless communications", *SPIE Proceeding: Optical Wireless Communications III,* vol. 4214, pp. 26-37, 2001.

[104] R. Arora, S. Seth, J. C. H. Poh, J. D. Cressler, A. K. Sutton, H. M. Nayfeh, G. L. Rosa, and G. Freeman, "Impact of Source/Drain contact and gate finger spacing on the RF reliability of 45-nm RF nMOSFETs", *2011 IEEE International*

Reliability Physics Symposium (IRPS), pp. 5A.6.1 - 5A.6.6, 10-14 April 2011.

[105] M. Bettayeb and S. F. A. Shah, "State of the art ultra-wideband technology for communication systems: a review," *Proceedings of the 2003 10th IEEE International Conference on Electronics, Circuits and Systems, 2003,* vol. 3, pp. 1276-1279, 2003.

[106] I. Kim, "10 G FSO systems position technology for the future," Light wave online pp. 19-21, July 2009.

[107] K. Wang, A. Nirmalathas, C. Lim, and E. Skafidas, "High speed 4×12.5Gbps WDM optical wireless communication systems for indoor applications," *the National Fiber Optic Engineers Conference Optical Fiber Communication Conference and Exposition 2011,* pp. 1-3, 2011.

[108] K. Kazaura, K. Omae, T. Suzuki, M. Matsumoto, E. Mutafungwa, T. Murakami, K. Takahashi, H. Matsumoto, K. Wakamori, and Y. Arimoto, "Performance evaluation of next generation free-space optical communication system," *IEICE Transaction of Electronics,* vol. E90-C, pp. 381-388, February 2007.

[109] M. Sjodin, E. Agrell, P. Johannisson, G. W. Lu, P. A. Andrekson, and M. Karlsson, "Filter optimization for self-homodyne coherent WDM systems using interleaved polarization division multiplexing," *Journal of Lightwave Technology,* vol. 29, pp. 1219-1226, 2011.

[110] H. Willebrand and B. S. Ghuman, *Free space optics: enabling optical connectivity in today's network*: SAMS publishing: 1 edition, December 31,2001.

[111] C. Abou-Rjeily, "On the optimality of the selection transmit diversity for MIMOFSO links with feedback," *IEEE Communications Letters,* vol. 15, pp. 641-643, 2011.

[112] T. Plank, M. Czaputa, E. Leitgeb, S. S. Muhammad, N. Djaja, B. Hillbrand, P. Mandl, and M. Schonhuber, "Wavelength selection on FSO-links," *Proceedings of the 5th European Conference on Antennas and Propagation (EUCAP),* pp. 2508-2512, 2011.

[113] S. A. Zabidi, W. A. Khateeb, M. R. Islam, and A. W. Naji, "Investigating of rain attenuation impact on free space optics propagation in tropical region," *4th International Conference on Mechatronics 2011,* pp. 1-6, 2011.

[114] X. Wu, P. Liu, and M. Matsumoto, "A study on atmospheric turbulence effects in full-optical free-space communication systems," *6th International Conference on Wireless Communications Networking and Mobile Computing 2010 (WiCOM),* pp. 1-5, 2010.

[115] M. S. Khan, M. S. Awan, S. S. Muhammad, V. Kvicera, M. Grabner, C. Capsoni, E. Leitgeb, and P. Mandl, "Linearity in optical attenuations for free-space optical links in continental fog," *Proceedings of the 5th European Conference on Antennas and Propagation,* pp. 2504-2507, 2011.

[116] E. Dadrasnia, S. Ebrahimzadeh, and F. R. M. Adikan, "Influence of short range free space optical atmospheric attenuation in modulated radio signal," *The 2nd International Conference on Computer and Automation Engineering (ICCAE) 2010,* vol. 5, pp. 569-571, 2010.

[117] M. Niu, J. Cheng, and J. F. Holzman, "Diversity reception for coherent free-space optical communications over K-distributed atmospheric turbulence channels,"*IEEE Wireless Communications and Networking Conference (WCNC)*

2010, pp. 1-6, 2010.

[118] T. Yamashita, M. Morita, M. Shimizu, D. Eto, K. Shiratama, and S. Murata, "The new tracking control system for free-space optical communications," *2011 International Conference on Space Optical Systems and Applications (ICSOS),* pp. 122-131, 2011.

[119] A. K. Majumdar and J. C. Ricklin, "*Free-space laser communications: principles and advances",* New York: NY: Springer, 2008.

[120] R. M. Langer, "Effects of atmospheric water vapour on near infrared transmission at sea level", in *Report on Signals Corps Contract DA-36-039-SC-723351*. J.R.M. Bege Co., Arlington, Mass, May-1957.

[121] R. K. Long, "Atmospheric attenuation on ruby lasers", *Proc. of the IEEE*, vol. 51, no. 5, pp. 859-860, May-1963.

[122] H. Weichel, *Laser Beam Propagation in the Atmosphere*. SPIE, Bellingham, WA, 1990.

[123] S. Karp, E. L. O'Neill and R. M. Gagliardi, "Communication theory for the free-space optical channel", *Proc. of the IEEE*, vol. 58, pp. 1626-1650, 1970.

[124] D. K. Borah and D. G. Voelz, "Pointing error effects on free-space optical communication links in the presence of atmospheric turbulence," *Journal of Lightwave Technology,* vol. 27, pp. 3965-3973, 2009.

[125] H. Guo, B. Luo, Y. Ren, S. Zhao and A. Dang, "Influence of beam wander on uplink of ground-to-satellite laser communication and optimization for transmitter beam radius," *Opt. Lett.*, vol. 35, no. 12, pp. 1977-1979, 2010.

[126] J. Akella, M. Yuksel, and S. Kalyanaraman, "Multi-channel communication in free-space optical networks for the last-mile," *15th IEEE Workshop on Local & Metropolitan Area Networks, 2007,* pp. 43 - 48 10-13 June 2007.

[127] I. Ahmed, H. Karvonen, T. Kumpuniemi and M. Katz, "Wireless Communications for the Hospital of the Future: Requirements, Challenges and Solutions" International Journal of Wireless Information Networks, vol. 27, pp. 4-17, October-2019.

[128] M. N. Khan and W. G. Cowley, "Signal dependent Gaussian noise model for FSO communications," *Australian Communications Theory Workshop 2011,* pp. 142-147, 2011.

[129] J. Armstrong, "OFDM for optical communications," Journal of Lightwave Technology, vol. 27, no. 3, pp. 189-204, Feb-2009.

[130] C. Chen, Z. Wen-De and D. Wu, "Non-Hermitian Symmetry Orthogonal Frequency Division Multiplexing for Multiple-Input Multiple-Output Visible Light communications" *Journal of OPT. COMMUN. NETW.,* vol. 9, no. 1, pp. 36-44, Jan-2017.

[131] W. K. Pratt, Laser Communication Systems, 1st ed. New York: John Wiley & Sons, Inc., 1969.

[132] S. F. Clifford, "The classical theory of wave propagation in a turbulent medium," in Laser Beam Propagation in the Atmosphere, J. W. Strobehn, Ed.: Springer-Verlag, 1978.

[133] H. E. Nistazakis, T. A. Tsiftsis and G. S. Tombras, "Performance analysis of free-space optical communication systems over atmospheric turbulence hannels," *IET Commun.,* Vol. **3**(8), pp. 1402–1409 (2009).

[134] N. Mehta, H. Kaushal, V. K. Jain and S. Kar, "Experimental Study on Aperture Averaging in Free Space Optical Communication Link", Conference paper, Feb 2013, DOI:10.1109/NCC.2013.6487941.

[135] H. Kaushal, V. Kumar, A. Dutta, H. Aennam, V. Jain, S. Kar, and J. Joseph, Experimental study on beam wander under varying atmospheric turbulence conditions," IEEE Photon. Tech. Lett., vol. 23, no. 22, pp. 1691–1693, 2011.

[136] P. J. Titterton, "Power reduction and fluctuations caused by narrow laser beam motion in the far field," Appl. Opt., vol. 12, no. 2, pp. 423–425, 1973.

[137] J. H. Churnside and R. J. Lataitis, 'Wander of an optical beam in the turbulent atmosphere," Appl. Opt., vol. 29, no. 7, pp. 926–930, 1990.

[138] H. Kausal and G. Kaddoum, "Optical Communication in Space: Challenges and Mitigation Techniques," accepted in IEEE Communication Survey & Tutorials, DOI: 10.1109/COMST.2016.2603518.

[139] D. Chen, X. Z. Ke, and Q. Sun, "Outage probability and average capacity research on wireless optical communication over turbulence channel," *2011 10th International Conference on Electronic Measurement & Instruments (ICEMI),* vol. 1, pp. 19-23, 2011.

[140] T. Singh, "Calculation of the impact on atmospheric turbulence conditions on free space optical communication links using Gamma-Gamma model", 4th ICCCNT, IEEE-31661, Tiruchengode, India, 1-5 (2013).

[141] W. G. Stephen, B. Maïté, C. Qianling and H. James, " Optical Repetition MIMO Transmission with Multipulse PPM" IEEE journal on selected areas in communications, Vol. 23, No. 9, pp. 1901-1910, September, 2005.

[142] Z. Sodnik, B. Furch, and H. Lutz, "Free-space laser communication activities in Europe: SILEX and beyond," *19th Annual Meeting of the IEEE Lasers and Electro-Optics Society 2006,* pp. 78-79, October 2006.

[143] S. G. Wilson, M. Brandt-Pearce, Q. Cao, and J. H. Leveque, "Free-space optical MIMO transmission with Q-ary PPM," *IEEE Transactions on Communications,* vol. 53, pp. 1402-1412 August 2005.

[144] D. Clarke and J. F. Grainger, *Polarized light and optical measurement (monographs in natural philosophy)* vol. 35. Oxford: Pergamon Press; 1st edition, 1971.

[145] E. Collett, *Polarized light: fundamentals and applications*. New York: Marcel Dekker, Inc., 1993.

[146] M. Winter, C. A. Bunge, D. Setti and K. Petermann, "A statistical treatment of cross polarization modulation in DWDM systems", *J. of Lightwave Technol*.27 (2009) 3739-3751.

[147] J. Zhang and A. Dang, "Performance analysis of free space optical communication under atmospheric polarization effect", Asia Communication and Photonics Conference (ACP), OSA, 2017.

[148] C. Glauco, P. Simoes, C. Floridia, C. Franciscangelis, M. C. Argentato and M. A. Romero, "Simultaneous nominal and effective differential group delay in service monitoring method for optical communication systems", Opt. Express, 21 (2013) 8190-8200.

[149] J. M. Ostermann and P. Debernardi, "Polarization Division Multiplexed data Transmission using Surface Grating VCSELs", Institute of Optoelectronics, Ulm

University, Annual report (2008), pp. 71-76.

[150] S. Bloom, E. Korevaar, J. Schuster, and H. Willebrand, "Understanding the performance of free-space optics," Journal of OpticalNetworking, vol. 2, no. 6, pp. 178–200, Jan. 2003.

[151] I. S. Gradshteyn and I. M. Ryzhik, *Table of Integrals, Series and Products,* 5th ed. London, U. K.: Academic, 1994.

[152] M. Torabi, S. Aissa and M. R. Soleymani, ''On the BER Performance of Space-Frequency Block Coded OFDM Systems in Fading MIMO Channels,'' IEEE Transactions on wireless communications, 6(4), 1366-1373 (2006).

[153] S. M Alamouti, "A Simple Transmit Diversity Technique for Wireless Communications", IEEE Journal on select area in Communications, Vol.16, no.8, pp. 1451-1458, October 1998.

[154] M. R. Bhatnagar and S. Anees, "On the performance of Alamouti Scheme in Gamma-Gamma fading FSO links with Pointing errors," IEEE wireless communications letters, vol. 4, no.1, pp. 94-97, 2015.

[155] M. Simon and V. Vilnrotter, "Alamouti-type space-time coding for freespace optical communication with direct detection," IEEE Trans. Wireless Commun., vol. 4, no. 1, pp. 35–39, 2005.

List of Publications

Journal:

1. M. Shariful Islam and S. P. Majumder, "Performance Analysis of a Non-Hermitian OFDM Optical DQPSK FSO Link over Atmospheric Turbulent Channel," Journal of optical communication, De-Gruyter, aop, 2019.

2. M. Shariful Islam and S. P. Majumder, "Performance analysis of a 2-Channel Polarization Division Multiplexed Optical DQPSK FSO Link with the effect of Atmospheric Turbulence" Journal of Optics, Springer, vol. 49(3), pp. 357-363, Jul-2020, DOI: 10.1007/s12596-020-00628-0.

3. M. Shariful Islam and S. P. Majumder, "Analytical Evaluation of the Cross-polarization induced Crosstalk on BER Performance of an OFDM FSO Link with Polarization Diversity" Optics Communication, Elsevier, vol. 474(C), May-2020, DOI: 10.1016/j.optcom.2020.126095.

4. M. Shariful Islam and S. P. Majumder, "BER Performance Evaluation of a non-Hermitian Coherent-Optical OFDM FSO System with SFBC and Polarization Diversity", Optics communication, Elsevier, vol. 475(C), Jul-2020, DOI: 10.1016/j.optcom.2020.126288.

5. M. Shariful Islam and S. P. Majumder, "Comparative performance analysis between STBC and SFBC on a non-Hermitian OFDM free-space optical system with polarization diversity", Optical and Quantum Electronics, Springer, vol. 53(603), October-2021.

6. M. Shariful Islam and S. P. Majumder, "BER Performance Analysis of a non-Hermitian coherent optical OFDM FSO System with Polarization Diversity using various Atmospheric Turbulent Channel Models", Optical and Quantum Electronics, Springer, vol. 54(302), April-2022.

Conference:

1. M. Shariful Islam and S. P. Majumder, "Performance Analysis of an OFDM Optical DQPSK FSO Link considering Strong Atmospheric Turbulence with Pointing Error" 3rd IEEE ICTP conference, Dec-2019.

2. M. Shariful Islam and S. P. Majumder, "Aperture Averaged BER Performance Analysis of a non-Hermitian coherent optical OFDM FSO System with Polarization Diversity," 11th International Conference on Electrical and Computer Engineering (ICECE), Dec-2020.